

**CALCIUM/CALMODULIN-DEPENDENT PROTEIN KINASE II  
REGULATION OF THE SLOW DELAYED RECTIFIER  
POTASSIUM CURRENT, I(KS), DURING SUSTAINED BETA-  
ADRENERGIC RECEPTOR STIMULATION**

by

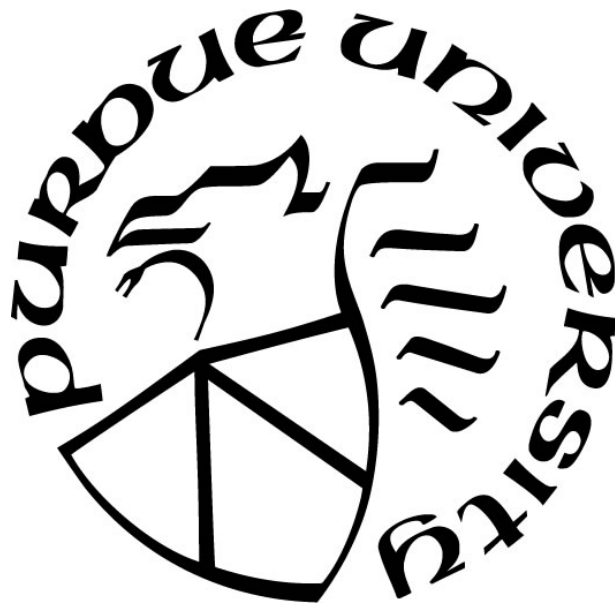
**Tyler Andrew Shugg**

**A Dissertation**

*Submitted to the Faculty of Purdue University*

*In Partial Fulfillment of the Requirements for the degree of*

**Doctor of Philosophy**



Department of Pharmacy Practice

West Lafayette, Indiana

December 2018

**THE PURDUE UNIVERSITY GRADUATE SCHOOL**  
**STATEMENT OF COMMITTEE APPROVAL**

Dr. Brian R. Overholser, Chair

Department of Pharmacy Practice

Dr. Andy Hudmon

Department of Medicinal Chemistry and Molecular Pharmacology

Dr. James E. Tisdale

Department of Pharmacy Practice

Dr. David R. Foster

Department of Pharmacy Practice

Dr. Kevin M. Sowinski

Department of Pharmacy Practice

Dr. Theodore Cummins

Department of Biology,

Indiana University-Purdue University Indianapolis

**Approved by:**

Dr. Duane Dunlap

Head of the Graduate Program

This work is dedicated to my parents, Joyce and Jack. Only through their continual love and support have I been fortunate enough to chase my dreams as a scientist and pharmacist. Below is an excerpt from the eulogy I prepared for my father's funeral in June 2015. The words remain true:

*"I come from a home of two very fostering and nurturing parents. And through their diligence and sacrifice, I was afforded the opportunity to pursue my dreams. When I used to thank my father for my parents' investment in me -- their time, their love, their money -- he used to say to me that what he wanted in life, more than anything, was for me to be successful. In my parents' example, I learned the meaning of unconditional love."*

## ACKNOWLEDGMENTS

I am eternally grateful to my many mentors and colleagues during my graduate tenure, who have provided me with expertise, training, advice, and support.

Foremost, I express my sincerest gratitude to my primary mentor, Dr. Brian Overholser. During the past five years, Brian has been my scientific mentor, my professional role model, and my trusted friend. I cannot thank Brian enough for his unwavering investment in my professional and personal development. I owe my positive momentum as an aspiring scientist to Brian's tutelage. In turn, Brian owes his ability to properly use commas to my time in his lab.

I also owe a great deal of thanks to the other members of my committee. Dr. Andy Hudmon has served as an unofficial co-mentor to me during my training, providing hands on scientific training, timely and expert reviews for my training grants, and invaluable career advice. My training has been significantly enriched by Andy's efforts. Dr. Jim Tisdale has greatly contributed to my training as well, being a key clinical collaborator and an incredible professional role model. I greatly appreciate Dr. Ted Cummins for his role on my committee as the electrophysiology guru; his ability to clearly and concisely articulate complex topics is remarkable and has been of great assistance to me during my training. Finally, I appreciate the efforts of Drs. Dave Foster and Kevin Sowinski who have been excellent professional role models and have facilitated numerous instances for me to hone my teaching skills. I am also thankful to the other members of Purdue's Department of Pharmacy Practice who have provided me with daily support and assistance.

Many members within the Division of Clinical Pharmacology at the Indiana University School of Medicine have also made essential contributions to my graduate training. Through formal didactic sessions, departmental seminars, and research collaborations, the Division has contributed enormously to my graduate training.

I also owe a great deal of gratitude to my graduate colleagues in Purdue's Department of Pharmacy Practice for their continual support throughout my time in the program, including scientific, social, and emotional support. I also am extremely thankful to the members of the Overholser lab, especially my fellow graduate trainees during my tenure, Ahmed Abdelhady, Noha Mourad, and Abdullah Assiri, for their immeasurable contributions to my scientific and professional development.

I would finally like to acknowledge the various organizations who have provided the Overholser lab with funding during my graduate career: the National Institutes of Health, the American Heart Association, the American College of Clinical Pharmacy, the Indiana Clinical and Translational Sciences Institute, and the Purdue University College of Pharmacy.

## TABLE OF CONTENTS

LIST OF TABLES .....	9
LIST OF FIGURES .....	10
LIST OF ABBREVIATIONS .....	15
ABSTRACT .....	17
INTRODUCTION .....	23
Delayed rectifier potassium currents regulate cardiac action potential duration and arrhythmogenesis .....	23
The slow delayed rectifier potassium current, $I_{Ks}$ .....	24
Functional significance of $I_{Ks}$ .....	24
Biology of the KCNQ1 carboxyl terminus .....	25
Functional changes in $I_{Ks}$ during $\beta$ -AR stimulation .....	27
Neurohormonal remodeling in heart failure .....	28
Changes in neurohormonal signaling during HF inhibit delayed rectifier potassium current function .....	30
CaMKII as a pathological regulator during HF .....	32
$\beta$ -AR stimulation activates CaMKII through an Epac-dependent pathway .....	34
CaMKII regulation of cardiac ion channels and APD .....	34
Mechanisms of $I_{Ks}$ inhibition during sustained $\beta$ -AR stimulation and HF .....	36
Study Rationale .....	38
Study Aims & Objectives .....	39
METHODS .....	41
DNA Constructs and Reagents .....	41
Cell Culture and cDNA Transfection .....	42
cDNA Amplification and Purification .....	43
Mass Spectrometry .....	45
Stable Lentiviral Expression .....	46
Cellular Electrophysiology .....	47
KCNQ1 Peptide Array .....	49
CaMKII Protein Immunoblot .....	50

Bimolecular Fluorescence Complementation (BiFC) .....	51
Cell Surface Biotinylation .....	56
Data Analysis .....	57
RESULTS .....	59
Specific Aim 1: Investigate the regulation of the KCNQ1 carboxyl terminus during sustained $\beta$ -AR stimulation and the associated functional implications on $I_{Ks}$ .....	59
The KCNQ1 carboxyl terminus demonstrates increased phosphorylation during sustained $\beta$ -AR stimulation.....	59
Sustained $\beta$ -AR stimulation inhibits $I_{Ks}$ activation currents and causes a depolarizing shift in the voltage dependence of activation.....	60
Mimics of phosphorylation at S457, T482, and S484 in combination decrease $I_{Ks}$ activation currents.....	62
Mimics of phosphorylation at S457 and S484, but not at T482, decrease $I_{Ks}$ activation currents and positively shift the voltage dependence of activation .....	65
Specific Aim 2: Assess the potential for CaMKII-mediated functional regulation of $I_{Ks}$ during sustained $\beta$ -AR stimulation and the associated functional implications.....	68
The KCNQ1 carboxyl terminus contains residues of CaMKII phosphorylation.....	68
CaMKII mediates functional changes in $I_{Ks}$ during sustained $\beta$ -AR stimulation .....	70
CaMKII mediates functional inhibition of $I_{Ks}$ through KCNQ1 phosphorylation at S484 but not S457 .....	74
PKA does not mediate functional changes in $I_{Ks}$ during sustained $\beta$ -AR stimulation	79
Specific Aim 3: Evaluate the mechanistic basis for how CaMKII-mediated S484 phosphorylation, in response to sustained $\beta$ -AR stimulation, inhibits $I_{Ks}$ function .....	82
The KCNQ1 carboxyl terminus is differentially phosphorylated during co-expression with KCNE1.....	82
Mimics of phosphorylation at S484 inhibit KCNQ1 function only during co-expression with KCNE1 .....	83
Utilizing LQT1 mutations in the vicinity of KCNQ1 S484 as a translational tool to assess CaMKII regulation during sustained $\beta$ -AR stimulation .....	85
Sustained $\beta$ -AR stimulation and mimics of phosphorylation and dephosphorylation at S484 disrupt the interaction between KCNQ1 and KCNE1 subunits.....	87

CaMKII signaling disrupts the interaction between KCNQ1 and KCNE1 subunits during sustained $\beta$ -AR stimulation via regulation at S484 .....	90
Phosphorylation at S484 reduces plasma membrane expression of KCNQ1 and KCNE1 subunits .....	93
DISCUSSION .....	95
Regulation of the KCNQ1 carboxyl terminus by CaMKII during sustained $\beta$ -AR stimulation .....	95
Assessing the mechanistic basis through which KCNQ1 S484 phosphorylation mediates functional inhibition of $I_{Ks}$ during sustained $\beta$ -AR stimulation .....	103
SUMMARY & CONCLUSIONS .....	112
SUPPLEMENTARY TABLES .....	115
BIBLIOGRAPHY .....	120

## LIST OF TABLES

<b>Table 1.</b> Estimated Boltzmann equation parameters for WT KCNQ1 during treatment with 100 nM ISO or vehicle.....	61
<b>Table 2.</b> Estimated Boltzmann equation parameters for Triple-A and Triple-D KCNQ1 during treatment with 100 nM ISO or vehicle.....	65
<b>Table 3.</b> Estimated Boltzmann equation parameters for S457A, S457D, T482A, T482D, S484A, and S484D KCNQ1 in control conditions.....	67
<b>Table 4.</b> Estimated Boltzmann equation parameters for WT KCNQ1 during co-treatment with 100 nM ISO for 12-24 hours and 500 nM KN-92 or KN-93 for 4 hours.....	71
<b>Table 5.</b> Estimated Boltzmann equation parameters for WT KCNQ1 during co-treatment with 100 nM ISO for 12-24 hours and CN21 or CN21-Ala (10 $\mu$ M tat-CN21 or tat-CN21-Ala in culture media and 1 $\mu$ M CN21 or CN21-Ala in pipette solution).....	73
<b>Table 6.</b> Estimated Boltzmann equation parameters for WT $I_{Ks}$ when expressed in an HEK 293 cell line containing T287D $\delta$ CaMKII or lentiviral control.....	79
<b>Table 7.</b> Estimated Boltzmann equation parameters for WT, S484A, and S484D KCNQ1 when expressed in the absence of KCNE1 in HEK 293 cells.....	84

## LIST OF FIGURES

- Figure 1. Methods for analysis of electrophysiological data.** (Left) Representative traces of elicited activation and tail currents for WT  $I_{Ks}$  in control conditions are shown at test voltages from -50 mV to +60 mV (-60 mV not shown, but was similar to -50 mV). (Right) Procedures detailing how summary graphics (I-V plots [top] and activation curves [bottom]) were constructed from raw data. .... 48
- Figure 2.** Vector maps showing the KCNQ1 coding region expressed in the pBIFC-VN155 plasmid containing the amino half of the fluorescent protein Venus (left) and the KCNE1 coding region expressed in the pBIFC-VC155 plasmid containing the carboxyl half of Venus (right). Maps were created using PlasMapper: (<http://wishart.biology.ualberta.ca/PlasMapper/>)..... 52
- Figure 3. (Top)** A series of images showing transient expression of the cytosolic Cerulean fluorescent protein in HEK 293 cells. Displayed images were taken along the z-plane (vertical) at 1.5  $\mu$ M increments. (Bottom) Summed images of the same visual field showing co-expression of Cerulean (left panel) and Venus fluorescent proteins (middle panel). A merged image showing both fluorescent proteins is shown in the right panel. Expression of Venus signals requires interaction of complementary halves of the Venus protein that are contained within plasmids co-expressing WT or mutant KCNQ1 and WT KCNE1. Cerulean is a cytosolic protein that allows resolution of cell boundaries for analysis and allows normalization of Venus intensity to control for transfection and expression efficiency. .... 53
- Figure 4. Control Experiments for BiFC Methodology.** To verify that Venus signals in our BiFC experiments were specifically mediated by interaction of expressed KCNQ1 and KCNE1 subunits with complementary halves of Venus, we performed the following control experiments. First, we co-expressed the VN155 (containing the amino half of Venus without KCNQ1 expressed within the MCS), VC155 (containing the carboxyl half of Venus without KCNE1 expressed within the MCS), and Cerulean. As shown in the top panels, HEK 293 cells transiently co-expressing VN155, VC155, and Cerulean displayed fluorescent signals corresponding to Cerulean expression but not Venus expression in the absence of KCNQ1 and KCNE1. The middle and bottom panels displayed merged filters (in which intensities from both Venus and Cerulean signals are both displayed) for when VNQ, VCE, and Cerulean are co-expressed (middle left; representative trace for elicited currents during co-expression of VNQ and VCE shown in middle right), when VNQ and Cerulean are co-expressed (bottom left), when VCE and Cerulean are co-expressed (bottom center), and when no plasmids are transfected (bottom right). Together, these panels demonstrate Venus fluorescent signal only when complementary halves of Venus come in close proximity via interaction of KCNQ1 and KCNE1 subunits. .... 55

- Figure 5.** Basal phosphorylation was identified at five KCNQ1 carboxyl terminal residues (when co-expressed with KCNE1 in HEK 293 cells) via LCMS/MS: S407, S457, T482, S484, and T624. Phosphorylation was increased at S407, T482, S484, and T624 following four hour treatment with the  $\beta$ -AR agonist ISO (100 nM). Increased phosphorylation was sustained following 24 hour ISO treatment at T482 and S484. \*P<0.05 vs. control conditions ..... 59
- Figure 6.** (A) Representative traces of  $I_{Ks}$  currents from WT KCNQ1 co-expressed with KCNE1 in HEK 293 cells treated with 100 nM ISO or vehicle for 12-24 hours. (B) I-V plots (mean and SEM), (C) activation curves (normalized to voltage of maximum activation [+60 mV]), and rate constants of activation (D) and deactivation (E) following treatment with ISO or vehicle. \*p<0.05 vs. control conditions ..... 61
- Figure 7.** (A) Representative traces of elicited WT  $I_{Ks}$  currents during treatment with the  $I_{Ks}$  chemical inhibitor, HMR 1556 (100 nM or 10  $\mu$ M), or vehicle in the pipette solution. (B) I-V plots (mean and SEM) and (C) bar graphs of maximum WT  $I_{Ks}$  current density during treatment with HMR 1556 or vehicle. \*p<0.05 vs. control conditions, ns = not significant..... 62
- Figure 8.** (A) Representative traces of  $I_{Ks}$  activation currents from KCNQ1 combination mimics of phosphorylation (Triple-D) and dephosphorylation (Triple-D) co-expressed with KCNE1 in HEK 293 cells. (B) I-V plots (mean and SEM), (C) activation curves (normalized to voltage of maximum activation), and rate constants of activation (D) and deactivation (E) for Triple-A and Triple-D KCNQ1. (F) Bar graph of current density at the voltage of maximum activation (+60 mV) for combination mimic KCNQ1 or for WT KCNQ1 following treatment with ISO or vehicle. \*p<0.05 for comparison indicated, <sup>+</sup>p<0.05 for Triple-A vs. Triple-D, <sup>†</sup>p<0.05 for Triple-A+ISO vs. Triple-D+ISO ..... 64
- Figure 9.** (A) I-V plots (mean and SEM) of elicited currents during an activating voltage step protocol, bar graph of maximum  $I_{Ks}$  current density, and activation curves for WT, dephosphorylation (S457A), and phosphorylation (S457D) mimics of KCNQ1 at S457 when co-expressed with WT KCNE1 in HEK 293 cells. (B) I-V plots activation currents, bar graph of maximum  $I_{Ks}$  current density, and activation curves for WT, dephosphorylation (T482A), and phosphorylation (T482D) mimics of KCNQ1 at T482. (C) I-V plots activation currents, bar graph of maximum  $I_{Ks}$  current density, and activation curves for WT, dephosphorylation (S484A), and phosphorylation (S484D) mimics of KCNQ1 at S484. \*p<0.05 for S457A vs. S457D or S484A vs. S484D ..... 66

**Figure 10.** Peptide fragments of 15 residues in length corresponding to the intracellular regions of KCNQ1 were synthesized on a cellulose membrane and exposed to  $\text{Ca}^{2+}$ /calmodulin-activated  $\delta\text{CaMKII}$  for four minutes (**top**) and 30 seconds (**bottom**) with  $\text{Mg}$ - $[\gamma\text{-}^{32}\text{P}]\text{ATP}$ . Peptide fragments containing KCNQ1 carboxyl terminal residues T482 and S484 (indicated by the dashed boxes at D5-D7) were the strongest substrates for CaMKII phosphorylation. The solid box at F15-F19 in the top panel contains a mutant autocamtide-2 negative control (T $\rightarrow$ A mutation; F15), WT autocamtide-2 positive control (F17), and Kemptide control (classical PKA substrate; F19). The arrow in the bottom panel contains an additional mutant autocamtide-2 negative control. The full peptide map is shown in **Supplementary Table 1**. ..... 69

**Figure 11.** Schematic of KCNQ1 and KCNE1 subunits showing KCNQ1 carboxyl terminal sites of potential CaMKII regulation during sustained  $\beta$ -AR stimulation and HF. .... 70

**Figure 12.** (A) I-V plots (mean and SEM), (B) peak current density, and (C) normalized activation curves for WT KCNQ1/KCNE1 following treatment with 100 nM ISO for 12-24 hours and 500 nM KN-92 or KN-93 for 4 hours in culture media. (D) I-V plots and (E) peak current density for WT KCNQ1/KCNE1 following treatment with 500 nM KN-92 or KN-93 for 4 hours in culture media. \* $p < 0.05$ , ns = not significant for comparison indicated ..... 72

**Figure 13.** (A) I-V plots (mean and SEM) and (B) peak activation current density for WT KCNQ1/KCNE1 following co-treatment with ISO (100 nM for 12-24 hours) and CN21 or CN21-Ala (10  $\mu\text{M}$  tat-CN21 or tat-CN21-Ala in culture media and 1  $\mu\text{M}$  CN21 or CN21-Ala in pipette solution during recording). (C) Normalized activation curves following treatment with ISO and CN21 or CN21-Ala. \* $p < 0.05$  ..... 73

**Figure 14.** Representative protein immunoblots ( $n=7$  per condition) and percent changes in CaMKII and CaMKII T287 phosphorylation in HEK 293 cells following treatment with 100 nM ISO for 24 hours. \* $p < 0.05$  ..... 75

**Figure 15.** (A) Synthesized peptides corresponding to KCNQ1 carboxyl terminal residues that demonstrated basal phosphorylation were exposed to activated  $\delta\text{CaMKII}$ . Each row contains peptides corresponding to the labeled KCNQ1 residue with columns for WT, A (phospho-acceptor site mutated to alanine), or KO (all serines and threonines mutated to alanines with the exception of T482 wherein S484 was not mutated;  $n=5$  for each condition). (B) Quantification of phosphostimulated luminescence for WT, A, and KO peptides corresponding to KCNQ1 T482 and S484 during exposure to activated  $\delta\text{CaMKII}$ . \* $p < 0.05$  ..... 77

**Figure 16.** (A) I-V plots (mean and SEM) and (B) peak current density at +60 V for elicited currents during an activating voltage protocol when WT or mutant KCNQ1 was co-expressed with KCNE1 in HEK 293 cells stably overexpressing YFP-tagged constitutively active (T287D)  $\delta$ CaMKII or YFP-tagged control. (C) Normalized activation curves for WT KCNQ1 when expressed in CaMKII overexpression and control lines. Rate constants of activation (D) and deactivation (E) for WT and S484A KCNQ1 when expressed in the CaMKII overexpression line +p<0.05 for Control, WT vs. CaMKII, WT, †p<0.05 for CaMKII, S484A vs. CaMKII, WT, \*\*p<0.05 for comparison indicated, \*p<0.05 for CaMKII, WT vs. CaMKII, S484A (tau analyses)..... 79

**Figure 17.** (A) I-V plots and (B) peak activation current density for WT KCNQ1/KCNE1 following treatment with vehicle, ISO, or co-treatment with ISO (100 nM for 12-24 hours) and myristoylated PKI (1  $\mu$ M in culture media and in pipette solution during recording). (C) Normalized activation curves following treatment with vehicle, ISO, and co-treatment with ISO and myristoylated PKI. \*p<0.05 ..... 80

**Figure 18.** Fifteen residue peptides corresponding to the KCNQ1 carboxyl terminal residues S407, S457, T482, S484, and T624, positive control (kemptide for PKA and autocalmitide-2 for CaMKII), negative controls (threonine and serine mutated to alanines on kemptide and autocalmitide-2, respectively) were synthesized on a cellulose membrane and exposed to activated PKA or  $\delta$ CaMKII for 30 seconds with [ $\gamma$ -<sup>32</sup>]ATP. Relative to kemptide control, peptides corresponding to S457, T482, and S484 (with nearby serines and threonines mutated to alanines), and T624 do not demonstrate phosphorylation signals when exposed to activated PKA. While S407 peptides demonstrate weak phosphorylation signals when exposed to activated PKA, analysis of the S407KO peptide, wherein all serines and threonines have been mutated to alanines, does not reduce the phosphorylation signal, indicating that the signal is being produced by a non-specific interaction of PKA and the peptide fragment. Relative to autocalmitide-2 control, peptides corresponding to S457, T482 (with nearby serines and threonines, including S484, mutated to alanines), and T624 do not demonstrate phosphorylation signals when exposed to activated  $\delta$ CaMKII. S484 (with nearby serines and threonines, including T482, mutated to alanines) demonstrates strong phosphorylation signals when exposed to activated  $\delta$ CaMKII. While S407 peptides demonstrate weak phosphorylation when exposed to activated  $\delta$ CaMKII, analysis of S407A, wherein S407 has been mutated to an alanine, does not reduce the phosphorylation signal, indicating that the signal is likely mediated by another serine or threonine on the peptide fragment..... 81

**Figure 19.** Phosphorylation was assessed via LCMS/MS at the five KCNQ1 carboxyl terminal residues that previously demonstrated basal phosphorylation (S407, S457, T482, S484, T624) in the presence (white bars) and absence (black bars) of co-expression with KCNE1. Phosphorylation was reduced at S457, T482, and S484 when KCNQ1 was co-expressed with KCNE1. Phosphorylation at T624 was not detected in the assay. \*P<0.05 vs. KCNQ1 expression alone..... 83

**Figure 20.** (A) I-V plots and (B) peak activation current density for WT, S484A, and S484D KCNQ1 expressed in the absence of KCNE1 in HEK 293 cells. (C) Normalized activation curves for WT, S484A, and S484D KCNQ1. .... 84

**Figure 21.** Peptide fragments corresponding to S457 on KCNQ1 and LQT1 mutations surrounding the site (R452W, H455Y, or G460S) did not display phosphorylation signals when exposed to activated CaMKII and radiolabeled ATP..... 86

**Figure 22.** Peptide fragments corresponding to S484 were substrates for CaMKII phosphorylation, and CaMKII phosphorylation was disrupted by R481I but not S484T LQT1 mutations..... 87

**Figure 23. (Left)** Representative summed images of HEK 293 cells transiently co-expressing cytosolic Cerulean fluorescent proteins (cyan) and Venus fluorescent proteins (yellow) encoded in plasmids containing WT KCNQ1 in control conditions, WT KCNQ1 during treatment with 100 nM ISO for 12-24 hours, S484A KCNQ1 in control conditions, and S484D KCNQ1 in control conditions along with WT KCNE1. **(Right)** Mean ratios of Venus:Cerulean fluorescent intensities for WT KCNQ1/KCNE1 in control conditions and during 12-24 hour treatment with 100 nM ISO, S484A KCNQ1/KCNE1, and S484D KCNQ1/KCNE1. \* $p < 0.05$ , \*\* $p < 0.01$  for comparison indicated..... 89

**Figure 24. (Left)** Representative summed images of HEK 293 cells transiently co-expressing cytosolic Cerulean fluorescent proteins (cyan) and Venus fluorescent proteins (yellow) encoded in plasmids containing WT KCNQ1 and KCNE1 during 12-24 hour co-treatment with 100 nM ISO and the specific CaMKII chemical inhibitor, KN-93, or its inactivate analogue, KN-92 (500 nM for both). **(Right)** Mean ratios of Venus:Cerulean fluorescent intensities for WT KCNQ1/KCNE1 during co-treatment with ISO and KN-93 or KN-92. \*\* $P < 0.01$  for comparison indicated..... 90

**Figure 25. (Left)** Representative summed images of HEK 293 cells transiently co-expressing cytosolic Cerulean fluorescent proteins (cyan) and Venus fluorescent proteins (yellow) encoded in plasmids containing R481I or S484T KCNQ1 during 12-24 hour treatment with 100 nM ISO. **(Right)** Mean ratios of Venus:Cerulean fluorescent intensities for R481I or S484T KCNQ1/WT KCNE1 during treatment with ISO. \*\* $P < 0.01$  for comparison indicated..... 92

**Figure 26. (A)** Representative protein immunoblot from HEK 293 cells transiently co-expressing WT KCNQ1/KCNE1 (no biotinylation), S484A KCNQ1/WT KCNE1 (after isolation of plasma membrane-bound proteins via biotinylation), and S484D KCNQ1/WT KCNE1 (after biotinylation) following treatment with KCNQ1, KCNE1, and  $\text{Na}^+/\text{K}^+ \text{-ATPase}$  (membrane-bound loading control) antibodies. **(B)** Percent change in  $\text{KCNQ1}:\text{Na}^+/\text{K}^+ \text{-ATPase}$  ratios relative to S484A. **(C)** Percent change in  $\text{KCNE1}:\text{Na}^+/\text{K}^+ \text{-ATPase}$  ratios relative to S484A. \* $p < 0.05$ ..... 94

**Figure 27.** Proposed pathway of CaMKII regulation of  $\text{I}_{\text{Ks}}$  during sustained  $\beta$ -AR stimulation..... 100

## LIST OF ABBREVIATIONS

A (amino acid) = Alanine  
ACE = Angiotensin-converting enzyme  
AKAP = Alpha-kinase anchoring protein  
AP = Action potential  
APD = Action potential duration  
APD<sub>90</sub> = Action potential duration at 90% of the return to the resting membrane potential  
ARB = Angiotensin II receptor blocker  
AT<sub>1</sub> = Angiotensin II receptor type 1  
AV = Atrioventricular  
β-AR = Beta-adrenergic receptor  
β<sub>1</sub>-AR = Beta<sub>1</sub>-adrenergic receptor  
β<sub>2</sub>-AR = Beta<sub>2</sub>-adrenergic receptor  
BSA = Bovine serum albumin  
C (amino acid) = Cysteine  
CaM = calmodulin  
CaMKII = Calcium/calmodulin-dependent protein kinase II  
cAMP = cyclic adenosine monophosphate  
CDF = Calcium-dependent facilitation  
CHO = Chinese hamster ovary  
CICR = Calcium-induced calcium release  
D (amino acid) = Aspartic acid  
E (amino acid) = Glutamate  
EAD = Early afterdepolarizations  
Epac = Exchange protein activated by cyclic adenosine monophosphate  
FBS = Fetal bovine serum  
G (amino acid) = Glycine  
GPCR = G-protein-coupled receptor  
H (amino acid) = Histidine  
HF = Heart failure  
hiPSC = Human inducible pluripotent stem cell  
hiPSC-CM = Cardiomyocyte derived from human inducible pluripotent stem cell  
I (amino acid) = Isoleucine  
ISO = Isoproterenol  
K (amino acid) = Lysine  
L (amino acid) = Leucine  
LCMS/MS = Tandem liquid chromatography- mass spectrometry/ mass spectrometry  
LQT1 = Long QT syndrome phenotype 1

LQT5 = Long QT syndrome phenotype 5  
M (amino acid) = Methionine  
MEM = Minimum essential medium  
Na<sup>+</sup>/K<sup>+</sup>-ATPase = Sodium-potassium adenosine triphosphatase (sodium-potassium exchange pump)  
P (amino acid) = Proline  
PIP<sub>2</sub> = Phosphatidylinositol 4,5-bisphosphate  
PKA = Protein kinase A  
PKC = Protein kinase C  
PKC-ε = Epsilon isoform of protein kinase C  
PLC = Phospholipase C  
PLC-ε = Epsilon isoform of phospholipase C  
PLN = Phospholamban  
PP1 = Protein phosphatase 1  
RAAS = Renin-angiotensin-aldosterone system  
ROS = Reactive oxygen species  
RyR = Ryanodine receptor  
R (amino acid) = Arginine  
S (amino acid) = Serine  
SERCA2 = Sarcoplasmic reticulum calcium-ATPase  
T (amino acid) = Threonine  
TBST = Tris-buffered saline with 0.1% (v/v) Tween 20  
TdP = Torsades des pointes  
TIRF = Total internal reflection fluorescence  
VF = Ventricular fibrillation  
VT = Ventricular tachycardia  
W (amino acid) = Tryptophan

## ABSTRACT

Author: Shugg, Tyler, A. Ph.D.

Institution: Purdue University

Degree Received: December 2018

Title: Calcium/Calmodulin-Dependent Protein Kinase II Regulation of the Slow Delayed Rectifier Potassium Current,  $I_{Ks}$ , During Sustained Beta-Adrenergic Receptor Stimulation

Major Professor: Brian R. Overholser, PharmD.

**Background:** Sustained elevations in catecholaminergic signaling, mediated primarily through  $\beta$ -adrenergic receptor ( $\beta$ -AR) stimulation, are a hallmark neurohormonal alteration in heart failure (HF) that contribute to pathophysiologic cardiac remodeling. An important pathophysiological change during sustained  $\beta$ -AR stimulation is functional inhibition of the slow delayed rectifier potassium current,  $I_{Ks}$ , which has been demonstrated to prolong action potential duration (APD) and increase ventricular arrhythmogenesis in HF. Though functional inhibition of  $I_{Ks}$  has been consistently reproduced in cellular, animal, and limited human studies of HF, the mechanisms that mediate  $I_{Ks}$  inhibition during HF remain poorly understood.

In addition, HF results in aberrant calcium handling that is known to contribute to the disease. HF has been demonstrated to increase the expression and function of calcium/calmodulin-dependent protein kinase II (CaMKII), a key regulator of calcium homeostasis and excitation-contraction coupling in cardiomyocytes. Enhanced CaMKII signaling has been consistently demonstrated to contribute to increased arrhythmogenesis in a number of cardiac diseases, including HF. CaMKII is a known pathological regulator of many cardiac ion channels resulting in APD prolongation and the development of arrhythmias.

**Objective:** This investigation aims to assesses the potential for CaMKII regulation of KCNQ1 (pore-forming subunit of  $I_{Ks}$ ) during sustained  $\beta$ -AR stimulation and to characterize the potential functional implications on  $I_{Ks}$ . Furthermore, this investigation seeks to elucidate the mechanism underlying CaMKII-mediated  $I_{Ks}$  inhibition during sustained  $\beta$ -AR stimulation.

**Methods:** Phosphorylation of KCNQ1 was assessed using a tandem liquid chromatography- mass spectrometry/ mass spectrometry (LCMS/MS) approach during sustained  $\beta$ -AR stimulation via treatment with 100 nM isoproterenol (ISO) for 4-24 hours and during co-expression with KCNE1. Whole-cell, voltage-clamp patch clamp electrophysiology experiments were performed in HEK 293 cells transiently co-expressing wild-type (WT) or mutant KCNQ1 (mutations conferring mimics of dephosphorylation and phosphorylation were introduced at phosphorylation sites identified by LCMS/MS) and KCNE1 (auxiliary subunit) during ISO treatment, treatment with CaMKII or protein kinase A (PKA) inhibitors, or during lentiviral  $\delta$ CaMKII overexpression. A robotic peptide synthesizer was used to create fifteen residue peptide fragments on a nitrocellulose membrane corresponding to KCNQ1 intracellular domains and the KCNQ1 residues identified via LCMS/MS; membranes were incubated with activated CaMKII or PKA in the presence of radiolabeled ATP to identify potential sites of phosphorylation. Bimolecular fluorescence complementation (BiFC) experiments were performed in HEK 293 cells to assess the impact of CaMKII-mediated KCNQ1 phosphorylation on the interaction of KCNQ1 and KCNE1 subunits. Protein immunoblot experiments were performed to (1) assess CaMKII activation during ISO treatment and (2) to assess plasma membrane expression of KCNQ1 and KCNE1 subunits with mimics

of differential KCNQ1 phosphorylation following a membrane protein biotinylation procedure.

**Results:** In Aim 1, we investigated the regulation of the KCNQ1 carboxyl terminus during sustained  $\beta$ -AR stimulation and assessed the associated functional implications on  $I_{Ks}$ . An LCMS/MS approach identified five novel KCNQ1 carboxyl terminal sites that demonstrated basal phosphorylation, with T482 and S484 having enhanced phosphorylation during treatment with 100 nM ISO for 24 hours ( $p \leq 0.01$  at both sites). Using patch clamp electrophysiology, we demonstrated that treatment with 100 nM ISO for 12-24 hours reduced  $I_{Ks}$  current density ( $p=0.01$ ) and produced a depolarizing shift in the voltage dependence of activation ( $p < 0.01$ ) relative to vehicle. Mimics of phosphorylation (mutations to aspartic acid; Triple-D KCNQ1) at S457, T482, and S484 in combination, meanwhile, reduced  $I_{Ks}$  activation current density relative to dephosphorylation (mutations to alanine; Triple-A KCNQ1) mimics ( $p=0.02$ ) but did not affect the voltage dependence of activation ( $p=0.66$ ). Functional assessment of these sites individually revealed that phosphorylation mimics at S457 ( $p=0.02$ ) and S484 ( $p=0.04$ ), but not at T482 ( $p=0.53$ ), reduced  $I_{Ks}$  current density relative to mimics of dephosphorylation. Similarly, the voltage dependence of activation was right-shifted with phosphorylation mimics at S457 ( $p=0.03$ ) and S484 ( $p=0.02$ ), but not at T482 ( $p=0.99$ ), relative to mimics of dephosphorylation.

The focus of Aim 2 was to assess the potential for CaMKII signaling to regulate increased KCNQ1 phosphorylation and reduced  $I_{Ks}$  function during sustained  $\beta$ -AR stimulation. Peptide fragments corresponding to the KCNQ1 carboxyl terminal sites demonstrating basal phosphorylation via LCMS/MS analysis were synthesized on a

nitrocellulose membrane and exposed to activated  $\delta$ CaMKII. Only peptide fragments corresponding to S484 demonstrated CaMKII phosphorylation. Patch clamp experiments demonstrated that CaMKII inhibition via the chemical inhibitor KN-93 ( $p=0.02$ ) and the peptide inhibitor CN21 ( $p<0.01$ ) reversed ISO-treatment associated inhibition of  $I_{Ks}$  activation current density relative to appropriate controls (KN-92 and CN21-Alanine, respectively). Inhibition with KN-93 and CN21 ( $p<0.01$  for both) also reversed ISO-treatment associated right shifts in the voltage dependence of activation relative to appropriate controls. The ability of ISO treatment to activate CaMKII in HEK 293 cells was confirmed via protein immunoblot wherein T287 phosphorylation (CaMKII residue conferring constitutive activity) was increased during ISO treatment ( $p<0.05$ ). Lentiviral overexpression of  $\delta$ CaMKII inhibited  $I_{Ks}$  activation current density with WT  $I_{Ks}$  ( $p=0.01$ ) but not with Triple-A  $I_{Ks}$  ( $p=0.20$ ) relative to lentiviral control. Inhibition of  $I_{Ks}$  activation current density during  $\delta$ CaMKII overexpression was attenuated with S484A  $I_{Ks}$  ( $p=0.04$ ) but not with S457A ( $p=0.99$ ) relative to WT  $I_{Ks}$  during  $\delta$ CaMKII overexpression. The voltage dependence of activation was also right-shifted during  $\delta$ CaMKII overexpression relative to lentiviral control ( $p=0.03$ ). PKA inhibition with the peptide inhibitor PKI did not reverse ISO-treatment associated inhibition of  $I_{Ks}$  activation current density ( $p=0.51$ ), and PKA did not phosphorylate peptide fragments corresponding to any of residues identified via LCMS/MS.

Aim 3 investigated the mechanism through which CaMKII-mediated phosphorylation at KCNQ1 S484 inhibits  $I_{Ks}$  function. To assess whether interaction with KCNE1 affects KCNQ1 phosphorylation, we performed LCMS/MS experiments during expression of KCNQ1 alone and during co-expression with KCNE1.

Phosphorylation at S484 was reduced during co-expression with KCNE1 relative to expression of KCNQ1 alone ( $p < 0.01$ ). In addition, mimics of phosphorylation at S484 (S484D) did not affect activation current density ( $p = 0.96$ ) or the voltage dependence of activation ( $p = 0.51$ ) relative to dephosphorylation mimics (S484A). Based on these results, we hypothesized that S484 phosphorylation affected the interaction between KCNQ1 and KCNE1 subunits; accordingly, we assessed the KCNQ1-KCNE1 interaction using BiFC experiments in HEK 293 cells. In accordance with our hypothesis, Venus fluorescent intensity (corresponding to KCNQ1-KCNE1 interaction) was reduced during ISO treatment relative to vehicle ( $p < 0.05$ ) and with S484D KCNQ1 relative to S484A ( $p < 0.01$ ). The role of CaMKII in mediating this disruption of KCNQ1-KCNE1 interaction was demonstrated BiFC experiments that showed co-treatment with ISO and KN-93 attenuated reduced Venus intensity during co-treatment with ISO and KN-92 ( $p < 0.01$ ). These results were corroborated by BiFC experiments with Long QT Syndrome Phenotype 1 (LQT1) mutations that demonstrated that an LQT1 mutation predicted to disrupt CaMKII phosphorylation at S484 (R481I) attenuated reduced Venus intensity during ISO treatment relative to an LQT1 mutations predicted to not affect CaMKII regulation of S484 (S484T;  $p < 0.01$ ). The ability of S484 phosphorylation to affect KCNQ1 and/or KCNE1 trafficking was assessed via protein immunoblot experiments to detect KCNQ1 and KCNE1 following a biotinylation procedure to isolate plasma membrane-bound proteins. Biotinylation experiments demonstrated that KCNQ1 and KCNE1 plasma membrane expression were reduced by ~15% and ~33%, respectively, with S484D KCNQ1 relative to S484A ( $p < 0.05$  for both).

**Conclusion:** CaMKII phosphorylates KCNQ1 S484 during sustained  $\beta$ -AR stimulation to inhibit  $I_{Ks}$  function. S484 phosphorylation inhibits  $I_{Ks}$  function by disrupting the interaction between KCNQ1 and KCNE1 subunits and by reducing the plasma membrane expression of KCNQ1 and KCNE1. Pathological regulation of KCNQ1 by CaMKII (and subsequent inhibition of  $I_{Ks}$ ) during sustained  $\beta$ -AR stimulation may contribute to increased arrhythmogenesis during physiologic states of chronically increased catecholaminergic tone, such as during HF.

## INTRODUCTION

### **Delayed rectifier potassium currents regulate cardiac action potential duration and arrhythmogenesis**

Delayed rectifier potassium currents, which include distinct slow, rapid, and ultra-rapid components that are encoded by individual genes, contribute repolarizing ionic currents that function during Phase II and Phase III of the cardiac action potential.

During Phase II, delayed rectifiers aid in balancing inward calcium currents to produce the plateau phase of the action potential (AP) that allows for mechanical responses (i.e. cardiac muscle contraction) to electrical stimuli; during Phase III, delayed rectifiers function to repolarize the membrane to terminate the AP.<sup>1</sup> The ultra-rapid delayed rectifier potassium current,  $I_{Kur}$ , is expressed exclusively in the atria, while the rapid ( $I_{Kr}$ ) and slow ( $I_{Ks}$ ) delayed rectifiers are expressed within both atrial and ventricular cardiomyocytes.<sup>2</sup> Based on their prominent roles in terminating the ventricular AP,  $I_{Kr}$  and  $I_{Ks}$  play essential roles in regulating cardiac action potential duration (APD).

Accordingly, functional deficits in these currents may result in APD prolongation and the development of ventricular arrhythmias, including the fatal tachyarrhythmia torsades des pointes (TdP). Loss-of-function mutations within the genes that encode for the pore-forming subunits of  $I_{Kr}$  and  $I_{Ks}$  are among the most common causes of congenital long QT syndrome (LQTS), and are classified as Long QT Syndrome Phenotype II (LQT2; mutations in *KCNH2* [pore-forming subunit of  $I_{Kr}$ ]) and Long QT Phenotype I (LQT1; mutation in *KCNQ1* [pore-forming subunit of  $I_{Ks}$ ]), respectively.<sup>3,4</sup>

### **The slow delayed rectifier potassium current, $I_{Ks}$**

$I_{Ks}$  is a voltage-gated potassium current that is mediated by interaction of the pore-forming subunit (gene product of *KCNQ1*, located on the short arm of chromosome 11) with the auxiliary subunit (gene product of *KCNE1*, located on the long arm of chromosome 21).<sup>5</sup> The human *KCNQ1* subunit is 676 amino acids in length and contains a 120 residue intracellular amino terminus and a 325 residue intracellular carboxyl terminus.<sup>6</sup> These termini are separated by a transmembrane region with six membrane-spanning domains, with the region connecting the fifth and sixth segments serving as the pore and multiple positively charged residues in the fourth segment serving as the voltage sensor.<sup>7</sup> Physiologic  $I_{Ks}$  channels are formed when four *KCNQ1* subunits co-assemble via protein-protein interactions with *KCNE1* auxiliary subunits.<sup>8</sup> The intracellular amino and carboxyl termini contain residues and domains that are important for channel regulation, mainly via post-translational protein modifications (e.g. phosphorylation) by signaling cascades such as protein kinase A (PKA) and protein kinase C (PKC), co-assembly of *KCNQ1* tetramers, and interaction with *KCNE1* and other interacting proteins (e.g. calmodulin [CaM]).<sup>9-12</sup>

### **Functional significance of $I_{Ks}$**

$I_{Ks}$  is abundantly expressed in the human ventricle where it plays an essential role in Phase III cardiac repolarization.<sup>13,14</sup>  $I_{Ks}$  functions as a repolarization reserve, contributing modestly to Phase III repolarization during rest (during which time  $I_{Kr}$  is the predominant repolarizing current) and having the potential to be acutely activated by the sympathetic nervous system in response to increases in cardiac rate; accordingly, functional activation of  $I_{Ks}$  in response to acute neural release of norepinephrine and/or

other neurotransmitters enhances repolarization to stabilize cardiac conduction during rapid heart rates (e.g. exercise).<sup>15,16</sup> Functional activation of  $I_{Ks}$  during rapid heart rates involves multiple mechanisms, including enhancement of  $I_{Ks}$  current amplitude during individual ventricular depolarizations (i.e. heartbeats) but also via accumulation of  $I_{Ks}$  during rapid pacing due to incomplete current deactivation.<sup>17</sup> Functional activation of  $I_{Ks}$  occurs during acute or intermittent  $\beta$ -AR stimulation via a protein kinase A (PKA)-dependent signaling complex (DISCUSSED IN MORE DETAIL IN THE “FUNCTIONAL CHANGES IN  $I_{Ks}$  DURING  $\beta$ -AR STIMULATION” SECTION).<sup>18-20</sup>

Though acute  $\beta$ -AR signaling enhances  $I_{Ks}$  function by a PKA-dependent mechanism, it has been consistently demonstrated that sustained  $\beta$ -AR stimulation functionally inhibits  $I_{Ks}$  function in a pathologic manner.<sup>21,22</sup> Functional inhibition of  $I_{Ks}$  has been demonstrated to prolong APD and increase arrhythmia development in both HF models and in patients carrying LQT1 mutations.<sup>23-26</sup>

### **Biology of the KCNQ1 carboxyl terminus**

Due to its role as an important regulator of the cardiac action potential, loss of function mutations in the *KCNQ1* gene, called LQT1 mutations, comprise the most common form of congenital Long QT syndrome.<sup>27</sup> While there is a paucity of data investigating the functional effects of post-translational protein modifications of the KCNQ1 carboxyl terminus, many investigations have been undertaken to characterize the functional implications of specific identified LQT1 mutations. These investigations have revealed valuable insights regarding the physiologic functions of various KCNQ1 domains, including those in the carboxyl terminus. Based on these findings, domains within the KCNQ1 carboxyl terminus have been demonstrated to play essential roles in

channel gating, subunit trafficking to the plasma membrane, interaction with KCNE1 and CaM, subunit tetramerization, and channel regulation by PKC.<sup>7,9-12</sup>

Aromolaran, et al. assessed the functional impact of LQT1 mutations in KCNQ1 assembly domains (R555H in helix C; G589D and L619M in helix D) and report that these mutations inhibit  $I_{Ks}$  through alterations in biophysical properties and channel trafficking.<sup>6</sup> Dvir, et al. also investigated LQT1 mutations in helix C (S546L, R555C, R555H, K557E, R562E) and helix D (G589D), determining that mutations at these sites functionally inhibit  $I_{Ks}$  through disruption of the KCNQ1-KCNE1 interaction and channel regulation by phosphatidylinositol 4,5-bisphosphate (PIP<sub>2</sub>).<sup>9</sup> Specifically, they found that helix C KCNQ1 mutations reduced co-immunoprecipitation with KCNE1, and thereby reduced  $I_{Ks}$  function, but did not affect plasma membrane trafficking of KCNQ1 or KCNE1.

Studies investigating the functional implications of LQT1 mutations in helices A and B of the KCNQ1 carboxyl terminus have demonstrated that interaction of CaM with KCNQ1 is required for normal  $I_{Ks}$  function. A well characterized LQT1 mutant at R518X lies in the CaM-binding domain within helix B.<sup>28,29</sup> This mutation inhibits  $I_{Ks}$  through alterations in channel gating and disruption of channel tetramerization and assembly.<sup>10</sup> Shamgar et al. have shown that helix A mutations (R366W, A371T, S373P, and W392R) also disrupt CaM binding and reduce  $I_{Ks}$  function by altering channel assembly, stabilizing inactivation, and decreasing current density.<sup>30</sup>

Given the propensity for LQT1 mutants in the KCNQ1 carboxyl terminus to produce functionally significant effects on  $I_{Ks}$  across a variety of biophysical parameters,

post-translational protein modifications, such as phosphorylation, may functionally impact  $I_{Ks}$ .

### **Functional changes in $I_{Ks}$ during $\beta$ -AR stimulation**

Though it had long been demonstrated that acute  $\beta$ -AR stimulation functionally enhances  $I_{Ks}$  to shorten repolarization during rapid heart rates, discovery of the macromolecular signaling complex responsible for acute  $I_{Ks}$  enhancement was a key finding in allowing investigation of the mechanistic basis for  $I_{Ks}$  channel regulation. The work by Marx, et al. utilized co-immunoprecipitation to identify the alpha-kinase anchoring protein Yotiao (AKAP9), protein phosphatase 1 (PP1), and PKA as a required signaling complex that targeted S27 on the KCNQ1 amino terminus to mediate enhanced  $I_{Ks}$  function during acute  $\beta$ -AR stimulation.<sup>19</sup> Subsequent investigations further confirmed the necessary nature of this signaling complex. This was evidenced by the fact that LQT1 mutations that disrupt interaction with Yotiao reduce acute  $I_{Ks}$  adrenergic-responsiveness and that loss-of-function mutations in Yotiao produce long QT; in addition, these investigations demonstrate that a portion of the KCNE1 carboxyl terminus is required for formation of the functional  $I_{Ks}$  complex.<sup>31,32</sup> Later, more detailed molecular mechanisms by which  $I_{Ks}$  is functionally enhanced have been explored, demonstrating that a large amount of KCNQ1 subunits exist in subcellular compartments away from the plasma membrane under basal conditions and that, during periods of stress, this reserve of KCNQ1 subunits is rapidly trafficked to the plasma membrane to enhance  $I_{Ks}$  functionality.<sup>33</sup> These findings are supported by additional work that demonstrates RAB-4 GTPase-dependent translocation of KCNQ1 to the plasma membrane during acute  $\beta$ -AR stimulation, enabling protection from beat-to-beat

variability during adrenergic stimulation that was absent in a *KCNQ1* knock-out model.

34

In contrast to its regulation during acute  $\beta$ -AR stimulation, there is considerably less known regarding the regulation of  $I_{Ks}$  during sustained  $\beta$ -AR stimulation. While the bulk of available evidence demonstrates reduced expression and/or function of *KCNQ1* and/or *KCNE1* in human HF tissue and animal HF models, few investigations assess the mechanistic basis for reduced  $I_{Ks}$  function during sustained  $\beta$ -AR stimulation. A study by Aflaki, et al. investigates the functional regulation of  $I_{Ks}$  during *in vivo* and *ex vivo* sustained treatment with isoproterenol (ISO), a non-specific  $\beta_1$  and  $\beta_2$ -AR agonist, in a guinea pig model.<sup>21</sup> The work demonstrates reduced  $I_{Ks}$  function during sustained  $\beta$ -AR stimulation and utilizes specific inhibitors to implicate Epac signaling in mediating  $I_{Ks}$  inhibition via a calcineurin-NFAT signaling pathway that negatively regulates *KCNE1* mRNA and protein expression. The work by Aflaki, et al. also demonstrates that, contrary to its activating role during acute adrenergic stimulation, PKA does not regulate  $I_{Ks}$  during sustained  $\beta$ -AR stimulation. Finally, the investigation found that inhibition of calcium/calmodulin-dependent protein kinase II (CaMKII), a known regulator of aberrant calcium handling and ion channel function in HF, with the chemical CaMKII inhibitor, KN-93, reversed deficits in  $I_{Ks}$  function during sustained  $\beta$ -AR stimulation.

### **Neurohormonal remodeling in heart failure**

Heart failure (HF) refers to a clinically heterogeneous group of pathologic conditions that result in reduced cardiac function and a subsequent reduction in the systemic circulation of oxygenated blood.<sup>35</sup> HF affects nearly 6 million people in the

United States and constitutes a leading cause of morbidity, mortality, hospitalization, and healthcare expenditure.<sup>36,37</sup> Though HF mortality occurs through a variety of mechanisms, arrhythmogenic sudden cardiac death (SCD) accounts for up to 40% of mortality in patients with severe HF.<sup>38</sup> HF is a risk factor for ventricular arrhythmias, such as ventricular tachycardia (VT; including TdP) and ventricular fibrillation (VF), and HF thereby imparts up to a nine-fold increase in the risk for SCD.<sup>38</sup> Animal models of HF as well as cardiomyocytes isolated from failing hearts consistently demonstrate prolongation of cardiac action potential duration (APD), which is a risk factor for the development of ventricular arrhythmias, including TdP.<sup>39</sup>

HF is associated with pathological structural (i.e. changes in the expression of contractile and extracellular matrix proteins) and electrical (i.e. changes in the expression and activation of calcium handling proteins, gap junctions, and ion channels) cardiac remodeling processes that predispose to the development of arrhythmias.<sup>40</sup> These remodeling processes largely result from HF-associated changes in neurohormonal signaling, with the most pharmacologically relevant being elevated circulating concentrations of catecholamines and angiotensin II. Alterations in neurohormonal signaling during HF are known to be involved in the pathophysiology of the disease, with therapeutic strategies targeting increased catecholaminergic (beta-adrenergic receptor [ $\beta$ -AR] blockers) and angiotensin II (angiotensin-converting enzyme [ACE] inhibitors or angiotensin II-receptor blockers [ARBs]) signaling having demonstrated increased survival in HF patients.<sup>41,42</sup> While the mechanistic basis for the pathophysiologic role of alterations in neurohormonal signaling during HF is not fully understood, various investigations have demonstrated that sustained increases in circulating catecholamines

and angiotensin II functionally inhibit a variety of species of ion channels that are important regulators of the cardiac action potential.<sup>43</sup> In particular, the potential for catecholaminergic signaling to inhibit L-type calcium and various species of potassium currents, including  $I_{Ks}$  (DISCUSSED IN MORE DETAIL IN THE “EFFECTS OF HF-ASSOCIATED CHANGES IN NEUROHORMONAL SIGNALING ON THE FUNCTION OF DELAYED RECTIFIER POTASSIUM CURRENTS” SECTION), have been consistently established.<sup>43,44</sup>

### **Changes in neurohormonal signaling during HF inhibit delayed rectifier potassium current function**

Given the essential role of delayed rectifier potassium currents in regulating APD, investigations have been undertaken to assess the potential for HF-associated changes in neurohormonal signaling to mediate functional inhibition of these currents. Though conflicting data exist, these investigations have largely found functional deficits in all species of delayed rectifier potassium currents in limited human studies and in animal and cellular HF models. Furthermore, isolated ventricular cardiomyocytes from HF patients demonstrate reduced  $I_{Ks}$  function relative to healthy patients.<sup>45</sup>

Specifically, increased angiotensin II signaling has been demonstrated to functionally inhibit both the rapid ( $I_{Kr}$ ) and slow ( $I_{Ks}$ ) delayed rectifier potassium currents.<sup>46-48</sup> Angiotensin II-dependent inhibition of  $I_{Ks}$  is mediated through signaling of the epsilon isoform of protein kinase C (PKC- $\epsilon$ ) and involves phosphorylation of two amino terminal sites on KCNQ1 (S95 and T96) as well as a distal site on KCNE1 (S102).<sup>47</sup>

Sustained catecholaminergic stimulation, mediated primarily via signaling through cardiac  $\beta_1$ -adrenergic receptors, has been shown to functionally regulate multiple

species of delayed rectifier potassium currents.<sup>49</sup>  $\beta_1$ -adrenergic receptors ( $\beta_1$ -ARs) are abundantly expressed in both cardiac nodal tissue and cardiomyocytes and comprise the primary cardiac target for catecholaminergic signaling, transducing cellular signals to increase the rate and force of cardiac contraction.  $\beta$ -ARs are G-protein coupled receptor (GPCR) that couple to stimulatory  $G_s$  alpha subunits. When the  $\beta$ -AR is stimulated by binding of a ligand, like various species of catecholamines or isoproterenol (ISO), the  $G_s$  subunit activates adenylyl cyclase which catalyzes formation of the second messenger cAMP from ATP. Increased cAMP concentrations trigger a number of downstream signaling cascades in cardiomyocytes, including activation of protein kinase A (PKA; also known as cAMP-dependent protein kinase) that has been established to regulate both  $I_{Kr}$  and  $I_{Ks}$  (DISCUSSED IN MORE DETAIL IN THE “FUNCTIONAL CHANGES IN  $I_{Ks}$  DURING  $\beta$ -AR STIMULATION” SECTION).<sup>19,50</sup>

In addition, increases in cAMP signaling through the  $\beta$ -AR also activate the exchange protein activated by cAMP (Epac), a guanine nucleotide exchange factor that regulates excitation-contraction coupling in cardiomyocytes and has been demonstrated to be associated with cardiac hypertrophy.<sup>51</sup> In fact, expression of Epac is increased during heart failure where it has been shown to modulate key regulators of cardiac contraction, including the ryanodine receptor (RyR) and CaMKII.<sup>52</sup> Epac signaling has also been demonstrated to mediate functional inhibition of  $I_{Ks}$  during sustained  $\beta$ -AR stimulation within animal and cellular HF models (DISCUSSED IN MORE DETAIL IN THE “FUNCTIONAL CHANGES IN  $I_{Ks}$  DURING  $\beta$ -AR STIMULATION” SECTION).<sup>21</sup>

### **CaMKII as a pathological regulator during HF**

CaMKII is a multi-functional serine/threonine kinase that is ubiquitously expressed throughout the body.<sup>53</sup> CaMKII is able to regulate a wide range of substrates, and the kinase has many documented regulatory targets both in normal physiology and in pathophysiologic disease processes.<sup>54</sup> The  $\delta$  and  $\gamma$  isoforms of CaMKII are expressed in cardiac tissue, with the  $\delta$  isoform having the highest expression in ventricular cardiomyocytes and being the isoform implicated in pathologic cardiac remodeling during sustained  $\beta$ -AR stimulation and HF.<sup>55</sup> Classical activation of CaMKII requires the presence of calcium-bound CaM that causes a conformational change in the enzyme complex that reveals the catalytic domain. Alternatively, CaMKII can also demonstrate hyperactive and calcium-bound CaM-independent enzymatic activity either via autophosphorylation at threonine (T) 287 (on  $\delta$ CaMKII) or through oxidation at methionine (M) 281 or 282, nitrosylation at cysteine (C) 273, or glycosylation at S279.<sup>56-59</sup> These modes of constitutive enzymatic activity have been shown to be increased in HF where they contribute to pathologic regulation of ion channels, cardiac hypertrophy, and a predisposition to the development of arrhythmias.<sup>60</sup>

$\delta$ CaMKII demonstrates increased functional activation and/or expression in response to a number of HF-related stimuli, including sustained  $\beta$ -AR stimulation, increased renin-angiotensin-aldosterone system (RASS) signaling, increased intracellular calcium handling, and the accumulation of reactive oxygen species (ROS).<sup>61</sup> Ligands for the  $\alpha_1$ -adrenergic receptor as well as endothelin have also been demonstrated to increase CaMKII activity.<sup>62,63</sup> Sustained treatment with ISO has been demonstrated to increase both CaMKII activity and T287 autophosphorylation in cardiomyocytes through an Epac-dependent pathway.<sup>64-66</sup> Constitutive CaMKII activation causes pathologic regulation of

many cellular targets that are essential for action potential regulation and cardiac contraction, including various species of ion channels (DISCUSSED IN MORE DETAIL IN THE “CAMKII REGULATION OF CARDIAC ION CHANNELS AND APD” SECTION) and calcium handling proteins like the ryanodine receptor (RyR), phospholamban (PLN), and potentially the sarcoplasmic reticulum calcium-ATPase (SERCA2; DISCUSSED IN MORE DETAIL IN THE “ $\beta$ -AR STIMULATION ACTIVATES CAMKII THROUGH AN EPAC-DEPENDENT PATHWAY” SECTION).<sup>53</sup> In fact, overexpression of  $\delta$ CaMKII has been independently shown to induce dilated cardiomyopathy and reduced cardiac contractility within in a transgenic mouse model, while genetic deletion of  $\delta$ CaMKII prevents the onset of HF even after physical HF-induction procedures.<sup>55,67,68</sup>

Through pathologic regulation of ion channels and calcium handling proteins, CaMKII activation has been linked to the development of arrhythmias in a variety of cardiac diseases, including HF where it is associated with VT and VF.<sup>61</sup> Transgenic overexpression of CaMKII and calcineurin have been demonstrated to increase arrhythmogenesis in mouse models, and CaMKII inhibition prevented ISO-induced arrhythmias in a dilated cardiomyopathy mouse model.<sup>68-70</sup> Increased activation and expression of CaMKII have also been demonstrated to prolong APD in a mouse HF model, while inhibition of CaMKII has been shown to reduce APD by preventing CaMKII-mediated regulation of the potassium channels  $I_{to}$  and  $I_{K1}$ .<sup>71-73</sup> Given CaMKII's established role as a pathologic regulator in HF that predisposes to arrhythmia development, the potential for CaMKII-mediated regulation of  $I_{Ks}$  may contribute to the increased incidence of arrhythmia development in HF.

### **$\beta$ -AR stimulation activates CaMKII through an Epac-dependent pathway**

Since aberrant calcium handling is known to be involved in the pathogenesis of HF, it was initially believed that increases in intracellular calcium signaling were the primary mechanism of enhanced CaMKII signaling during HF.<sup>74</sup> While this classical, calcium-dependent mechanism of CaMKII activation likely plays an important role during HF, a number of investigations have characterized calcium-independent mechanisms of CaMKII activation in cardiomyocytes that are mediated through Epac signaling.<sup>65,75-78</sup> These investigations have found that, in response to sustained  $\beta$ -AR stimulation, enhanced Epac activity functionally enhances the action of phospholipase C epsilon (PLC- $\epsilon$ ) that, through Rap-GEF signaling, mediates functional enhancement of PKC- $\epsilon$  via enhanced membrane translocation.<sup>76</sup> Finally, CaMKII is activated through a PKC- $\epsilon$ -dependent pathway to regulate calcium-induced calcium release (CICR) and excitation-contraction coupling in cardiomyocytes through known CaMKII regulatory sites on RyR (S2815) and PLN (T17).<sup>76,79</sup>

### **CaMKII regulation of cardiac ion channels and APD**

While CaMKII activity is essential in regulating intracellular calcium handling in basal conditions and in response to acute  $\beta$ -AR stimulation, sustained  $\beta$ -AR stimulation and HF have been associated with pathological constitutive activation of CaMKII.<sup>80</sup> During constitutive activation, CaMKII is known to aberrantly regulate a wide array of ion channels and calcium handling proteins to promote APD prolongation and the development of arrhythmias.<sup>81</sup> As previously mentioned, CaMKII has been demonstrated to manipulate intracellular calcium handling through regulation of the RyR and PLN.<sup>53</sup> In addition, CaMKII also influences intracellular calcium handling through direct

regulation of L-type calcium channels, where CaMKII-dependent phosphorylation has been demonstrated to mediate calcium-dependent facilitation (CDF), a process by which L-type calcium current density increases over several heart beats due to slower channel inactivation.<sup>82,83</sup> While CDF plays important roles in normal physiological processes (e.g. during exercise), enhanced CDF, as may occur during HF when CaMKII is functionally activated, has been demonstrated to have arrhythmogenic consequences.<sup>84</sup> CaMKII has also been demonstrated to regulate T-type calcium channels, wherein CaMKII phosphorylation functionally enhances current by increasing the open channel probability.<sup>85</sup> While T-type calcium channels are minimally expressed in the ventricle of healthy individuals, investigations have shown that cardiac hypertrophy and changes in neurohormonal signaling during HF, such as enhanced endothelin-1 and angiotensin II signaling, cause increased ventricular expression of T-type calcium channels.<sup>86,87</sup> Therefore, functional enhancement of T-type calcium channels by CaMKII may have arrhythmogenic consequences in HF.<sup>81</sup>

In addition to its regulation of calcium channels, CaMKII has been demonstrated to regulate various types of sodium and potassium channels through phosphorylation of their pore-forming or auxiliary subunits. Multiple investigations have demonstrated a role for CaMKII in functionally regulating the cardiac voltage-gated sodium channel Nav1.5 via direct phosphorylation at T594 and/or S516; CaMKII regulation of Nav1.5 results in functional enhancement of sodium current that has been shown to result in APD prolongation and arrhythmia development in transgenic rabbit models.<sup>88-90</sup> CaMKII also regulates inactivation of the transient outward potassium current,  $I_{to}$ , an important regulator of Phase I of the cardiac action potential that has significant effects on APD.<sup>91</sup>

The precise mechanism of CaMKII regulation of  $I_{to}$  remains controversial, with some investigations demonstrating direct phosphorylation of S550 on Kv4.3 (pore-forming subunit of  $I_{to}$ ) that prolongs open-state inactivation; other studies have shown CaMKII-mediated downregulation of Kv4.3 in canine cardiomyocytes in response to pacing-induced HF.<sup>92,93</sup> Regardless of mechanism, CaMKII regulation of  $I_{to}$  results in APD prolongation in transgenic mouse models that are predicted to have pro-arrhythmogenic consequences.<sup>71</sup> CaMKII overexpression and HF have also been independently demonstrated to reduce expression and function of the inwardly rectifying potassium current,  $I_{K1}$ , which is an important regulator of cardiomyocyte resting membrane potential and action potential termination.<sup>94-97</sup> Therefore, via aberrant regulation of the aforementioned ion channels, increased CaMKII activity, as occurs in HF, has been consistently demonstrated to mediate APD prolongation and arrhythmogenesis.<sup>81</sup>

### **Mechanisms of $I_{Ks}$ inhibition during sustained $\beta$ -AR stimulation and HF**

Although functional inhibition of  $I_{Ks}$  and APD prolongation during sustained  $\beta$ -AR stimulation and HF have been observed clinically and in cellular and animal HF models, the mechanism of inhibition remains elusive. Isolated right ventricular cardiomyocytes from patients with HF demonstrate reduced  $I_{Ks}$  current density and subsequent APD prolongation relative to healthy patients.<sup>45</sup> Findings of reduced  $I_{Ks}$  function have been corroborated in various animal and cellular HF models: HF induced by tachycardiac pacing reduced  $I_{Ks}$  current density by ~30% in canine atrial cardiomyocytes<sup>22</sup>; HF induced by tachycardiac pacing triggered early afterdepolarizations (EADs), a mechanism for TdP development, and inhibited  $I_{Ks}$  current density by 57%, 49%, and 58% in epicardial, midmyocardial, and endocardial cardiomyocytes

(respectively) isolated from canine left ventricles<sup>98</sup>; HF induced by chronic atrioventricular (AV) nodal blockade reduced KCNQ1 and KCNE1 mRNA (KCNQ1 reduced by 80%, KCNE1 reduced by 70%) and protein expression (KCNQ1 reduced by 50%, KCNE1 reduced by 60%) in cardiomyocytes isolated from canine ventricles<sup>99</sup>; HF induced by tachycardiac pacing prolonged APD and functionally inhibited composite  $I_K$  current (primarily a composite of  $I_{Kr}$  and  $I_{Ks}$ ) but did not affect mRNA expression of KCNQ1 and KCNE1 (or Erg which encodes for the pore-forming subunit of rabbit  $I_{Kr}$ ) in cardiomyocytes isolated from rabbit ventricles<sup>100</sup>; HF induced from tachycardiac pacing prolonged action potential duration at the return to 90% of resting membrane potential ( $APD_{90}$ ) and reduced  $I_{Ks}$  maximum tail current density by ~50% in cardiomyocytes isolated from rabbit ventricles<sup>101</sup>; HF induced by chronic AV block and bradycardiac or tachycardiac pacing reduced KCNQ1 and KCNE1 mRNA (~60% reduction in KCNQ1, 50% reduction in KCNE1) and protein (~50% reduction in KCNQ1, ~30% reduction in KCNE1) and inhibited  $I_{Ks}$  maximum tail currents by ~60% in cardiomyocytes isolated from rabbit ventricles<sup>102</sup>; HF induced by chronic ISO treatment reduced  $I_{Ks}$  maximum tail current density by 58% and decreased KCNE1 mRNA and protein expression by 45% and 51%, respectively (no change in KCNQ1 expression), in cardiomyocytes isolated from guinea pig ventricles.<sup>21</sup>

However, reductions in mRNA and protein expression of KCNQ1 and/or KCNE1 in HF patients and in animal HF models have not been consistently reproduced, suggesting that another mechanism may mediate reduced  $I_{Ks}$  function in HF.<sup>100,102-105</sup> Apart from changes in expression of KCNQ1 and/or KCNE1, a number of other molecular mechanisms could potentially mediate inhibition of  $I_{Ks}$  function during

sustained  $\beta$ -AR stimulation. Aberrant regulation by kinases known to be functionally activated during sustained  $\beta$ -AR stimulation and HF (e.g. CaMKII, PKC- $\epsilon$ ) could alter KCNQ1 phosphorylation and thereby regulate  $I_{Ks}$  via alteration of: (1) the biophysical properties of the channel (e.g. open channel probability, the rate and/or voltage dependence of activation or inactivation); (2) plasma membrane trafficking of KCNQ1 and/or KCNE1; (3) tetramerization of KCNQ1 subunits; (4) interaction of KCNQ1 with required auxiliary subunits, such as KCNE1 and CaM. Regardless of mechanism, the arrhythmogenic potential of functional reductions in  $I_{Ks}$  has been corroborated in animal experiments that have shown torsades des pointes development with pharmacological inhibition of  $I_{Ks}$  and in animal HF models (canine and leporine) wherein  $I_{Ks}$  is functionally inhibited.<sup>23,25,98,101,106</sup>

### **Study Rationale**

While detailed mechanistic data regarding the potential for CaMKII to regulate  $I_{Ks}$  are lacking, it has previously been shown that CaMKII inhibition with the chemical inhibitor KN-93 attenuates inhibition of  $I_{Ks}$  during sustained ISO treatment in guinea pig cardiomyocytes, suggesting that functional inhibition of  $I_{Ks}$  during sustained  $\beta$ -AR stimulation may be mediated through CaMKII signaling.<sup>21</sup> In addition, the KCNQ1 carboxyl terminus contains CaM-binding domains in helices A and B, and it has been previously demonstrated that CaM is a required beta subunit for normal  $I_{Ks}$  function.<sup>10,107</sup> Finally, the KCNQ1 carboxyl terminus contains a number of putative CaMKII phosphorylation sites.

Multiple investigations have also established CaMKII as a downstream regulator of Epac signaling.<sup>65,75,76,78</sup> Since Epac has been demonstrated to mediate pro-

arrhythmogenic cardiac remodeling during HF, including via regulation of  $I_{Ks}$ , CaMKII may be a key pathological downstream regulator following Epac activation.<sup>52</sup> Given these pieces of evidence and CaMKII's role as an established pro-arrhythmogenic regulator during HF, the potential for CaMKII to mediate functional inhibition of  $I_{Ks}$  during sustained  $\beta$ -AR stimulation warrants investigation.

### **Study Aims & Objectives**

The overarching objective of this work is to assess the functional regulation of  $I_{Ks}$  during sustained  $\beta$ -AR stimulation, including an assessment of the potential for regulation of KCNQ1 by CaMKII. Discovery of the molecular mechanism that mediates  $I_{Ks}$  inhibition in response to sustained  $\beta$ -AR stimulation may elucidate a therapeutic target to prevent the development of ventricular arrhythmias in HF. Towards this objective, the following specific aims were pursued:

**Specific Aim 1:** Investigate the regulation of the KCNQ1 carboxyl terminus during sustained  $\beta$ -AR stimulation and the associated changes in  $I_{Ks}$  function. This objective utilizes an LCMS/MS phosphoproteomics approach, peptide arrays, and cellular electrophysiology.

**Specific Aim 2:** Assess the potential for CaMKII signaling to mediate regulation of  $I_{Ks}$  in response to sustained  $\beta$ -AR stimulation and the associated CaMKII-mediated functional changes in  $I_{Ks}$ . This objective employs peptide arrays, Western blots to assess CaMKII activity, and cellular electrophysiology experiments.

**Specific Aim 3:** Evaluate the molecular mechanism(s) for how CaMKII regulation of KCNQ1 disrupts  $I_{Ks}$  function. This objective utilizes an LCMS/MS phosphoproteomics approach, cellular electrophysiology experiments, bimolecular

fluorescence complementation live-cell imaging, and Western blots following surface biotinylation to isolate membrane-bound proteins.

## METHODS

### DNA Constructs and Reagents

Complementary DNA (cDNA) encoding for human *KCNQ1* and *KCNE1* expressed within pCDNA3.1 (constructs generously provided by the laboratory of Dr. Robert Kass) were co-transfected into human embryonic kidney cells (HEK 293 cells; a durable cell line for heterologous expression and electrophysiological investigation of ion channels) for eukaryotic expression of  $I_{Ks}$ . Point mutations to alanine (A) and aspartic acid (D) were performed at S457, T482, and S484 on *KCNQ1* alone and in combination via site-directed mutagenesis (performed commercially by GenScript®) and were verified via sequencing. Enhanced green fluorescent protein (GFP) that was expressed in pCEP4 was co-transfected with *KCNQ1* and *KCNE1* plasmids and was used to identify cells transiently expressing *KCNQ1* and *KCNE1* via microscopic analysis. For experiments that employed lentiviral overexpression of CaMKII, activated  $\delta$ CaMKII (wherein T287 was mutated to an aspartic acid [T287D] to confer constitutive kinase activity) was inserted into a lentiviral packaging plasmid that contained a fused yellow fluorescent protein (YFP) tag on the amino terminus. This packaging plasmid was transfected along with additional viral gene plasmids (pRRE, pRSV-Rev, pCMV-VSV-G) in HEK 293T cells to generate  $\delta$ CaMKII-containing lentivirus that was collected and filtered before it was added to the media of HEK 293 cells in order to stably express T287D  $\delta$ CaMKII. The red fluorescent protein tdTomato expressed in pSCSMV was co-transfected along with *KCNQ1* and *KCNE1* plasmids and was used to identify cells transiently expressing *KCNQ1* and *KCNE1* in YFP-expressing cells. Isoproterenol (Cat. #: I5627) was purchased from Sigma-Aldrich®. KN-92 (Cat. #: sc-311369) and KN-93 (Cat. #: sc-

202199) were purchased from Santa Cruz Biotech<sup>®</sup>. Myristoylated protein kinase A inhibitor (Myr-PKI; Cat.#: 476485) was purchased from EMD Millipore<sup>®</sup>. The CaMKII peptide inhibitor CN21 and the inactive analog, CN21-Alanine, were purchased from Biopeptide Co. Inc.<sup>®</sup> along with tat-conjugated versions of each. The catalytic subunit of protein kinase A (Cat. #: P2645) was purchased from Sigma Aldrich<sup>®</sup>.

### **Cell Culture and cDNA Transfection**

HEK 293 cells were purchased from American Type and Culture Collection (ATCC<sup>®</sup>) and maintained in Modified Essential Medium (MEM) with 10% fetal bovine serum (FBS) and 1% Pen-Strep (5,000 Units/mL Penicillin; 5,000 µg/mL Streptomycin) at 37°C and 5% CO<sub>2</sub> (complete media). For electrophysiology experiments, HEK 293 cells were subcultured into 35 mm tissue-culture treated culture dishes (Corning<sup>®</sup>) at ~30-40% confluence. At 24 hours following subculture, cDNA transfections were performed (3-8 transfections per experimental group) via the following protocol: cDNAs containing wild-type or mutated KCNQ1, wild-type KCNE1, and GFP or tdTomato were co-transfected into HEK 293 cells using Lipofectamine 2000 (ThermoFisher<sup>®</sup>) in MEM (without the additives mentioned above) per the manufacturer's instructions at the following mass ratio: 750 ng KCNE1, 500 ng KCNQ1, 100 ng GFP. After 4 hours, transfection media was aspirated and cells were maintained in complete media. Electrophysiology experiments were performed ~48 hours after transfection on cells expressing GFP, YFP, or tdTomato as seen by fluorescent microscopy for all experimental groups.

To achieve β-AR stimulation, isoproterenol (ISO; β<sub>1</sub>, β<sub>2</sub> adrenergic receptor agonist; Sigma-Aldrich<sup>®</sup>) was dissolved in water and added directly to complete media at

a concentration of 100 nM.  $I_{Ks}$  responsiveness to stimulation of endogenous  $\beta$ -ARs has been previously demonstrated in HEK cells.<sup>108</sup> For LCMS/MS experiments, separate plates were incubated with ISO for 3 minutes, 4 hours, 12 hours, and 24 hours before cultures were lysed and prepared for LCMS/MS experiments. For electrophysiology experiments, cells were treated with ISO for 12-24 hours before experiments were performed. As cells were pre-treated with ISO as described previously, ISO was not included in the internal (pipette) or external (bath) patch solutions during recording. In experiments assessing the impact of CaMKII or PKA inhibition, 500 nM KN-93 or KN-92, 10  $\mu$ M tat-CN21 or tat-CN21-Alanine, or 1  $\mu$ M Myr-PKI were added to complete media 4-6 hours before whole-cell, voltage-clamp experiments were performed. In experiments utilizing peptide inhibition of CaMKII and PKA, 1  $\mu$ M CN21 or CN21-Alanine and Myr-PKI, respectively, were also added to the internal patch solution.

### **cDNA Amplification and Purification**

The cDNAs used in this investigation were amplified via bacterial transformation into NEB5-alpha competent *E. coli* (Cat. #: C2988J; New England BioLabs®) using a heat shocking transformation technique, as follows. ~1  $\mu$ L of cDNAs were aseptically added to 150  $\mu$ L of thawed *E. coli* competent cell solution in plastic culture tubes and incubated on ice for 20 minutes. Following this incubation, the mix was heat shocked at 42 °C (via water bath) for 60 seconds before being returned to ice for 2-3 minutes. 500  $\mu$ L of sterile Luria-Bertani (LB; Cat. #: L3152; Sigma Aldrich®) broth (sterilized by autoclaving) was aseptically added to the mixture. The mixture was then incubated while shaking for 40 minutes at 37 °C. Following this incubation, 100  $\mu$ L of the mixture was pipetted into culture dishes containing LB agar (Cat. #: L3027; Sigma Aldrich®) to which

selective antibiotic (kanamycin for pCEP4 plasmid, ampicillin for all others) had been added at a concentration of 50 µg/mL. The transformation mix was spread around the plate using a plastic spreader and the plates were incubated overnight in a 37 °C incubator.

On the next day, 2-3 colonies were selected via pipette tip and placed into culture tubes containing 5 mL pre-warmed antibiotic-containing (50 µg/mL) LB broth and were shaken in a 37 °C incubator overnight. On the following day, the bacterial culture was purified by centrifugation at 8,000 rpm for 10 min on a bench top centrifuge. Following centrifugation, the supernatant was discarded and replaced by fresh pre-warmed LB broth with antibiotic. The same centrifugation process was repeated an additional time before cells were re-suspended in 1 mL of pre-warmed LB broth with antibiotic. 500 µL of the bacterial culture were then added to were Erlenmeyer flasks containing 50 mL of pre-warmed LB broth with antibiotic (50 µg/mL) and the flasks were shaken in an incubator at 37 °C for 8 hours. Finally, 1 mL of the bacterial culture was transferred to Erlenmeyer flasks containing 1 L of pre-warmed LB broth with antibiotic (50 µg/mL) and were agitated in an incubator at 37°C overnight.

Plasmid cDNAs were isolated and purified from bacterial cultures using the NucleoBond® Xtra Maxi Plasmid Purification Kit (Cat. #: 740410.10; Macherey-Nagel®) or HiSpeed® Plasmid Maxi Kit (Cat. #: 12662; Qiagen®) per the manufacturer's protocol. Purified cDNA concentration was determined by a Qubit® 2.0 bench-top fluorometer using the Qubit® dsDNA BR Assay Kit (Cat. #: Q32850). Purified cDNAs were aliquoted and stored at 4°C (short-term) or -20 °C (long-term).

## Mass Spectrometry

Enriched membrane preparations (100  $\mu\text{g}$ ) were reconstituted in 200  $\mu\text{L}$  of 4 M urea and reduced and alkylated using 200  $\mu\text{L}$  of a TEP/iodoethanol cocktail as previously described.<sup>109,110</sup> Samples were then incubated at 37°C for 120 min, dried by SpeedVac, and reconstituted with 100  $\mu\text{L}$  of 100 mM  $\text{NH}_4\text{HCO}_3$  at pH 8.0. 150  $\mu\text{L}$  aliquots of 20  $\mu\text{g}/\text{mL}$  trypsin solution were then added to samples and incubated at 37°C for 3 hours. Following three hour incubation, another 150  $\mu\text{L}$  of trypsin solution was added and samples were incubated at 37°C overnight in order to complete digestion.

Following digestion, a linear ion-trap (LTQ) mass spectrometer coupled with a Surveyor autosampler and MS HPLC system (ThermoFinnigan®) was used to analyze samples. Tryptic peptides were injected onto the C18 microbore RP column (Zorbax SBC18, 1.0 mm x 150 mm) using a flow rate of 50  $\mu\text{L}/\text{min}$ . Mobile phases A, B, and C consisted of the following: 0.1% formic acid in water, 50% acetonitrile with 0.1% formic acid in water, and 80% acetonitrile with 0.1% formic acid in water, respectively. Samples were exposed to a gradient elution process as follows: 10% B (90% A) for 5 min, 10–95% B (90–5% A) for 120 min, 100% C for 5 min, and 10% B (90% A) for 12 min. Data were collected in the “Triple-Play” (MS scan, Zoom scan, and MS/MS scan) mode using a normalized collision energy of 35% within the ESI interface. The dynamic exclusion settings were set to the following: repeat count equal to 1, repeat duration equal to 30 seconds, exclusion duration equal to 120 seconds, and exclusion mass width equal to 0.75 m/z (low) and 2.0 m/z (high).

Acquired data were queried against the current UniProtKB human database using the SEQUEST (v.28 rev.12) algorithms within Bioworks software (v.3.3). For this process, the general parameters were as follows: peptide tolerance equal to 2.0 amu,

fragment ion tolerance set to 1.0 amu, enzyme limits set as “fully enzymatic - cleaves at both ends”, and missed cleavage sites set to 2, static modification set at + 44 @C, and potential modifications set at +80 @STY. Peptides and proteins returned via this search were validated using PeptideProphet and ProteinProphet in the TransProteomic Pipeline (<http://tools.proteomecenter.org/wiki/index.php?title=Software:TPP>).<sup>111,112</sup> Only proteins and peptides with protein probability  $\geq 0.9000$  and peptide probability  $\geq 0.8000$  were reported. Protein quantification was performed using a label-free quantification software package, IdentiQuantXL<sup>TM</sup>.<sup>113</sup>

### **Stable Lentiviral Expression**

YFP-tagged constitutively active human  $\delta$ CaMKII (T287D) was stably overexpressed in HEK 293 cells by means of lentiviral transduction. The packaging plasmid with  $\delta$ CaMKII (20  $\mu$ g) was co-transfected into HEK 293T cells along with additional viral gene plasmids [pRRE (10  $\mu$ g), pRSV-Rev (5  $\mu$ g), pCMV-VSV-G (6  $\mu$ g)] using polyethylenimine (50  $\mu$ g) in Opti-MEM (ThermoFisher<sup>®</sup>) and the media was refreshed on the day following transfection with complete media (MEM + 10% FBS + 5% penicillin-streptomycin + 1% NEAA + 1% sodium pyruvate). At 36 hours following transfection, the virus-containing media was aspirated from the transfected cells and filtered with a 0.45  $\mu$ m syringe filter (ThermoFisher<sup>®</sup>). Filtered media was added to low passage HEK 293 cells along with polybrene (Sigma-Aldrich<sup>®</sup>; 8  $\mu$ g: 1 mL viral media) for 6 hours, after which time the viral media was aspirated and the cells were maintained in complete media. Effective CaMKII transduction was confirmed by YFP expression at 2 days following HEK 293 cell infection and YFP expression was visualized via fluorescent microscopy in all cells used in whole-cell patch clamp experiments.

## Cellular Electrophysiology

Functional measurements of  $I_{Ks}$  were assessed using the whole-cell, patch-clamp configuration in the voltage-clamp mode at room temperature ( $\sim 22^\circ\text{C}$ ). Activation currents were measured during an activating voltage step protocol with 10 mV steps from -60 mV to +60 mV for 4 secs from a holding potential of -80 mV using an EPC-9 amplifier and PatchMaster software (HEKA Elektronik<sup>®</sup>). The voltage dependence of activation was assessed through analysis of elicited tail currents when the voltage was returned to -40 mV after the activating steps described previously. A diagram depicting how current (I) vs. voltage (V), also called I-V plots, and fractional activation vs. voltage plots, referred to as activation curves, were constructed from elicited current traces is shown in **Figure 1** below.

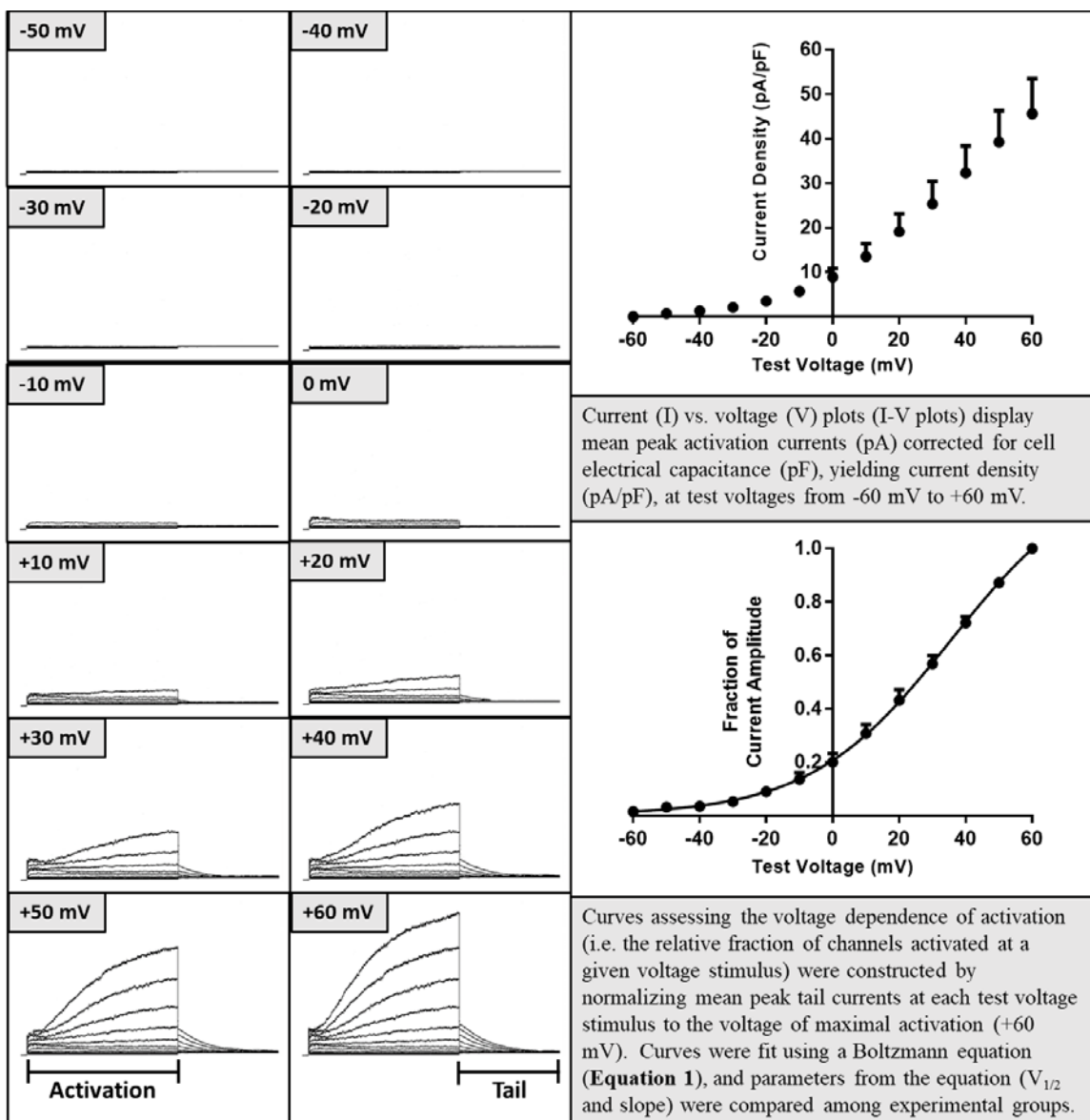


**Figure 1. Methods for analysis of electrophysiological data.** (Left) Representative traces of elicited activation and tail currents for WT  $I_{K_S}$  in control conditions are shown at test voltages from -50 mV to +60 mV (-60 mV not shown, but was similar to -50 mV). (Right) Procedures detailing how summary graphics (I-V plots [top] and activation curves [bottom]) were constructed from raw data.

The internal patch solution (pipette) was composed of (in mM): K-Aspartate 110, KCl 20,  $MgCl_2 \cdot 6H_2O$  1.0, HEPES 10, Mg-ATP 5.0, EGTA 5.0, while the external patch solution (bath) was composed of (in mM): NaCl 140, KCl 5.4,  $NaH_2PO_4$  0.33,  $CaCl_2 \cdot 2H_2O$  1.8,  $MgCl_2 \cdot 6H_2O$  1.0, HEPES 5.0, Glucose 10. The internal solution was

adjusted to a pH of 7.2 using KOH and the external solution was adjusted to a pH of 7.4 using NaOH. Pipettes were pulled from borosilicate glass (with filament, outer diameter: 1.2 mm, inner diameter: 0.69 mm; Sutter Instruments<sup>®</sup>) using a Sutter Instruments<sup>®</sup> P-2000 Puller. Pipettes were pulled via four loops in a repeating protocol with the Heat function set to 385, the Filament function set to 4, the Velocity function set to 30, the Delay function set to 200, and the Pull function set to 0. Pipettes with a resistance in bath solution of 2-7 M $\Omega$  were used for patch clamp experiments. The average liquid junctional potential for all experimental groups was manually estimated to be  $14.2 \pm 2.7$  (mean  $\pm$  SEM) mV using a salt-bridge. Series resistance compensation was not performed during the collection of any data. The sampling rate was set to 20,000 samples per minute in all experiments. The average cell capacitance was  $18.6 \pm 0.4$  pF and the average series resistance was  $18.1 \pm 0.5$  M $\Omega$ .

### **KCNQ1 Peptide Array**

Peptides corresponding to intracellular regions of KCNQ1, including the full amino and carboxyl termini as well as the intracellular segments linking S2-S3 and S4-S5, were constructed using a robotic peptide synthesizer (Intavis<sup>®</sup> MultiPep). Each peptide was 15 amino acids in length. For the global KCNQ1 experiment, tiled peptides were shifted by two amino acids (13 overlapping amino acids per peptide), allowing for several opportunities for each serine and/or threonine residue(s) to be phosphorylated via their presence in a number of overlapping peptides. For the peptide array focused on the spots identified by LCMS analysis, 15-mer peptides containing the putative phospho-acceptor site at the eighth residue were constructed (1) as in KCNQ1 (columns labeled wild-type [WT] in **Figure 15**), (2) with the putative phospho-acceptor spot mutated to an

alanine (columns labeled alanine [A]), and (3) with all serine and/or threonine residue(s) on the peptide knocked out via mutation to alanine (columns labeled knockout [KO]).

Immobilized peptides were synthesized on a modified cellulose membrane using routine Fmoc (N-(9-fluorenyl)methoxycarbonyl) chemistry as previously described.<sup>88,114</sup>

In peptide arrays using CaMKII, CaMKII was activated with Mg-ATP to allow for autophosphorylation before Mg- $[\gamma\text{-}^{32}\text{P}]\text{ATP}$  was applied to the membrane.<sup>88</sup> In peptide arrays using PKA, the catalytic subunit of PKA was applied to the membrane.

Phosphorylated peptides were imaged on autoradiographic film or visualized with a phosphoimager (Fujifilm<sup>®</sup>) and quantified using MultiGauge version 3.0 (Fujifilm<sup>®</sup>).

### **CaMKII Protein Immunoblot**

HEK 293 cells were transiently co-transfected with KCNQ1 and KCNE1 as previously described. At 24 hours following transfection, cells were treated with 100 nM ISO or vehicle (water) before cells were lysed at 48 hours post-transfection using a RIPA Buffer Lysis System (Cat. #: sc-24948; Santa Cruz Biotechnology<sup>®</sup>) per the manufacturer's instructions. Following lysis, 20  $\mu\text{g}$  of total protein was loaded and run on 10% SDS-polyacrylamide gel in a 25mM Trisma base/ 190 mM glycine/ 0.1% sodium dodecyl sulfate (SDS) running buffer for 1.25 hours at a constant voltage of 125 V. Proteins were then transferred to PVDF membranes (ThermoFisher<sup>®</sup>) at 4°C in a 25 mM Trisma base/ 190 mM glycine/ 20% methanol transfer buffer for 1 hour at a constant voltage of 100 V. Membranes were then blocked with 5% bovine serum albumin (BSA; Cat. #: 2905; EMD Millipore<sup>®</sup>) in Tris-buffered saline with 0.1% (v/v) Tween 20 (TBST; Tween 20: Cat. #: P1379; Sigma Aldrich<sup>®</sup>) for one hour at room temperature before being exposed to primary CaMKII (1:1000; Cat. #: M03964; Boster Biological

Technology<sup>®</sup>) or CaMKII Phospho-T287 (1:1000, Cat. #: NBP1-64741; Novus Biologicals<sup>®</sup>) antibodies and primary GAPDH (1:2000; Cat. #: FL-335; Santa Cruz Biotechnology<sup>®</sup>) antibodies for 12 hours at 4°C. Membranes were then washed with TBST and exposed to secondary anti-mouse (1:5000; Cat. #: sc-358914; Santa Cruz Biotechnology<sup>®</sup>) antibody for one hour at room temperature. Finally, membranes were washed again before being developed using Pierce ECL Western Blotting Substrate (Cat. #: 32106; ThermoFisher<sup>®</sup>) and a Chemi-Doc Imager (Bio-Rad<sup>®</sup>). Images were analyzed with ImageJ<sup>®</sup> version 1.4.3.67.

### **Bimolecular Fluorescence Complementation (BiFC)**

The coding regions of WT and mutant KCNQ1 (S484A, S484D, R481I, and S484T) and WT KCNE1 were subcloned into the multiple cloning sites of BiFC plasmids to produce expression of the channel subunit followed by a flexible linker region and complementary halves of the YFP fluorescent protein, Venus. KCNQ1 BiFC plasmids encoded for the amino half of Venus while KCNE1 BiFC plasmids encoded for the carboxyl half of Venus. Schematic vector maps of the KCNQ1 coding region (with the stop codon removed) subcloned between the EcoRI and XhoI sites within the multiple cloning site of the pBiFC-VN155 plasmid and the KCNE1 coding region (with the stop codon removed) subcloned between the EcoRI and XhoI sites of the multiple cloning site of the pBiFC-VC155 plasmid are shown below in **Figure 2**.

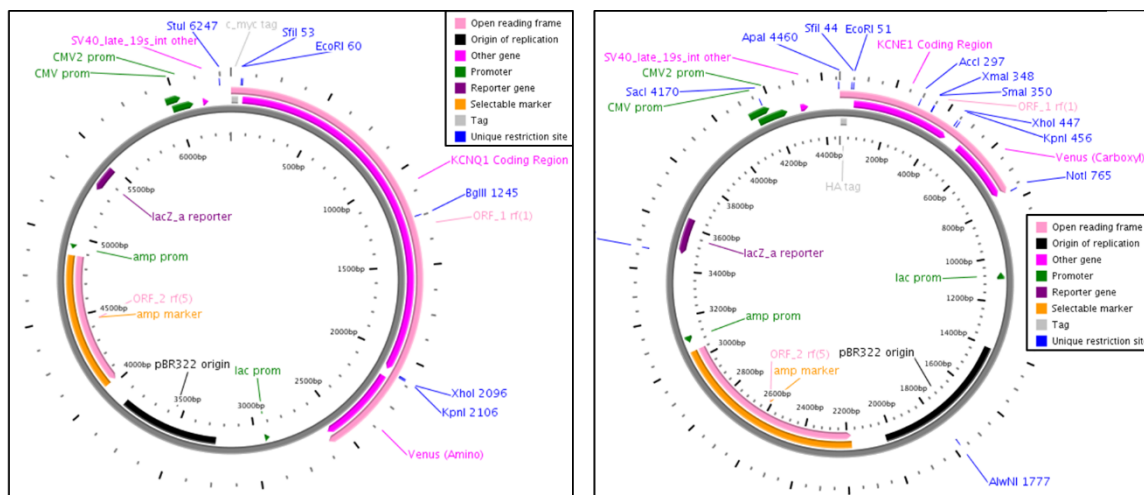


**Figure 2.** Vector maps showing the KCNQ1 coding region expressed in the pBIFC-VN155 plasmid containing the amino half of the fluorescent protein Venus (left) and the KCNE1 coding region expressed in the pBIFC-VC155 plasmid containing the carboxyl half of Venus (right). Maps were created using PlasMapper: (<http://wishart.biology.ualberta.ca/PlasMapper/>).

At 24 hours post-subculture, KCNQ1 and KCNE1 BiFC plasmids (500 ng each) were transiently co-transfected along with 500 ng of a cytosolic variant of the cyan fluorescent protein, Cerulean, using Lipofectamine 2000 (ThermoFisher®; transfection protocol detailed previously) in HEK 293 cells plated on 35 mm<sup>2</sup> glass-bottom (MatTek®) cell culture dishes. When applicable, cells were treated with ISO and CaMKII inhibitors at ~24 hours following transfection for 14-16 hours before microscopy experiments were initiated. Cells were imaged with a Leica P8 Resonant-scanning confocal/multiphoton microscope at ~48 hours following transfection. Z-series were acquired at 0.5 μm increments in the vertical plane, and summed image projections were created using Fiji software as shown in **Figure 3**.

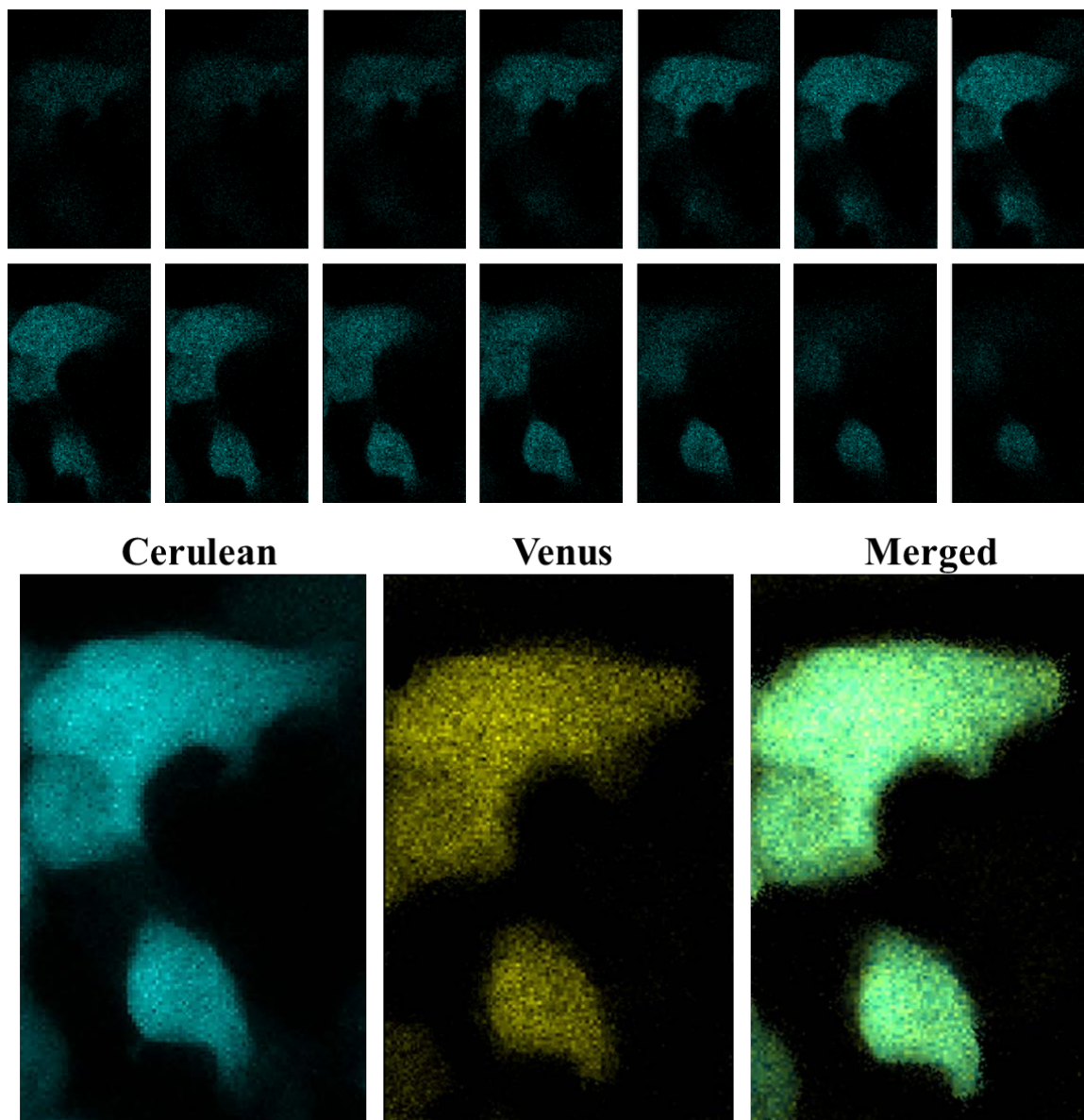


**Figure 3. (Top)** A series of images showing transient expression of the cytosolic Cerulean fluorescent protein in HEK 293 cells. Displayed images were taken along the z-plane (vertical) at  $1.5 \mu\text{M}$  increments. **(Bottom)** Summed images of the same visual field showing co-expression of Cerulean (left panel) and Venus fluorescent proteins (middle panel). A merged image showing both fluorescent proteins is shown in the right panel. Expression of Venus signals requires interaction of complementary halves of the Venus protein that are contained within plasmids co-expressing WT or mutant KCNQ1 and WT KCNE1. Cerulean is a cytosolic protein that allows resolution of cell boundaries for analysis and allows normalization of Venus intensity to control for transfection and expression efficiency.

Data were analyzed as the ratio of Venus fluorescent intensity (indicating reconstitution of the Venus fluorescent protein by close proximity/interaction of KCNQ1

and KCNE1 subunits) to the ratio of Cerulean fluorescent intensity (cytosolic protein assisting in visualization of cell boundaries and also controlling for transfection/expression efficiency) in images summing measured intensities throughout all acquired Z-planes. Regions of interest (ROIs) were drawn freehand around cellular boundaries and held constant between channels measuring Venus and Cerulean intensities using the ROI Manager within Fiji. Mean fluorescent intensities of all pixels within ROIs were tabulated within Fiji, and mean Venus:Cerulean fluorescent intensity ratios were calculated from these data for each individual cell in the analysis.

The potential for non-specific Venus intensity was assessed in cells in which Cerulean and only one half of Venus plasmids were transiently co-transfected. Measured mean Venus intensities in these cells were approximately 3.6% of the intensity of mean Venus intensities in the vehicle control group. Cerulean detection in cells only expressing both Venus plasmids was also tested and was also minimal. Finally, complementary halves of Venus were expressed without KCNQ1 and KCNE1, respectively, and the resulting Venus intensity was  $< \sim 10\%$  of mean Venus intensity in the vehicle control group. Representative summed image projections of these control experiments are shown in **Figure 4**.

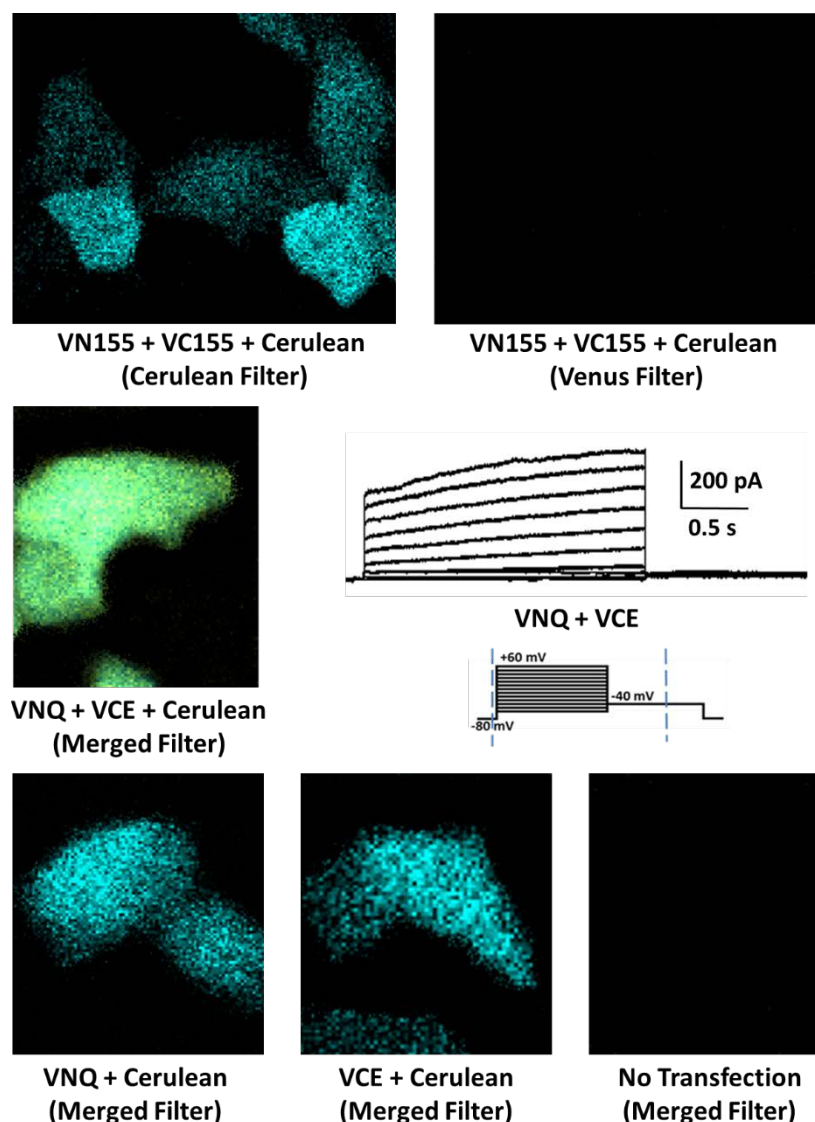


**Figure 4. Control Experiments for BiFC Methodology.** To verify that Venus signals in our BiFC experiments were specifically mediated by interaction of expressed KCNQ1 and KCNE1 subunits with complementary halves of Venus, we performed the following control experiments. First, we co-expressed the VN155 (containing the amino half of Venus without KCNQ1 expressed within the MCS), VC155 (containing the carboxyl half of Venus without KCNE1 expressed within the MCS), and Cerulean. As shown in the top panels, HEK 293 cells transiently co-expressing VN155, VC155, and Cerulean displayed fluorescent signals corresponding to Cerulean expression but not Venus expression in the absence of KCNQ1 and KCNE1. The middle and bottom panels displayed merged filters (in which intensities from both Venus and Cerulean signals are both displayed) for when VNQ, VCE, and Cerulean are co-expressed (middle left; representative trace for elicited currents during co-expression of VNQ and VCE shown in middle right), when VNQ and Cerulean are co-expressed (bottom left), when VCE and Cerulean are co-expressed (bottom center), and when no plasmids are transfected (bottom right). Together, these panels demonstrate Venus fluorescent signal only when complementary halves of Venus come in close proximity via interaction of KCNQ1 and KCNE1 subunits.

### **Cell Surface Biotinylation**

Isolation of plasma membrane-bound proteins was performed using the Pierce Cell Surface Protein Isolation Kit (Cat. #: 89881; ThermoScientific®) on HEK 293 cells transiently co-expressing (lipofection) WT or mutant KCNQ1 (S484A, S484D, R481I, S484T) and WT KCNE1. Isolation of cell surface proteins was performed per the manufacturer's instructions, and are described in the following.

At ~48 hours following transfection and 12-24 hours following treatment with ISO (when applicable), complete media was removed, cells were washed with ice-cold PBS twice, and the Sulfo-NHS-SS-Biotin reagent was dissolved in ice-cold PBS and exposed (10 mL/10 cm culture dish) to cells for 30 minutes at 4°C on a rocking platform. Quenching solution (500 µL) was then added to each dish and cells were scraped into 15 mL conical flasks and centrifuged at 500 x g for 3 minutes. The supernatant was discarded and cells were re-suspended in 5 mL TBS and centrifuged again at 500 x g for 3 minutes to wash them before the supernatant was discarded. Cells were then re-suspended in lysis buffer (500 µL) with protease inhibitor cocktail added. Cells were sonicated for five 1-second bursts using a probe sonicator at 35% intensity and then centrifuged at 10,000 x g for 2 minutes at 4°C. The supernatant was transferred to new tubes while 500 µL of the NeutrAvidin Agarose reagent was placed into new biotinylation columns (included in the kit) and centrifuged for 1 minute at 1000 x g and the flow-through was discarded. Columns were washed with wash buffer twice (centrifugation at 1000 x g for 1 minute) and then lysate was added to the biotinylation columns and allowed to incubate a room temperature for 1 hour while rocking. Columns were then centrifuged at 1000 x g for 1 minute and the flow-through was discarded. Wash buffer (500 µL) with protease inhibitor cocktail was then added to the columns, the

columns were centrifuged at 1000 c g for 1 minute, and the flow-through was discarded. The DTT solution was then reconstituted and 23.7  $\mu$ L was added to 450  $\mu$ L SDS-PAGE Sample Buffer (Cat. #: 161-0791; Bio-Rad<sup>®</sup>). DTT-sample buffer (400  $\mu$ L) was then added to the column and incubated at room temperature for 1 hour while rocking. The column was then centrifuge at 1000 x g for 2 minutes and then flow-through was collected. Total protein concentration was assessed via NanoDrop One<sup>®</sup> (“1 Abs = 1 mg/mL” setting), and protein lysates were stored at -20°C until immunoblot experiments were performed.

Protein immunoblots for isolated membrane proteins were performed using the general methods described in the “CaMKII Protein Immunoblot” section. Membranes were exposed to primary antibodies for KCNQ1 (Cat. #: sc-365186; Santa Cruz Biotechnology<sup>®</sup>), KCNE1 (Cat. #: sc-16796; Santa Cruz Biotechnology<sup>®</sup>), and Na<sup>+</sup>/K<sup>+</sup>-ATPase (used as loading control for membrane-bound proteins; Cat. #: sc-374050; Santa Cruz Biotechnology<sup>®</sup>) overnight at 4°C on a rocking platform and secondary anti-mouse (Cat. #: sc-516102; Santa Cruz Biotechnology<sup>®</sup>) and anti-goat (Cat. #: sc-2354; Santa Cruz Biotechnology<sup>®</sup>) antibodies for one hour at room temperature on a rocking platform. All primary and secondary antibodies in his experiment were diluted 1:1000 in 5% (w/v) BSA in TBST.

### **Data Analysis**

Analysis of electrophysiology data was performed using FitMaster software (Version 2x73.1; HEKA<sup>®</sup>) and GraphPad Prism (Version 6.03). Mean peak corrected activation current density at +60 mV (voltage of maximal I<sub>Ks</sub> current density) was compared among experimental groups by means of one-factor ANOVA with post-hoc

Tukey's HSD test or independent sample t-test with Welch correction, as appropriate. A Boltzmann distribution was used to fit normalized activation curves (analyzed using normalized tail currents) in GraphPad Prism with the equation:

$$\text{(Equation 1.) } I/I_{\max} = 1 / (1 + \exp[(V_{1/2} - V)/\text{slope}]).$$

The voltages of half-maximal activation ( $V_{1/2}$ ) were compared among experimental groups by one-way ANOVA or t-test as above.  $V_{1/2}$ s and slope factors for all experimental groups are displayed in **Supplementary Table 1**. Mono-exponential curves were fit to activation and tail currents in order to estimate mean rate constants of activation and deactivation, respectively, at each voltage that elicited measurable channel activation (0 to +60 mV). Rate constants of activation and deactivation were compared between experimental conditions via Welch corrected t-tests, as above.

Mean protein abundance from LCMS/MS experiments and mean phospho-stimulated luminescence from CaMKII peptide array experiments were compared via one-way ANOVA with Tukey's HSD post-hoc test. Normalized (normalized to GAPDH band intensity) luminescent intensities for total CaMKII, T287-phospho CaMKII, KCNQ1, KCNE1, and Na<sup>+</sup>/K<sup>+</sup>-ATPase bands in Western blots were compared to a hypothesized  $\mu=1$  via one-way T test. All data are expressed as mean  $\pm$  standard error of the mean (SEM) and the *a priori* alpha was set to 0.05 for all experiments.

## RESULTS

**Specific Aim 1: Investigate the regulation of the KCNQ1 carboxyl terminus during sustained  $\beta$ -AR stimulation and the associated functional implications on  $I_{Ks}$**

*The KCNQ1 carboxyl terminus demonstrates increased phosphorylation during sustained  $\beta$ -AR stimulation*

The phosphorylation status of the KCNQ1 carboxyl terminus was assessed by tandem LCMS/MS during sustained  $\beta$ -AR stimulation via treatment with 100 nM ISO in HEK 293 cells transiently co-transfected with plasmids encoding for human KCNQ1 and KCNE1. Basal phosphorylation of KCNQ1 was identified at five residues on the carboxyl terminus (S407, S457, T482, S484, T624; n=5 for all experimental conditions; **Figure 5**). Phosphorylation was significantly enhanced at four of these residues (S407, T482, S484, p < 0.01; T624, p = 0.02) following sustained ISO treatment for 4 hours. Increased phosphorylation was maintained following 24 hours of ISO treatment at T482 (p < 0.01) and S484 (p = 0.01).

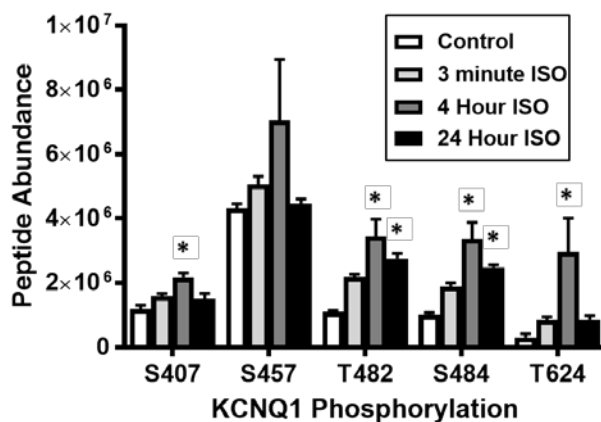


**Figure 5.** Basal phosphorylation was identified at five KCNQ1 carboxyl terminal residues (when co-expressed with KCNE1 in HEK 293 cells) via LCMS/MS: S407, S457, T482, S484, and T624. Phosphorylation was increased at S407, T482, S484, and T624 following four hour treatment with the  $\beta$ -AR agonist ISO (100 nM). Increased phosphorylation was sustained following 24 hour ISO treatment at T482 and S484. \*P<0.05 vs. control conditions

***Sustained  $\beta$ -AR stimulation inhibits  $I_{Ks}$  activation currents and causes a depolarizing shift in the voltage dependence of activation***

As past investigations have demonstrated functional inhibition of  $I_{Ks}$  during sustained  $\beta$ -AR stimulation, including during sustained ISO treatment, in a variety of experimental models, we first sought to assess the responsiveness of our HEK 293 expression system to sustained ISO treatment. Of note, the responsiveness of expressed  $I_{Ks}$  to endogenous  $\beta$ -ARs has been previously demonstrated in HEK 293 cells.<sup>108</sup> Functional assessment of expressed  $I_{Ks}$  currents, and the potential of  $I_{Ks}$  to respond to sustained  $\beta$ -AR stimulation, was investigated within our HEK 293 model using whole-cell, voltage-clamp cellular electrophysiology experiments in control conditions and following treatment with 100 nM ISO for 12-24 hours.

The activating voltage protocol used in these experiments along with representative current traces are displayed in **Figure 6A**. As shown in **Figure 6B**, wild-type KCNQ1 (when transiently co-expressed with KCNE1) demonstrated reduced mean peak corrected activation currents at +60 mV (the voltage of maximum activation) following sustained ISO treatment ( $45.6 \pm 7.9$  pA/pF,  $n = 20$  with vehicle vs.  $21.5 \pm 4.0$ ,  $n = 14$  following ISO treatment,  $p = 0.01$ ). ISO treatment also resulted in a depolarizing shift in the voltage dependence of activation, obtained using elicited tail currents from the same activating voltage protocol ( $V_{1/2}$  of  $20.6 \pm 0.8$ ,  $n = 19$  with vehicle vs.  $26.1 \pm 0.8$  mV,  $n = 12$  following ISO treatment,  $p < 0.01$ ; **Figure 6C**). Parameter estimates of  $V_{1/2}$  and slopes from fitted Boltzmann distributions are displayed in **Table 1**. Rate constants

of activation and deactivation were not different in control cells and those treated with ISO (**Figures 6D and 6E**).

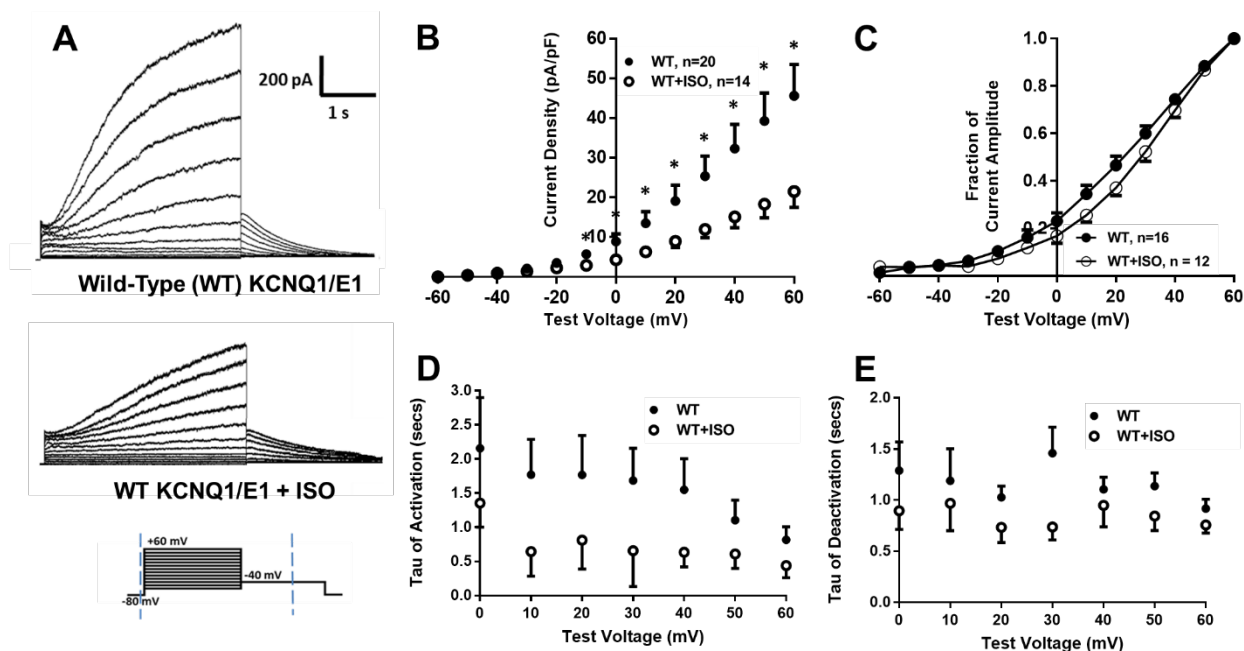


**Figure 6.** (A) Representative traces of  $I_{Ks}$  currents from WT KCNQ1 co-expressed with KCNE1 in HEK 293 cells treated with 100 nM ISO or vehicle for 12-24 hours. (B) I-V plots (mean and SEM), (C) activation curves (normalized to voltage of maximum activation [+60 mV]), and rate constants of activation (D) and deactivation (E) following treatment with ISO or vehicle. \* $p < 0.05$  vs. control conditions

**Table 1.** Estimated Boltzmann equation parameters for WT KCNQ1 during treatment with 100 nM ISO or vehicle.

Mutant/Treatment	$V_{1/2}$ (mV)	Slope Factor
WT KCNQ1 + Vehicle	20.61 (0.82)	16.77 (0.75)
WT KCNQ1 + ISO	26.10 (0.79)	14.80 (0.73)

Since KCNQ1 phosphorylation was highest following 4 hours of 100 nM ISO treatment at all identified sites in our LCMS/MS analysis (**Figure 5**), patch clamp experiments were performed following 4 hour ISO treatment to assess whether the functional inhibition of  $I_{Ks}$  was similar following 4 hour and 12-24 hour ISO treatment. As shown in **Figure 7B and 7C**,  $I_{Ks}$  activation currents were similar following 4 hour and 12-24 hour ISO exposure. In addition, experiments with the specific  $I_{Ks}$  chemical

inhibitor HMR 1556 (100 nM and 10  $\mu$ M added to the pipette solution) confirm that measured currents in our HEK 293 expression system are indeed  $I_{Ks}$ .

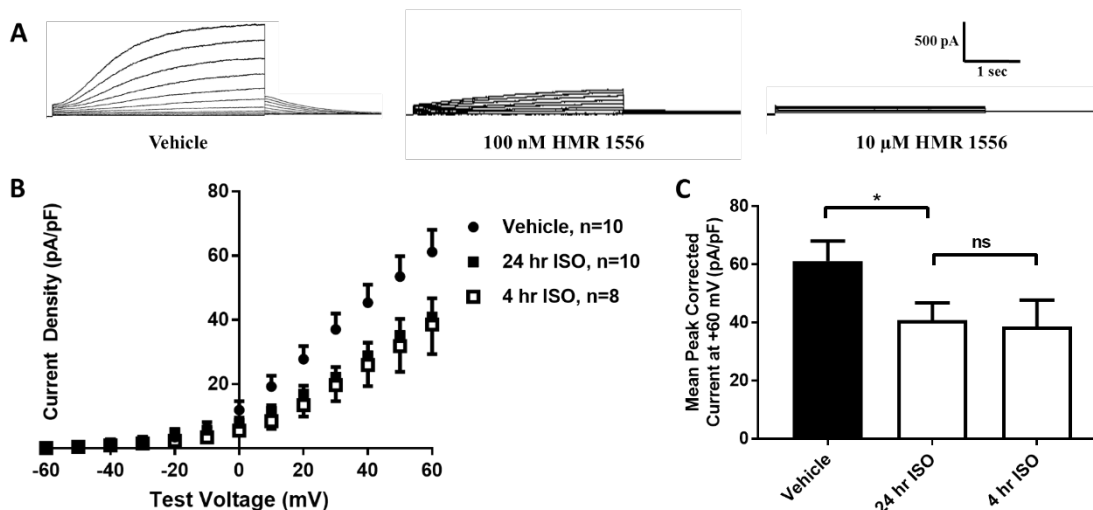


**Figure 7.** (A) Representative traces of elicited WT  $I_{Ks}$  currents during treatment with the  $I_{Ks}$  chemical inhibitor, HMR 1556 (100 nM or 10  $\mu$ M), or vehicle in the pipette solution. (B) I-V plots (mean and SEM) and (C) bar graphs of maximum WT  $I_{Ks}$  current density during treatment with HMR 1556 or vehicle. \* $p < 0.05$  vs. control conditions, ns = not significant

### *Mimics of phosphorylation at S457, T482, and S484 in combination decrease $I_{Ks}$ activation currents*

Based on LCMS/MS data from **Figure 5**, cellular electrophysiology experiments were planned to assess the functional implications of phosphorylation at T482 and S484. In addition, ScanSite3 (described in detail within the results of Specific Aim 2) identified S457 as a potential site of CaMKII regulation; resultantly, the functional implications of phosphorylation at all three sites were investigated by means of patch-clamp experiments in HEK 293 cells transiently expressing KCNE1 and KCNQ1 mutants conferring mimics of dephosphorylation or phosphorylation at S457, T482, and S484 in combination: triple-alanine KCNQ1 (Triple-A; dephosphorylated mimic) and triple-aspartic acid KCNQ1 (Triple-D; phosphorylated mimic).

As displayed in **Figure 8A and 8B**, Triple-A mutants demonstrate increased mean peak corrected activation currents ( $50.0 \pm 8.7$  pA/pF,  $n = 10$  at +60 mV) relative to Triple-D mutants ( $24.5 \pm 4.2$ ,  $n = 13$ ,  $p = 0.02$ ). In contrast to the effect seen with wild-type KCNQ1, sustained treatment with 100 nM ISO for 12-24 hours did not decrease  $I_{Ks}$  current amplitude with Triple-A ( $50.0 \pm 8.7$ ,  $n = 10$  with vehicle vs.  $70.5 \pm 13.3$ ,  $n = 18$  following ISO treatment,  $p = 0.21$ ) or Triple-D mutants ( $24.5 \pm 4.2$ ,  $n = 13$  with vehicle vs.  $32.9 \pm 5.1$ ,  $n = 13$  following ISO treatment,  $p = 0.22$ ; **Figure 8B**). The voltage dependence of activation was not different between Triple-A and Triple-D mutants ( $V_{1/2}$  of  $19.5 \pm 0.9$  mV,  $n = 10$  in Triple-A mutants vs.  $20.2 \pm 1.1$ ,  $n = 13$  in Triple-D mutants,  $p = 0.66$ ), and sustained ISO treatment did not alter the voltage dependence of activation in Triple-A ( $V_{1/2}$  of  $19.5 \pm 0.9$ ,  $n = 10$  with vehicle vs.  $22.3 \pm 0.6$ ,  $n = 18$  following ISO treatment,  $p = 0.25$ ) or Triple-D mutants ( $V_{1/2}$  of  $20.2 \pm 1.1$  mV,  $n = 13$  with vehicle vs.  $19.2 \pm 0.6$ ,  $n = 12$  following ISO treatment vs,  $p = 0.44$ ; **Figure 8C**). Parameter estimates of  $V_{1/2}$  and slopes from fitted Boltzmann distributions are displayed in **Table 2**. Rate constants of activation or deactivation were not different between Triple-A and Triple-D mutants (**Figure 8D and 8E**).

In summary, these experiments demonstrate that, relative to the combination dephosphorylated state mimics (Triple-A), the combination phosphorylated state mimics (Triple-D) demonstrate reduced activation currents in a manner similar to that observed when wild-type  $I_{Ks}$  was exposed to sustained  $\beta$ -AR stimulation (**Figure 8F**). In addition, the fact that both Triple-A and Triple-D mutants were unresponsive to sustained ISO

treatment suggests that the functional changes in  $I_{Ks}$  in response to ISO treatment are mediated specifically through changes in phosphorylation at one or more of these sites.

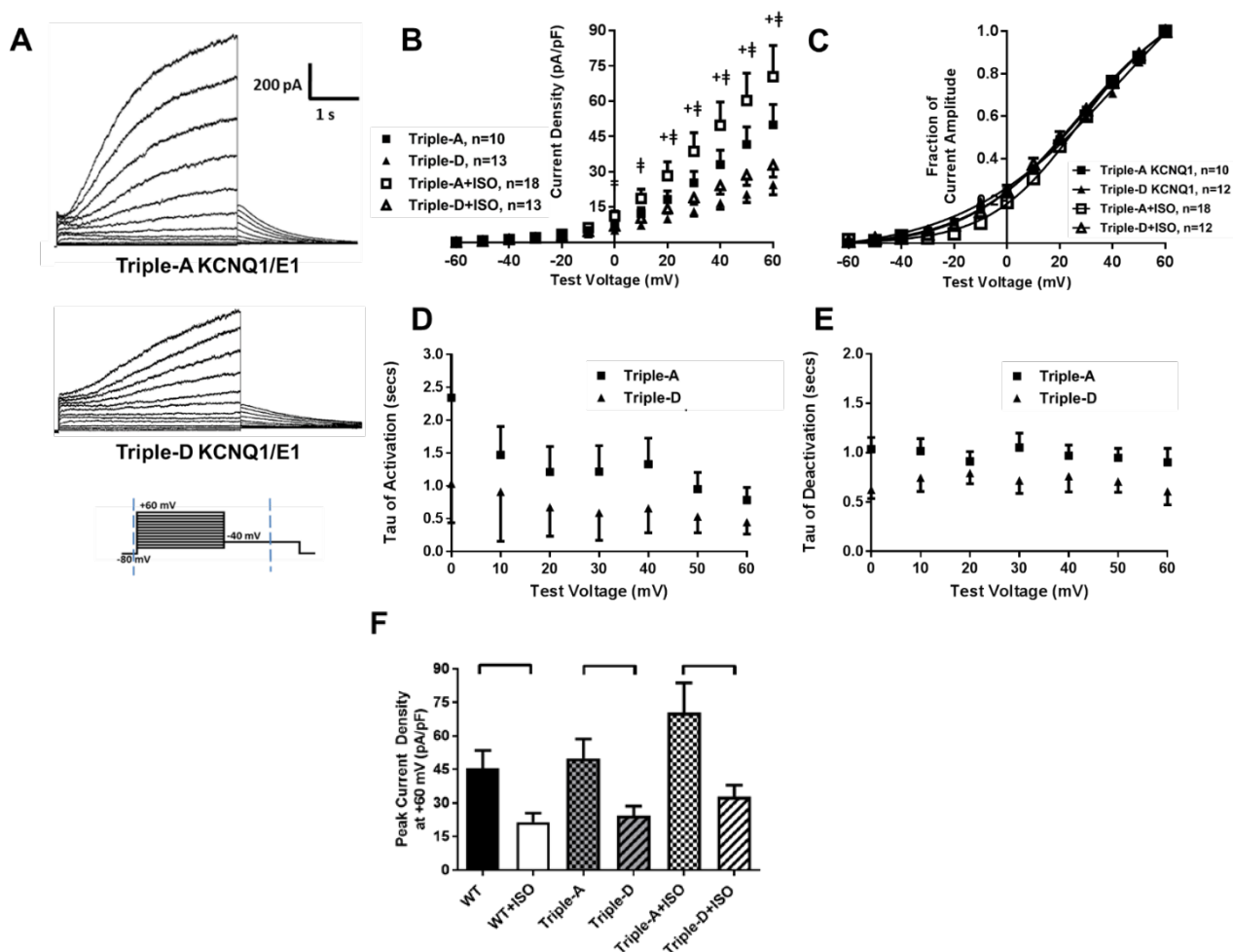


**Figure 8.** (A) Representative traces of  $I_{Ks}$  activation currents from KCNQ1 combination mimics of phosphorylation (Triple-A) and dephosphorylation (Triple-D) co-expressed with KCNE1 in HEK 293 cells. (B) I-V plots (mean and SEM), (C) activation curves (normalized to voltage of maximum activation), and rate constants of activation (D) and deactivation (E) for Triple-A and Triple-D KCNQ1. (F) Bar graph of current density at the voltage of maximum activation (+60 mV) for combination mimic KCNQ1 or for WT KCNQ1 following treatment with ISO or vehicle. \* $p < 0.05$  for comparison indicated,  $^{\dagger}p < 0.05$  for Triple-A vs. Triple-D,  $^{\ddagger}p < 0.05$  for Triple-A+ISO vs. Triple-D+ISO

**Table 2.** Estimated Boltzmann equation parameters for Triple-A and Triple-D KCNQ1 during treatment with 100 nM ISO or vehicle.

Mutant/Treatment	$V_{1/2}$ (mV)	Slope Factor
Triple-A KCNQ1	19.53 (0.90)	16.43 (0.82)
Triple-A KCNQ1 + ISO	22.34 (0.64)	14.38 (0.58)
Triple-D KCNQ1	20.18 (1.12)	18.44 (1.05)
Triple-D KCNQ1 + ISO	19.19 (0.58)	16.19 (0.53)

***Mimics of phosphorylation at S457 and S484, but not at T482, decrease  $I_{Ks}$  activation currents and positively shift the voltage dependence of activation***

To determine the specific KCNQ1 carboxyl terminal residue(s) at which phosphorylation affects  $I_{Ks}$  function, we individually investigated mimics of dephosphorylation and phosphorylation at each residue (S457, T482, and S484). Mimics of phosphorylation demonstrated significantly decreased  $I_{Ks}$  mean peak activation currents relative to dephosphorylation mimics at S457 ( $40.4 \pm 4.1$  pA/pF,  $n = 19$  in S457D mutants vs.  $70.7 \pm 12.3$ ,  $n = 16$  in S457A mutants at +60 mV,  $p = 0.02$ ) and also right shifted the voltage dependence of activation ( $V_{1/2}$  of  $28.6 \pm 2.5$  mV,  $n=15$  for S457D vs.  $21.6 \pm 1.7$ ,  $n=12$  for S457A,  $p=0.03$ ; **Figure 9A**). Conversely, activation currents elicited with mimics of phosphorylation at T482 were not significantly different from dephosphorylation mimics ( $64.3 \pm 11.4$ ,  $n = 22$  in T482D mutants vs.  $73.8 \pm 11.3$ ,  $n = 22$  in T482A mutants at +60 mV,  $p = 0.53$ ) and there was no shift in the voltage dependence of activation ( $V_{1/2}$  of  $24.8 \pm 4.2$  mV,  $n=14$  for T482D vs.  $24.7 \pm 2.2$ ,  $n=16$  for T482A,  $p=0.99$ ; **Figure 9B**). Mimics of phosphorylation at S484 also decreased  $I_{Ks}$  activation currents relative to dephosphorylation mimics ( $61.9 \pm 10.8$ ,  $n = 20$  in S484D mutants vs.  $100.4 \pm 13.7$ ,  $n = 22$  in S484A mutants at +60 mV,  $p = 0.04$ ) and produced a right shift in the voltage dependence of activation ( $V_{1/2}$  of  $28.3 \pm 3.1$  mV,  $n=15$  for S484D vs.  $19.6 \pm 1.8$ ,

n=11 for S484A, p=0.02; **Figure 9C**). Parameter estimates of  $V_{1/2}$  and slopes from fitted Boltzmann distributions are displayed in **Table 3**.

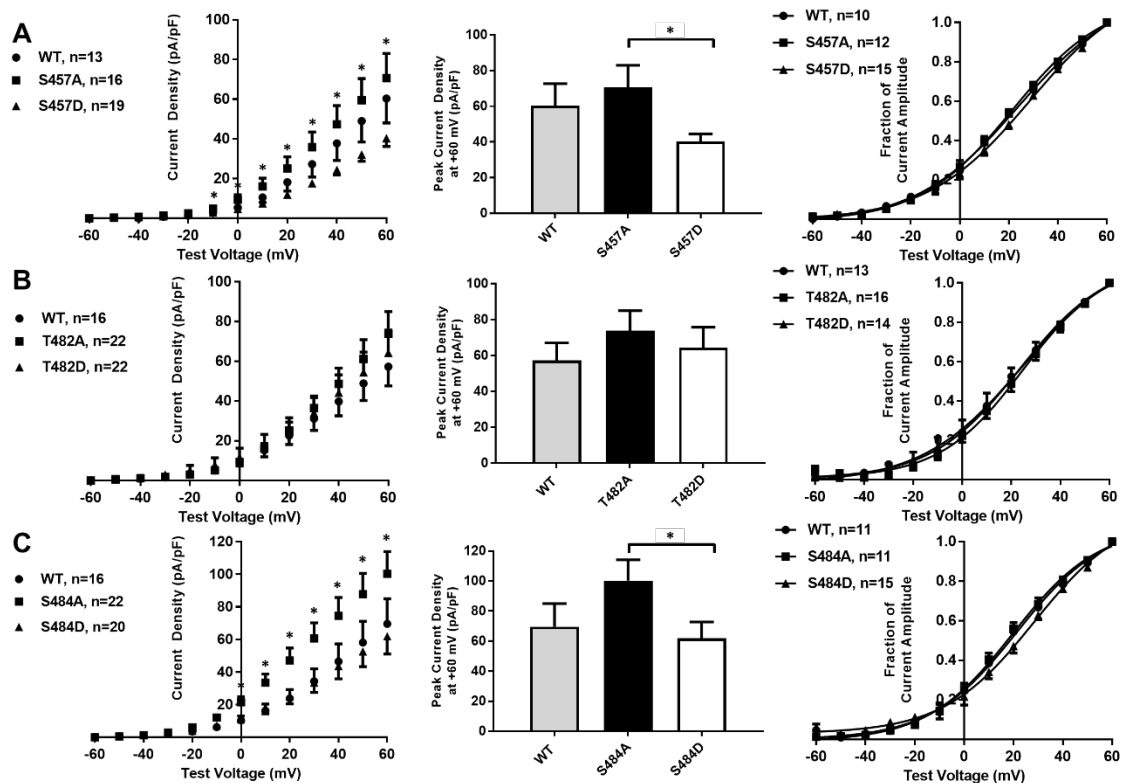


**Figure 9.** (A) I-V plots (mean and SEM) of elicited currents during an activating voltage step protocol, bar graph of maximum  $I_{Ks}$  current density, and activation curves for WT, dephosphorylation (S457A), and phosphorylation (S457D) mimics of KCNQ1 at S457 when co-expressed with WT KCNE1 in HEK 293 cells. (B) I-V plots activation currents, bar graph of maximum  $I_{Ks}$  current density, and activation curves for WT, dephosphorylation (T482A), and phosphorylation (T482D) mimics of KCNQ1 at T482. (C) I-V plots activation currents, bar graph of maximum  $I_{Ks}$  current density, and activation curves for WT, dephosphorylation (S484A), and phosphorylation (S484D) mimics of KCNQ1 at S484. \*p<0.05 for S457A vs. S457D or S484A vs. S484D

**Table 3.** Estimated Boltzmann equation parameters for S457A, S457D, T482A, T482D, S484A, and S484D KCNQ1 in control conditions.

<b>Mutant/Treatment</b>	<b><math>V_{1/2}</math> (mV)</b>	<b>Slope Factor</b>
<b>S457A KCNQ1</b>	21.55 (1.74)	18.89 (1.46)
<b>S457D KCNQ1</b>	28.55 (2.52)	20.83 (1.75)
<b>T482A KCNQ1</b>	24.72 (2.16)	16.92 (1.69)
<b>T482D KCNQ1</b>	24.77 (4.17)	20.56 (3.22)
<b>S484A KCNQ1</b>	19.62 (1.80)	17.41 (1.57)
<b>S484D KCNQ1</b>	28.34 (3.05)	18.41 (2.15)

**Specific Aim 2: Assess the potential for CaMKII-mediated functional regulation of  $I_{Ks}$  during sustained  $\beta$ -AR stimulation and the associated functional implications**

***The KCNQ1 carboxyl terminus contains residues of CaMKII phosphorylation***

The ability of  $Ca^{2+}$ /CaM-activated human  $\delta$ CaMKII to phosphorylate immobilized peptide fragments corresponding to the intracellular regions of KCNQ1, including the entire KCNQ1 carboxyl terminus, was assessed using a KCNQ1 peptide array. Phospho-stimulated luminescent signals corresponding to CaMKII phosphorylation were seen with peptides containing the carboxyl terminal residues T482

and/or S484 (the dashed boxes in the top, following four minute exposure to radiolabeled  $[\gamma\text{-}^{32}\text{P}]$  ATP and bottom, following 30 second exposure) in **Figure 10**; a map containing the complete peptide sequences is provided in

**Supplementary Table 2).**

The precise phosphorylation site(s) (T482 or S484) could not be resolved since both residues were located on the same three peptide

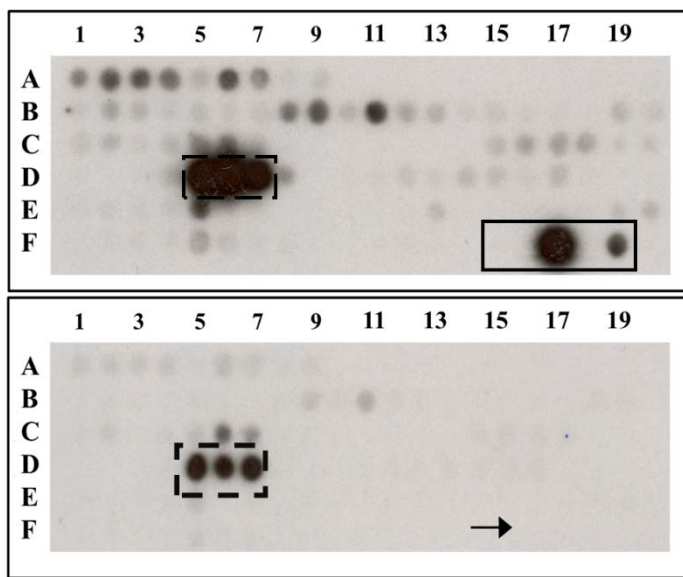


**Figure 10.** Peptide fragments of 15 residues in length corresponding to the intracellular regions of KCNQ1 were synthesized on a cellulose membrane and exposed to  $Ca^{2+}$ /calmodulin-activated  $\delta$ CaMKII for four minutes (**top**) and 30 seconds (**bottom**) with  $Mg\text{-}[\gamma\text{-}^{32}\text{P}]$ ATP. Peptide fragments containing KCNQ1 carboxyl terminal residues T482 and S484 (indicated by the dashed boxes at D5-D7) were the strongest substrates for CaMKII phosphorylation. The solid box at F15-F19 in the top panel contains a mutant autocalmitide-2 negative control (T $\rightarrow$ A mutation; F15), WT autocalmitide-2 positive control (F17), and Kemptide control (classical PKA substrate; F19). The arrow in the bottom panel contains an additional mutant autocalmitide-2 negative control. The full peptide map is shown in **Supplementary Table 1.**

fragments in the experiment given their close proximity within the KCNQ1 carboxyl terminus.

To complement the KCNQ1 peptide array, we utilized ScanSite3 (available at: <http://scansite3.mit.edu/#home>), a tool for predicting protein motifs that are kinase substrates, to assess the potential for CaMKII to regulate the residues identified in our LCMS/MS and peptide array experiments. Using the broadest stringency setting to minimize the potential for false negative results, ScanSite3 identified S484 and S457 as predicted sites of CaMKII phosphorylation. Interestingly, S457 was a residue that demonstrated basal KCNQ1 phosphorylation in our LCMS/MS analysis and also showed a large numerical (albeit not statistically significant) increase in phosphorylation during 4 hour ISO treatment (**Figure 5**). All three of these residues reside within a loop in the KCNQ1 carboxyl terminus that connects two known CaM-binding domains in helices A and B (**Figure 11**), suggesting the potential for pathological regulation by CaMKII during sustained  $\beta$ -AR stimulation and HF.

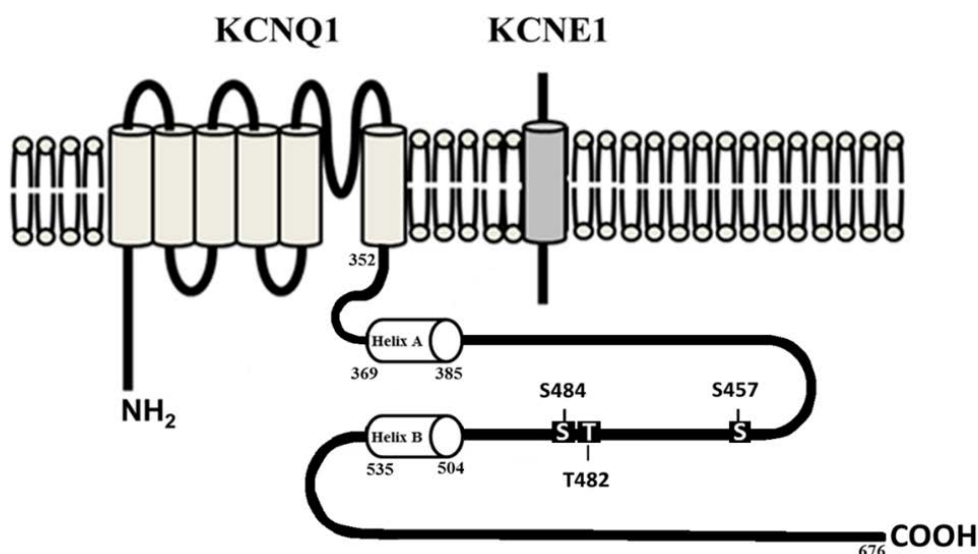


**Figure 11.** Schematic of KCNQ1 and KCNE1 subunits showing KCNQ1 carboxyl terminal sites of potential CaMKII regulation during sustained  $\beta$ -AR stimulation and HF.

***CaMKII mediates functional changes in  $I_{Ks}$  during sustained  $\beta$ -AR stimulation***

The potential for CaMKII signaling to regulate functional inhibition of  $I_{Ks}$  during sustained  $\beta$ -AR stimulation was investigated using whole-cell, voltage clamp patch clamp experiments as before. Wild-type  $I_{Ks}$  currents were assessed during sustained treatment with 100 nM ISO for 12-24 hours in the presence of the CaMKII chemical inhibitor, KN-93, or its inactive analogue, KN-92. As shown in **Figure 12A and 12B**, exposure to 500 nM KN-93 (4 hour incubation in culture media before the start of patch clamp experiments) attenuated reductions in  $I_{Ks}$  mean peak activation currents observed during sustained ISO treatment versus treatment with 500 nM KN-92 ( $37.4 \pm 5.9$  pA/pF,  $n = 17$  with KN-93 treatment vs.  $21.6 \pm 2.6$ ,  $n = 14$  with KN-92 treatment,  $p = 0.02$ ). The voltage dependence of activation was significantly right-shifted during co-treatment with ISO and KN-92 relative to co-treatment with ISO and KN-93 ( $V_{1/2}$  of  $21.4 \pm 0.6$  mV,  $n = 17$  with KN-93 treatment vs.  $26.4 \pm 0.8$ ,  $n = 14$  with KN-92 treatment,  $p < 0.01$ ; **Figure 12C**). Parameter estimates of  $V_{1/2}$  and slopes from fitted Boltzmann distributions are displayed in **Table 4**.

As KN-93 has been previously been shown to directly block the pore of  $I_{Kr}$  currents within rabbit and guinea pig cardiomyocytes, we assessed whether KN-93 or KN-92 had direct inhibitory effects on  $I_{Ks}$  currents expressed in our HEK 293 system.<sup>115</sup> As displayed in **Figure 12D and 12E**, 4 hour incubation with 500 nM KN-92 or KN-93 did not affect  $I_{Ks}$  activation currents when compared to vehicle ( $37.1 \pm 7.7$  pA/pF,  $n = 6$  with KN-93 treatment,  $45.3 \pm 8.8$ ,  $n = 5$  with KN-92 treatment, and  $47.7 \pm 8.4$ ,  $n=5$  with vehicle,  $p=0.63$ ) in the absence of co-treatment with 100 nM ISO for 12-24 hours.

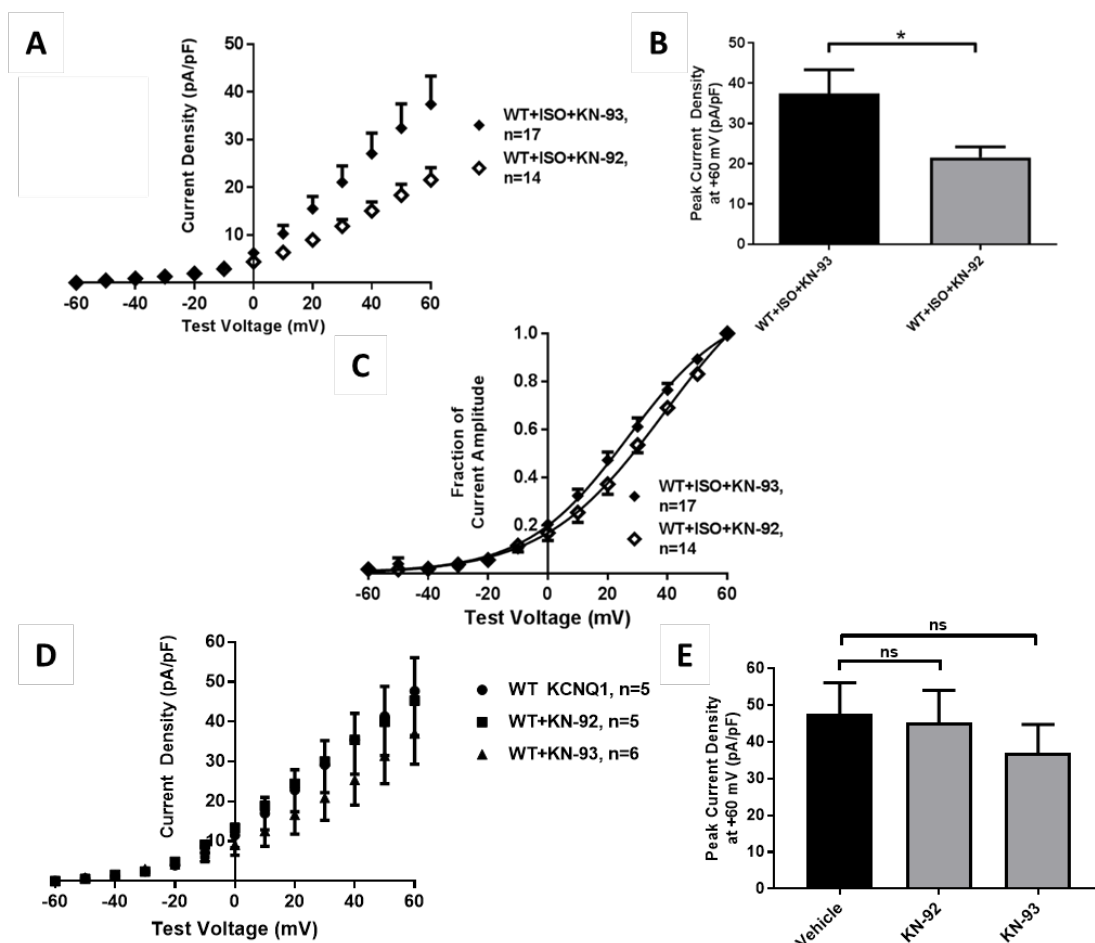


**Figure 12.** (A) I-V plots (mean and SEM), (B) peak current density, and (C) normalized activation curves for WT KCNQ1/KCNE1 following treatment with 100 nM ISO for 12-24 hours and 500 nM KN-92 or KN-93 for 4 hours in culture media. (D) I-V plots and (E) peak current density for WT KCNQ1/KCNE1 following treatment with 500 nM KN-92 or KN-93 for 4 hours in culture media. \* $p < 0.05$ , ns = not significant for comparison indicated

**Table 4.** Estimated Boltzmann equation parameters for WT KCNQ1 during co-treatment with 100 nM ISO for 12-24 hours and 500 nM KN-92 or KN-93 for 4 hours.

Mutant/Treatment	$V_{1/2}$ (mV)	Slope Factor
WT + ISO + KN-92	26.41 (0.76)	14.97 (0.70)
WT + ISO + KN-93	21.40 (0.65)	14.65 (0.59)

Similarly, 4 hour incubation with the CaMKII peptide inhibitor CN21, but not its inactive analogue, CN21-Alanine (10  $\mu$ M tat-CN21 or tat-CN21-Ala in culture media for 4 hours and 1  $\mu$ M CN-21 or CN21-Ala in pipette solution), reversed sustained ISO

induced reductions in  $I_{Ks}$  activation currents ( $71.9 \pm 5.1$  pA/pF,  $n=10$  with CN21 vs.  $47.2 \pm 5.9$ ,  $n=12$  with CN21-Ala,  $p<0.01$ ; **Figure 13A and 13B**). In addition, CN21 co-treatment, but not CN21-Alanine co-treatment, attenuated the depolarizing shift in the voltage dependence of activation that was seen during treatment with sustained ISO ( $V_{1/2}$  of  $13.8 \pm 1.3$  mV,  $n=6$  with CN21 vs.  $20.2 \pm 2.1$ ,  $n=6$  with CN21-Ala,  $p<0.01$ ; **Figure 13C**). Parameter estimates of  $V_{1/2}$  and slopes from fitted Boltzmann distributions are displayed in **Table 5**.

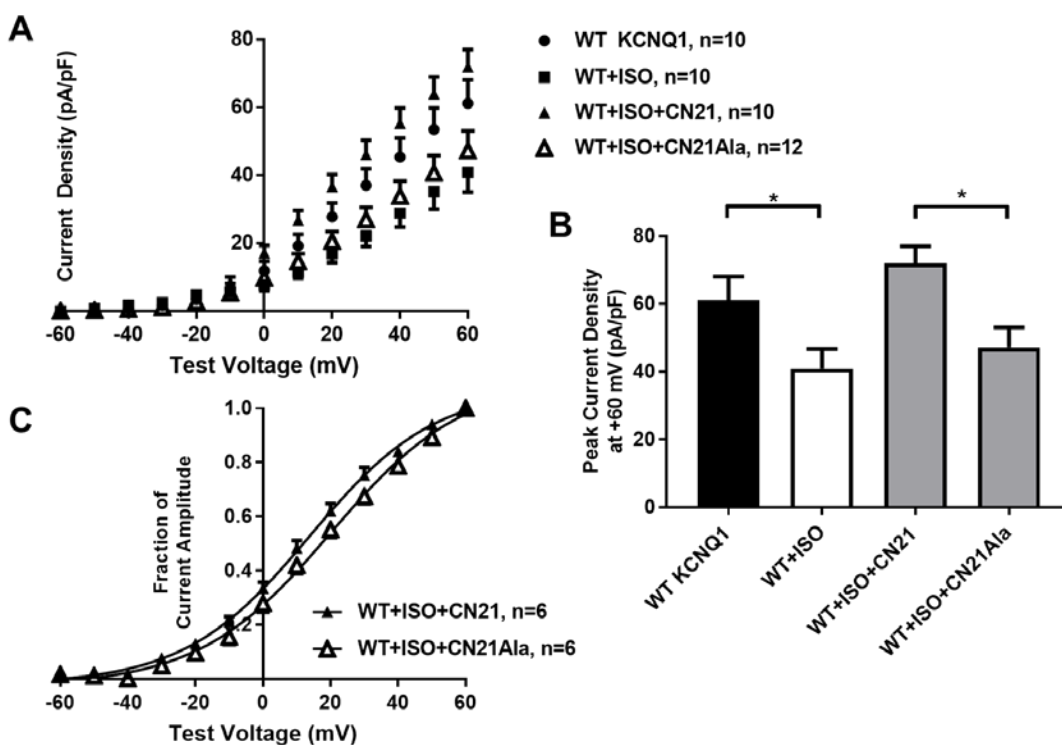


**Figure 13.** (A) I-V plots (mean and SEM) and (B) peak activation current density for WT KCNQ1/KCNE1 following co-treatment with ISO (100 nM for 12-24 hours) and CN21 or CN21-Ala (10  $\mu$ M tat-CN21 or tat-CN21-Ala in culture media and 1  $\mu$ M CN21 or CN21-Ala in pipette solution during recording). (C) Normalized activation curves following treatment with ISO and CN21 or CN21-Ala. \* $p<0.05$

**Table 5.** Estimated Boltzmann equation parameters for WT KCNQ1 during co-treatment with 100 nM ISO for 12-24 hours and CN21 or CN21-Ala (10  $\mu$ M tat-CN21 or tat-CN21-Ala in culture media and 1  $\mu$ M CN21 or CN21-Ala in pipette solution)

<b>Mutant/Treatment</b>	<b>V<sub>1/2</sub> (mV)</b>	<b>Slope Factor</b>
<b>WT + ISO + CN21</b>	13.81 (1.33)	18.60 (1.31)
<b>WT + ISO + CN21-Alanine</b>	20.21 (2.12)	19.67 (1.84)

To assess the potential for functional enhancement of CaMKII activity in response to sustained  $\beta$ -AR stimulation, HEK 293 cells co-expressing KCNQ1 and KCNE1 were treated with 100 nM ISO or vehicle for 24 hours before cells were lysed and total protein was isolated. Total protein lysates were separated via SDS-PAGE, transferred to PVDF membranes, and blocked with 5% BSA in TBST. Membranes were then exposed to primary antibodies for CaMKII, phospho-T287 CaMKII (an antibody detecting CaMKII phosphorylation at T287, the site wherein auto-phosphorylation confers constitutive kinase activity), and GAPDH overnight at 4°C. Membranes were then washed, exposed to secondary anti-rabbit antibodies, washed again, exposed to enhanced chemiluminescent (ECL) substrate, and imaged on a Bio-Rad ChemiDoc Imager. As shown in **Figure 14**, phosphorylation at T287 (and therefore enhanced CaMKII activity) was increased by 36.8% following 24 hour treatment with 100 nM ISO relative to vehicle control, when corrected for GAPDH expression ( $p < 0.05$ ). Total CaMKII expression, however, was not changed following ISO treatment relative to vehicle, when corrected for GAPDH expression (-5.6% change with ISO treatment relative to vehicle,  $p = 0.49$  for one-way T-test with hypothesized  $\mu = 1$ ).

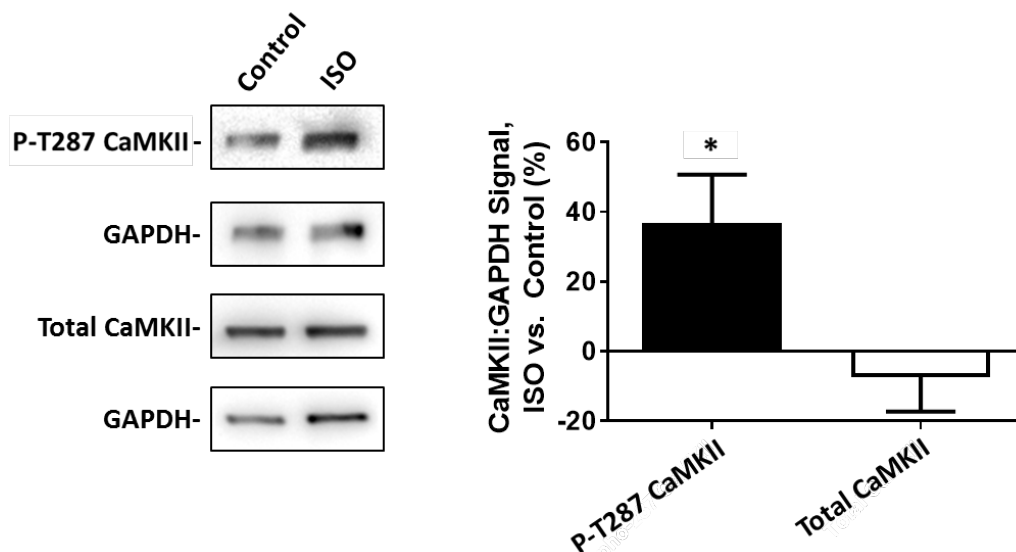


**Figure 14.** Representative protein immunoblots (n=7 per condition) and percent changes in CaMKII and CaMKII T287 phosphorylation in HEK 293 cells following treatment with 100 nM ISO for 24 hours. \*p<0.05

Taken together, these results suggest that CaMKII is functionally enhanced in response to sustained  $\beta$ -AR stimulation in our HEK 293 expression system and plays a role in mediating both the inhibition of  $I_{Ks}$  activation currents and the right-shift in the voltage dependence of activation observed when wild-type  $I_{Ks}$  was exposed to sustained  $\beta$ -AR stimulation.

***CaMKII mediates functional inhibition of  $I_{Ks}$  through KCNQ1 phosphorylation at S484 but not S457***

In order to determine the specific KCNQ1 carboxyl terminal sites of CaMKII phosphorylation, a peptide array was performed to assess the potential for  $Ca^{2+}$ /CaM-activated  $\delta$ CaMKII to phosphorylate each individual residue identified in our LCMS/MS analysis (**Figure 5**). As shown in the labeled rows in **Figure 15A**, peptide fragments corresponding to the KCNQ1 carboxyl terminal residues S457 and T624 did not demonstrate detectable phospho-stimulated luminescent signals (indicating

phosphorylation) when exposed to activated  $\delta$ CaMKII. The top row in **Figure 15A**, which contains peptide fragments corresponding to S407, displayed weak phosphorylation signals in WT 15 peptides, which contained S407 in addition to the nearby potential residues of phosphorylation S402, T404, and S409. When S407 was mutated to an alanine (shown in the columns with an A), the phosphorylation signals did not decrease relative to WT, indicating that the signals were due to one or more of the aforementioned serines or threonines on the 15 residue peptide ( $51.3 \pm 3.4$  units of phospho-stimulated luminescence for S407A vs.  $54.1 \pm 2.6$  for S407WT,  $p = 0.53$ ). The phosphostimulated luminescent signals decreased significantly in the phosphorylation knock-outs (shown in the columns with a KO) when all serines and threonines in the peptide fragment, including S407, were mutated to alanines ( $23.7 \pm 1.2$  for S407KO vs.  $54.1 \pm 2.6$  for S407WT,  $p < 0.01$ ). The strongest phosphostimulated luminescent signals were detected with peptide fragments corresponding to the T482 and S484 regions, as shown in **Figure 15B**. By mutating T482 and S484 to alanines individually (as well as mutating an additional potential phosphorylation site on the fragment [S475]), strong phosphostimulated luminescent signals were detected at all peptide fragments containing S484, including the T482KO (Spot 3) in which S484 was the only residue available for phosphorylation on the fragment. The peptides containing the T482 residue as the lone potential phosphorylation site (S484A, Spot 5) displayed greatly reduced signals relative to the peptides containing S484 alone ( $40.7 \pm 1.9$  for the S484A peptides containing just T482 vs.  $1605.3 \pm 67.8$  for the T482KO peptides containing just S484,  $p < 0.01$ ; **Figure 15B**). The peptides containing no serine or threonine sites (S484 KO, Spot 6) demonstrated negligible  $\delta$ CaMKII phosphorylation signals ( $34.5 \pm 3.4$ ) when all

phosphorylation sites were removed. Peptide sequences are defined in **Supplementary Table 3**. Together, results from our global carboxyl terminal and site-specific peptide arrays are consistent in demonstrating that KCNQ1 S484 is a site of CaMKII

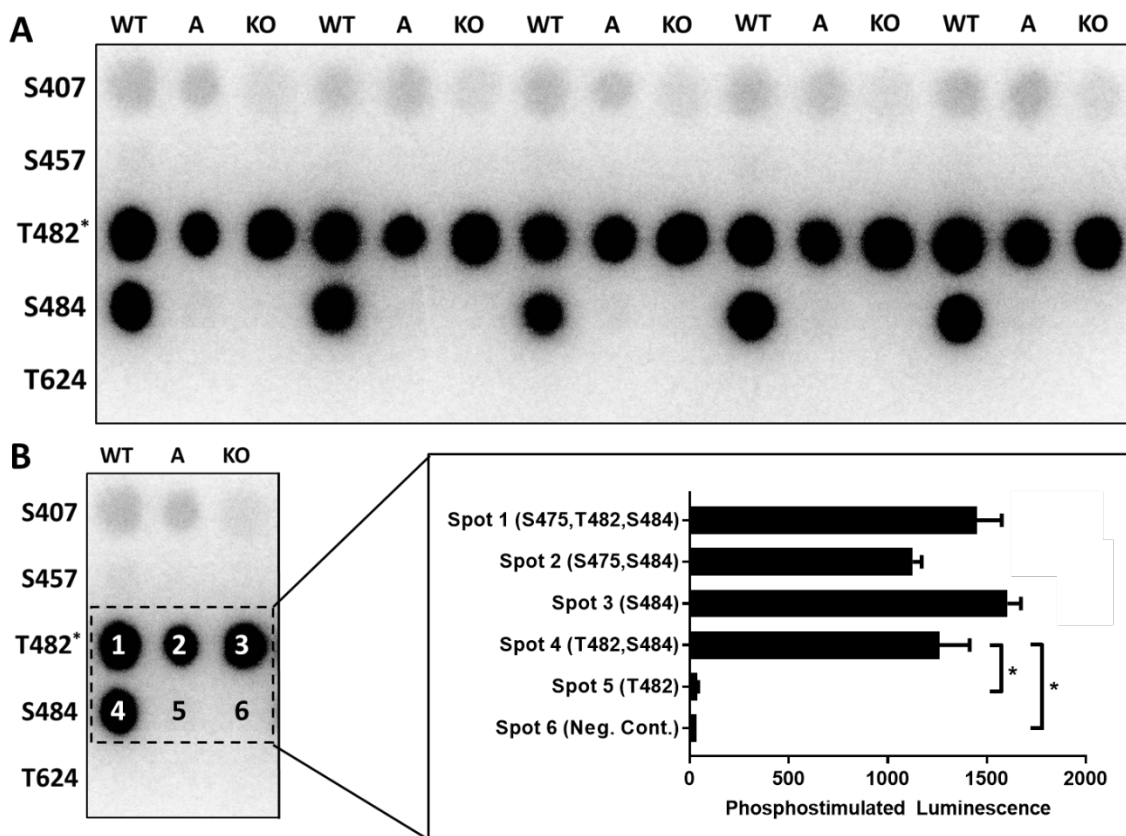


**Figure 15.** (A) Synthesized peptides corresponding to KCNQ1 carboxyl terminal residues that demonstrated basal phosphorylation were exposed to activated  $\delta$ CaMKII. Each row contains peptides corresponding to the labeled KCNQ1 residue with columns for WT, A (phospho-acceptor site mutated to alanine), or KO (all serines and threonines mutated to alanines with the exception of T482 wherein S484 was not mutated; n=5 for each condition). (B) Quantification of phosphostimulated luminescence for WT, A, and KO peptides corresponding to KCNQ1 T482 and S484 during exposure to activated  $\delta$ CaMKII. \*p<0.05

phosphorylation.

To assess the ability of CaMKII to inhibit  $I_{Ks}$  function via regulation at S457 and/or S484 (the residues which were previously shown to be critical for  $I_{Ks}$  function in **Figure 9**), constitutively active  $\delta$ CaMKII (T287D; YFP tagged) was stably expressed via lentiviral transduction in an HEK 293 cell line in which WT or mutant KCNQ1 with

KCNE1 were transiently co-expressed (methodology previously described). To control lentiviral transduction, a lentiviral vector containing only YFP was stably expressed within a control HEK 293 cell line. As shown in **Figure 16A and 16B**, mean peak corrected activation currents were reduced during CaMKII overexpression relative to the lentiviral control line when WT KCNQ1 (co-expressed with KCNE1;  $67.3 \pm 9.3$  pA/pF,  $n = 15$  in control vs.  $35.8 \pm 5.8$ ,  $n = 15$  in CaMKII overexpression at +60 mV,  $p = 0.01$ ), while activation currents with the combination dephosphorylated state mimic (Triple-A; co-expressed with KCNE1) were unchanged relative to the control line ( $78.2 \pm 7.1$ ,  $n = 14$  in control vs.  $63.7 \pm 8.5$ ,  $n = 15$  in CaMKII overexpression at +60 mV,  $p = 0.20$ ). Individual mimics of phosphorylation at S457 and S484 showed differential effects when assessed during CaMKII overexpression. In contrast to the functional inhibition seen with WT KCNQ1, S484A mutants did not demonstrate reduced activation currents during CaMKII overexpression ( $60.9 \pm 9.1$ ,  $n = 10$  for S484A mutants in CaMKII overexpression vs.  $35.8 \pm 5.8$ ,  $n = 15$  for wild-type KCNQ1 in CaMKII overexpression,  $p = 0.04$ ). Conversely, S457A demonstrated reduced activation currents during CaMKII overexpression similar to the inhibition seen with WT KCNQ1 ( $35.6 \pm 7.0$ ,  $n = 10$  for S457A mutants in CaMKII overexpression vs.  $35.8 \pm 5.8$ ,  $n = 15$  for wild-type KCNQ1 in CaMKII overexpression,  $p = 0.99$ ; **Figure 16A and 16B**). Relative to the lentiviral control cell line, the voltage dependence of activation was right-shifted with WT KCNQ1 relative to the T287D  $\delta$ CaMKII line ( $V_{1/2}$  of  $18.5 \pm 1.4$  mV,  $n = 11$  in control vs.  $22.2 \pm 0.8$ ,  $n = 11$  in CaMKII overexpression,  $p = 0.03$ ; **Figure 16C**). Rate constants of activation were not different between WT and S484A KCNQ1 when expressed in the

T287D  $\delta$ CaMKII line (**Figure 16D**); however, rate constants of deactivation were significantly reduced in cells expressing WT KCNQ1 relative to S484A (**Figure 16E**).

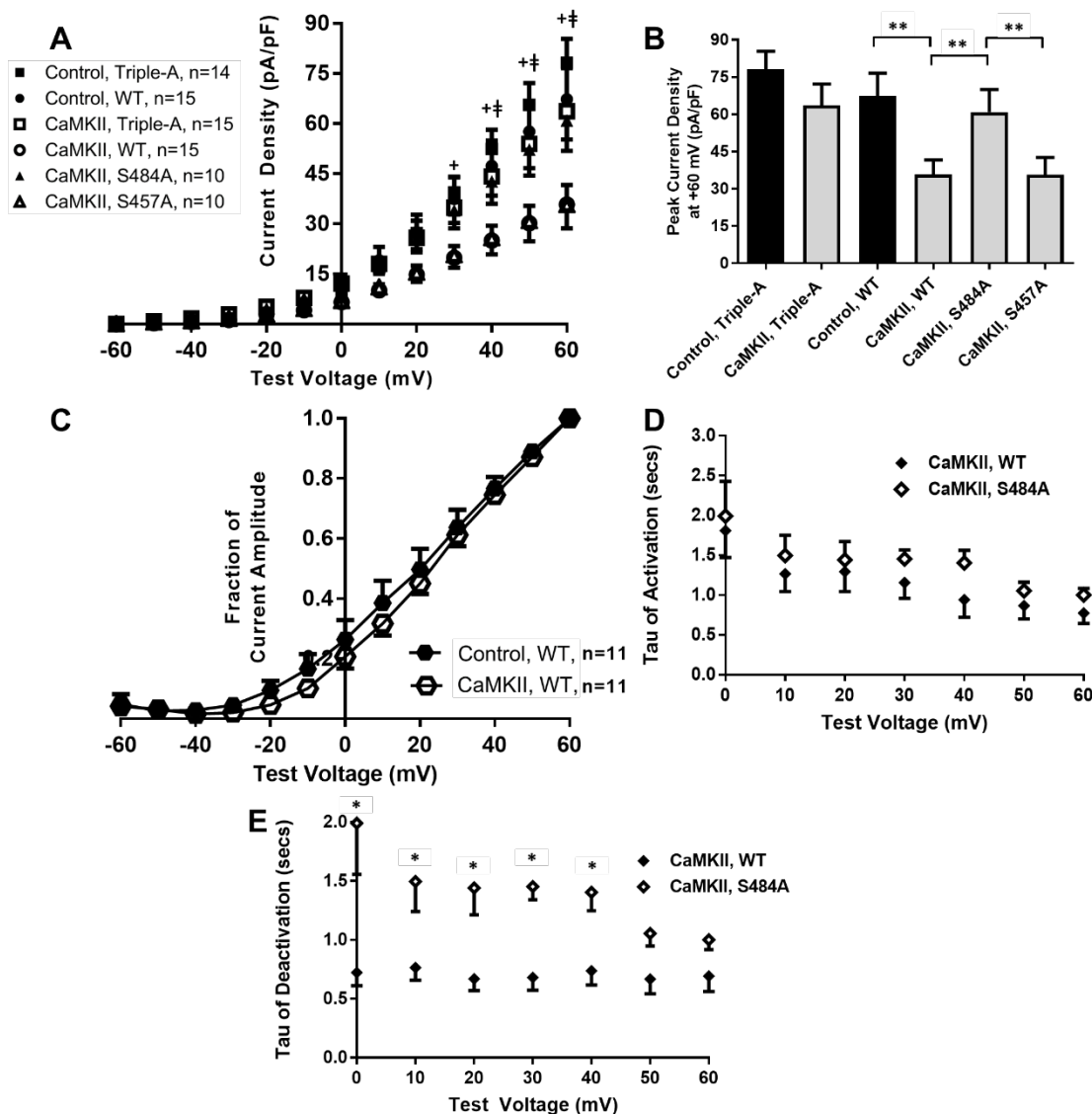


**Figure 16.** (A) I-V plots (mean and SEM) and (B) peak current density at +60 V for elicited currents during an activating voltage protocol when WT or mutant KCNQ1 was co-expressed with KCNE1 in HEK 293 cells stably overexpressing YFP-tagged constitutively active (T287D)  $\delta$ CaMKII or YFP-tagged control. (C) Normalized activation curves for WT KCNQ1 when expressed in CaMKII overexpression and control lines. Rate constants of activation (D) and deactivation (E) for WT and S484A KCNQ1 when expressed in the CaMKII overexpression line +p<0.05 for Control, WT vs. CaMKII, WT, †p<0.05 for CaMKII, S484A vs. CaMKII, WT, \*\*p<0.05 for comparison indicated, \*p<0.05 for CaMKII, WT vs. CaMKII, S484A (tau analyses)

**Table 6.** Estimated Boltzmann equation parameters for WT  $I_{Ks}$  when expressed in an HEK 293 cell line containing T287D  $\delta$ CaMKII or lentiviral control.

Mutant/Treatment	$V_{1/2}$ (mV)	Slope Factor
WT in Control Lentivirus	18.51 (1.37)	16.67 (1.26)
WT in CaMKII Lentivirus	22.21 (0.76)	14.83 (0.70)

***PKA does not mediate functional changes in  $I_{Ks}$  during sustained  $\beta$ -AR stimulation***

Based on PKA's established role as a regulator of  $I_{Ks}$  function in response to acute  $\beta$ -AR stimulation, we sought to (1) examine whether PKA signaling mediates functional inhibition of  $I_{Ks}$  in response to sustained  $\beta$ -AR stimulation and (2) assess whether the residues we previously identified in our LCMS/MS analysis (**Figure 5**) are substrates for PKA phosphorylation.

To assess the potential for PKA inhibition to reverse functional reduction of  $I_{Ks}$  activation currents during sustained ISO treatment, HEK 293 cells transiently co-expressing WT KCNQ1 and KCNE1 were treated with 100 nM ISO for 12-24 hours and co-treated with the PKA peptide inhibitor myristoylated-PKI (1  $\mu$ M in culture media for 4 hours and in pipette solution). As shown in **Figure 17**, PKI treatment did not attenuate ISO-induced inhibition of  $I_{Ks}$  activation currents ( $47.4 \pm 7.6$  pA/pF, n=10 with myr-PKI vs.  $40.9 \pm 5.9$ , n=10 with ISO, p=0.51; **Figure 17A and 17B**). Similarly, co-treatment with myr-PKI did not reverse the depolarizing shift in the voltage dependence of activation with ISO treatment ( $V_{1/2}$  of  $18.3 \pm 2.0$  mV, n=8 with myr-PKI vs.  $20.4 \pm 2.3$ , n=8 with ISO, p=0.50; **Figure 17C**).

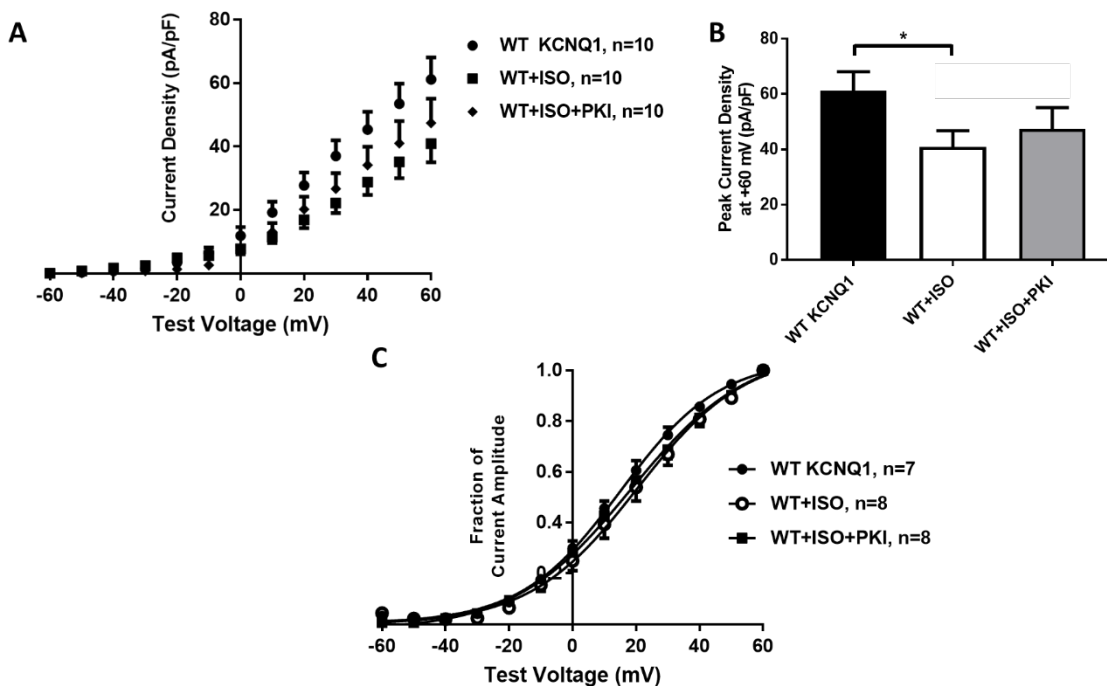


**Figure 17.** (A) I-V plots and (B) peak activation current density for WT KCNQ1/KCNE1 following treatment with vehicle, ISO, or co-treatment with ISO (100 nM for 12-24 hours) and myristoylated PKI (1  $\mu$ M in culture media and in pipette solution during recording). (C) Normalized activation curves following treatment with vehicle, ISO, and co-treatment with ISO and myristoylated PKI. \* $p < 0.05$

A peptide array was performed to assess the potential for activated PKA to phosphorylate peptide fragments corresponding to the residues identified in our LCMS/MS analysis (**Figure 5**). As shown in the top row of **Figure 18**, peptides corresponding to S457, T482, S484, and T624 on KCNQ1 showed negligible phosphorylation signals relative to kemptide positive control. While the WT S407 fragment displays a weak phosphorylation signal, this signal is not reduced in the S407 KO fragment, indicating a non-specific interaction between the peptide fragments and PKA. For comparison, the same spots when exposed to activated  $\delta$ CaMKII are shown wherein S484 is shown to be a specific site of CaMKII phosphorylation.

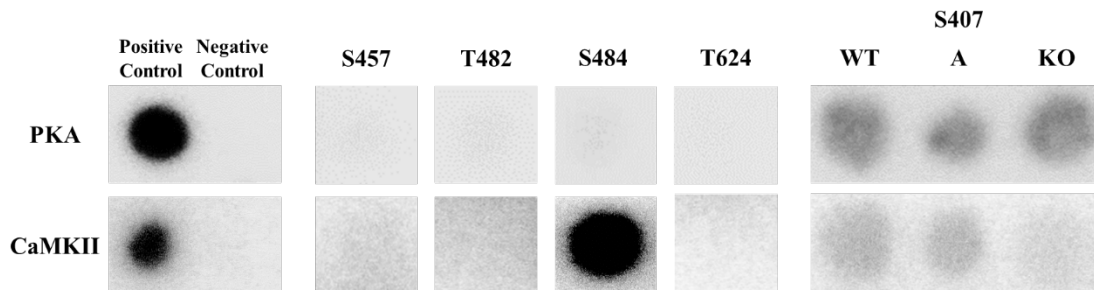


**Figure 18.** Fifteen residue peptides corresponding to the KCNQ1 carboxyl terminal residues S407, S457, T482, S484, and T624, positive control (kemptide for PKA and autocamtide-2 for CaMKII), negative controls (threonine and serine mutated to alanines on kemptide and autocamtide-2, respectively) were synthesized on a cellulose membrane and exposed to activated PKA or  $\delta$ CaMKII for 30 seconds with [ $\gamma$ - $^{32}$ ]ATP. Relative to kemptide control, peptides corresponding to S457, T482, and S484 (with nearby serines and threonines mutated to alanines), and T624 do not demonstrate phosphorylation signals when exposed to activated PKA. While S407 peptides demonstrate weak phosphorylation signals when exposed to activated PKA, analysis of the S407KO peptide, wherein all serines and threonines have been mutated to alanines, does not reduce the phosphorylation signal, indicating that the signal is being produced by a non-specific interaction of PKA and the peptide fragment. Relative to autocamtide-2 control, peptides corresponding to S457, T482 (with nearby serines and threonines, including S484, mutated to alanines), and T624 do not demonstrate phosphorylation signals when exposed to activated  $\delta$ CaMKII. S484 (with nearby serines and threonines, including T482, mutated to alanines) demonstrates strong phosphorylation signals when exposed to activated  $\delta$ CaMKII. While S407 peptides demonstrate weak phosphorylation when exposed to activated  $\delta$ CaMKII, analysis of S407A, wherein S407 has been mutated to an alanine, does not reduce the phosphorylation signal, indicating that the signal is likely mediated by another serine or threonine on the peptide fragment.

Taken together, these results demonstrate that PKA inhibition does not reverse sustained ISO-induced changes in  $I_{Ks}$  function and that the identified phosphorylation sites on the KCNQ1 carboxyl terminus are not substrates for PKA phosphorylation using our in vitro approaches. Therefore, our results indicate that, in contrast to CaMKII, PKA signaling does not mediate functional inhibition of  $I_{Ks}$  during sustained  $\beta$ -AR stimulation.

**Specific Aim 3: Evaluate the mechanistic basis for how CaMKII-mediated S484 phosphorylation, in response to sustained  $\beta$ -AR stimulation, inhibits  $I_{Ks}$  function**

As was discussed in the introductory section entitled “molecular mechanisms of  $I_{Ks}$  inhibition,” changes in the expression of KCNQ1 and/or KCNE1 mRNA and protein have not been consistently demonstrated in HF patients or in animal HF models. Likely potential mechanistic explanations for the inhibition of  $I_{Ks}$  during sustained  $\beta$ -AR stimulation include: changes in the biophysical properties of KCNQ1 (when expressed alone) or  $I_{Ks}$  (co-expression with KCNE1); reduced trafficking and/or plasma membrane expression of KCNQ1 and/or KCNE1; alteration of the interaction between KCNQ1 and its required auxiliary subunits (e.g. KCNE1, CaM). In our final specific aim, we performed experiments investigating the potential for the aforementioned mechanisms to mediate functional inhibition of  $I_{Ks}$  during sustained  $\beta$ -AR stimulation.

***The KCNQ1 carboxyl terminus is differentially phosphorylated during co-expression with KCNE1***

In order to assess whether functional interaction with KCNE1 affects the phosphorylation status of the KCNQ1 carboxyl terminus, we utilized the LCMS/MS approach that we employed previously to assess phosphorylation at the KCNQ1 residues that demonstrated basal phosphorylation (S407, S457, T482, S484, T624). cDNAs encoding for human KCNQ1 (and KCNE1 in the co-expression group) were transiently expressed in HEK 293 cells to assess KCNQ1 phosphorylation in the presence and absence of KCNE1 co-expression. As shown in **Figure 19**, phosphorylation was identified at S407, S457, T482, and S484 (phosphorylation was not identified at 624 in this assay). When KCNQ1 was co-expressed with KCNE1, phosphorylation was decreased at S457, T482, and S484 relative to KCNQ1 expression alone.

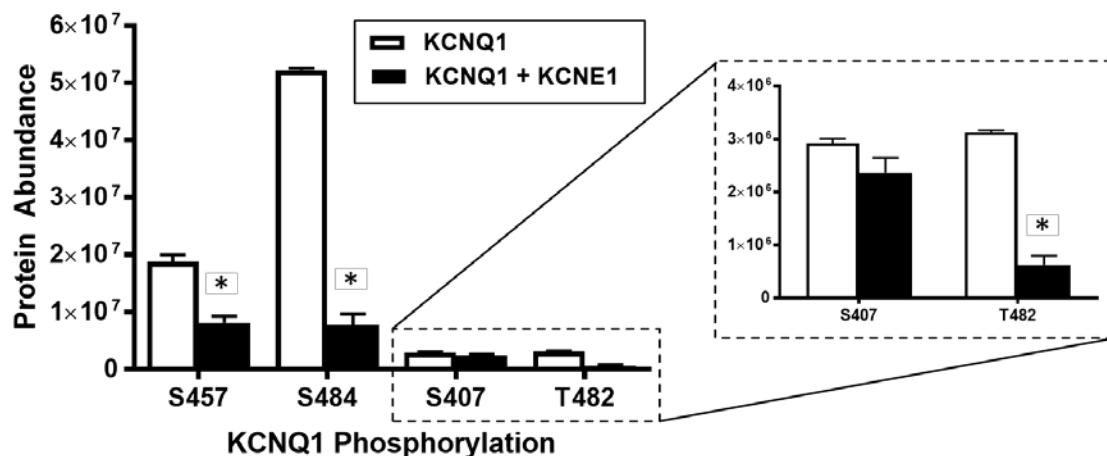


**Figure 19.** Phosphorylation was assessed via LCMS/MS at the five KCNQ1 carboxyl terminal residues that previously demonstrated basal phosphorylation (S407, S457, T482, S484, T624) in the presence (white bars) and absence (black bars) of co-expression with KCNE1. Phosphorylation was reduced at S457, T482, and S484 when KCNQ1 was co-expressed with KCNE1. Phosphorylation at T624 was not detected in the assay. \* $P < 0.05$  vs. KCNQ1 expression alone

Since the functional interaction between KCNQ1 and KCNE1 involves protein-protein interactions between the carboxyl termini of KCNQ1 and KCNE1, these results suggest that protein-protein interactions with KCNE1 reduce basal phosphorylation of KCNQ1 in the vicinity of S457 through S484. Based on this finding, we hypothesized that KCNQ1 phosphorylation at S484 might similarly reduce protein-protein interaction with KCNE1 and thereby inhibit  $I_{Ks}$  function.

***Mimics of phosphorylation at S484 inhibit KCNQ1 function only during co-expression with KCNE1***

To functionally assess the potential for competition between KCNQ1 phosphorylation at S484 and functional interaction with KCNE1, we performed patch clamp electrophysiology experiments with differential mimics of phosphorylation at S484 (S484A and S484D KCNQ1) in the presence and absence of KCNE1 co-expression. As displayed in **Figure 20A and 20B**, activation currents were not different

among WT ( $23.9 \pm 3.0$  pA/pF [mean  $\pm$  SEM] at +60 mV, n=15), S484A ( $22.8 \pm 3.8$ , n=15), and S484D ( $23.7 \pm 2.6$ , n=15) KCNQ1 when expressed in HEK 293 cells in the absence of KCNE1 co-expression ( $p=0.96$ ). Similarly, the voltage dependence of activation was not different between WT ( $V_{1/2}$ :  $15.9 \pm 3.8$  mV, n=13), S484A ( $10.6 \pm 1.5$ , n=15), or S484D ( $11.6 \pm 4.1$ , n=15) KCNQ1 when expressed with KCNE1 co-expression ( $p=0.51$ ; **Figure 20C**).

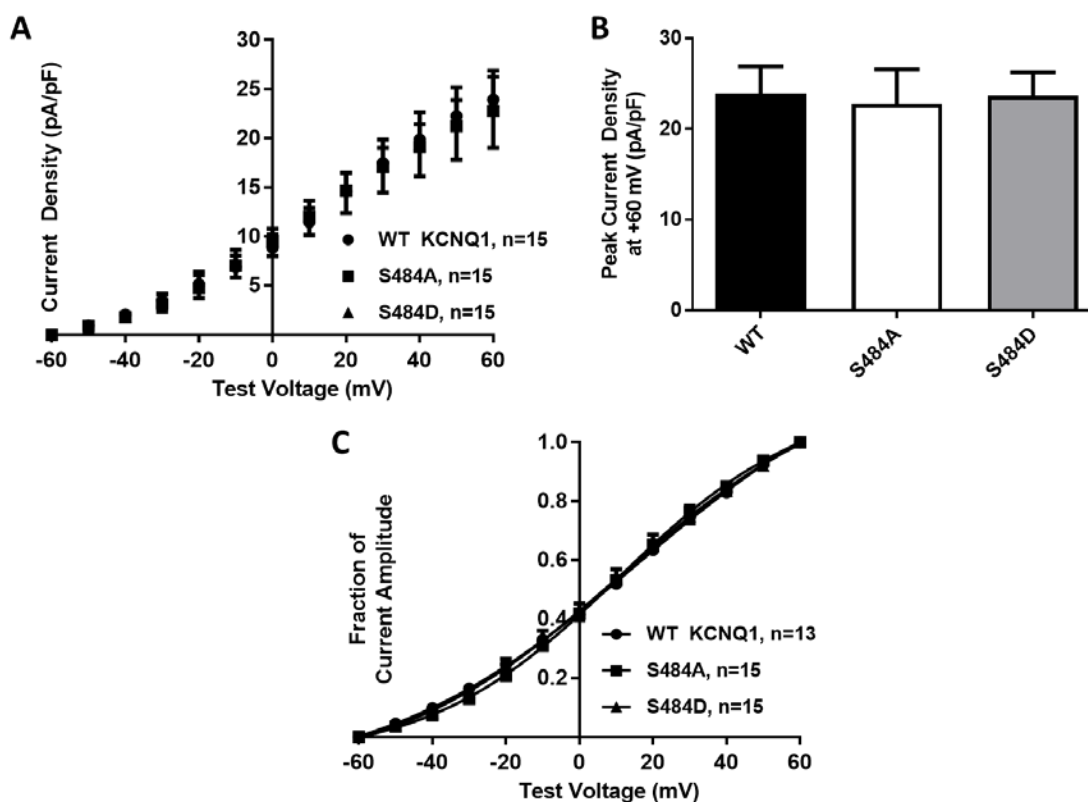


**Figure 20.** (A) I-V plots and (B) peak activation current density for WT, S484A, and S484D KCNQ1 expressed in the absence of KCNE1 in HEK 293 cells. (C) Normalized activation curves for WT, S484A, and S484D KCNQ1.

**Table 7.** Estimated Boltzmann equation parameters for WT, S484A, and S484D KCNQ1 when expressed in the absence of KCNE1 in HEK 293 cells.

Mutant	$V_{1/2}$ (mV)	Slope Factor
WT	15.9 (3.8)	35.0 (4.5)
S484A	10.6 (1.5)	25.6 (1.8)
S484D	11.6 (4.1)	31.3 (5.4)

The lack of a functional difference between S484A and S484D KCNQ1 in the absence of KCNE1 co-expression is in contrast to that seen during co-expression of KCNE1 (**Figure 9C**). This contrast suggests that the phosphorylation at S484 does not impact the inherent biophysical properties of KCNQ1 channels alone, but instead may impact the formation of functional protein-protein complexes with KCNE1.

Accordingly, our subsequent experiments pursued methodological techniques to assess the interaction of KCNQ1 and KCNE1 in response to S484 phosphorylation and sustained  $\beta$ -AR stimulation.

***Utilizing LQT1 mutations in the vicinity of KCNQ1 S484 as a translational tool to assess CaMKII regulation during sustained  $\beta$ -AR stimulation***

Large electronic long QT databases, which record mutations observed in genes known to affect the cardiac QT interval along with the phenotype associated with these mutations (when available), have been compiled to assist in both clinical and research applications. One such database, maintained by the Zhejiang University Center for Genetic and Genomic Medicine, contains nearly 850 entries for distinct LQT1 mutations that have been discovered clinically (database available at: [http://www.genomed.org/lovd2/home.php?select\\_db=KCNQ1](http://www.genomed.org/lovd2/home.php?select_db=KCNQ1)). In utilizing Scansite 4.0 to predict potential sites for CaMKII phosphorylation in the vicinity of the CaM-binding domains in KCNQ1 carboxyl terminal helices A and B, the sites of S457 and S484 were identified. The Zhejiang University database was then scanned for LQT1 mutations in close proximity to these sites, revealing three LQT1 mutations around S457 (R452W, H455Y, and G460S) and two LQT1 mutations in the vicinity of S484 (R481I and S484T).

Immobilized peptides corresponding to the predicted KCNQ1 sites of CaMKII regulation and the surrounding LQT1 sites were then synthesized on a cellulose membrane and exposed to calcium-CaM-activated CaMKII along with [ $\gamma$ - $^{32}$ P] ATP to identify sites of CaMKII phosphorylation. As shown in **Figure 21**, S457 was not a substrate for CaMKII phosphorylation, and the LQT1 mutations around the site, including G460S which introduced an additional potential phosphorylation site, did not enhance CaMKII phosphorylation.

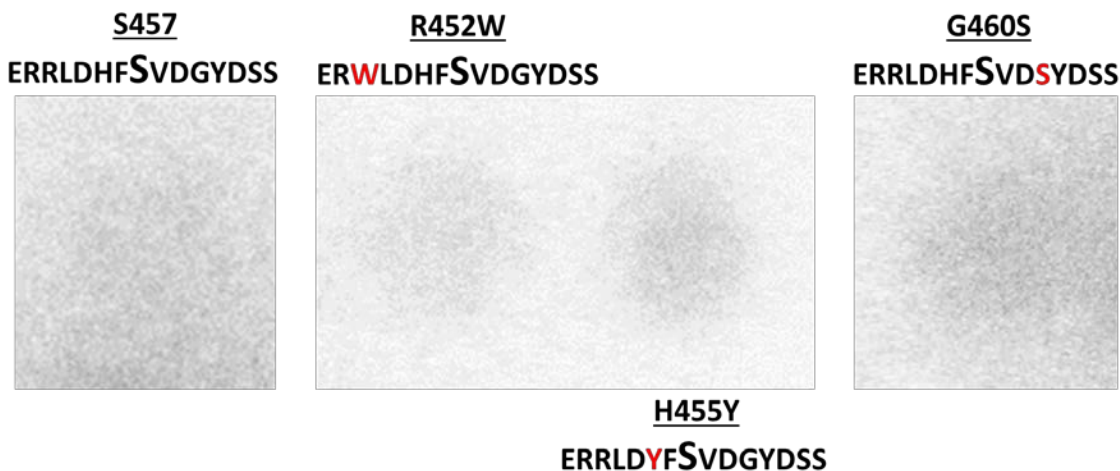


**Figure 21.** Peptide fragments corresponding to S457 on KCNQ1 and LQT1 mutations surrounding the site (R452W, H455Y, or G460S) did not display phosphorylation signals when exposed to activated CaMKII and radiolabeled ATP.

In contrast, strong CaMKII phosphorylation signals were seen at S484 (**Figure 22**). Interestingly, phosphorylation was prevented by the R481I LQT1 mutation, which removes an arginine residue from three places before S484, but was unaffected by the S484T LQT1 mutation. Based upon the differential abilities of these two LQT1 mutations to disrupt CaMKII phosphorylation at S484, these mimics will be used as experimental tools in assessing the mechanistic basis for S484 phosphorylation to disrupt

I<sub>Ks</sub> function. In addition, these analyses investigate the functional implications of these previously uncharacterized mutations on KCNQ1-KCNE1 biology.

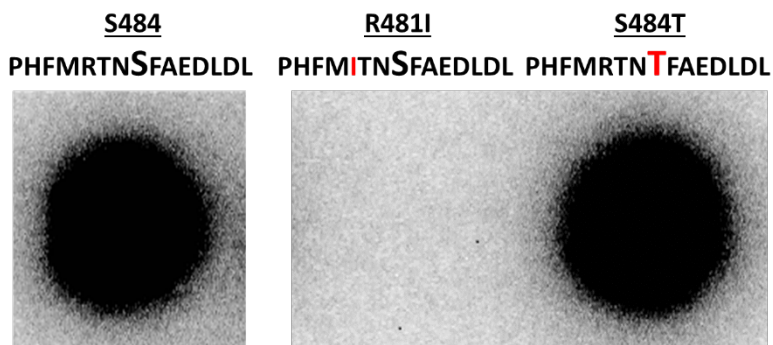


**Figure 22.** Peptide fragments corresponding to S484 were substrates for CaMKII phosphorylation, and CaMKII phosphorylation was disrupted by R481I but not S484T LQT1 mutations.

***Sustained  $\beta$ -AR stimulation and mimics of phosphorylation and dephosphorylation at S484 disrupt the interaction between KCNQ1 and KCNE1 subunits***

Bimolecular fluorescence complementation (BiFC) is a live-cell imaging technique in which complementary halves of a fluorophore (the yellow fluorescent protein Venus was used in this series of experiments) are expressed on the termini of putative interacting proteins. A primary advantage of BiFC relative to classical techniques to assess protein-protein interactions (e.g. protein-protein co-immunoprecipitation) is that it allows detection of protein-protein interactions within a living cell. In these experiments, cDNA plasmids encoding for KCNQ1 and KCNE1 with complementary halves of Venus connected to their carboxyl termini (plasmids with WT or mutant KCNQ1 contained the amino half of Venus while plasmids with WT KCNE1 contained the carboxyl half of Venus) were transiently co-expressed in HEK 293 cells along with the cytosolic cyan fluorescent protein, Cerulean. Venus fluorescent

signals were normalized to Cerulean fluorescent signals in all experiments to control for the efficiency of cDNA transfection and cellular expression of the encoded proteins.

In order to assess the potential for phosphorylation at S484 to disrupt the intracellular interaction of KCNQ1 and KCNE1 proteins, Venus BiFC plasmids encoding for WT KCNQ1 (in control conditions and during ISO treatment), S484A KCNQ1, and S484D KCNQ1 were transiently co-expressed (Lipofectamine 2000<sup>®</sup>) with Venus BiFC plasmids encoding WT KCNE1 in HEK 293 cells. Cells were visualized using a Leica<sup>®</sup> SP8 Resonant-scanning confocal/multiphoton microscope at ~48 hours follow transfection using a two sequence procedure that utilized a 405 nm laser to excite Cerulean followed by a 488 nm laser to excite Venus. Images were taken at 0.5  $\mu\text{m}$  increments in the Z-direction (vertical), and composite images were created that summed fluorescent intensity for each pixel in all Z planes using Fiji<sup>®</sup> software. Freehand regions of interest were used to trace cell boundaries based on Cerulean intensity, and the mean fluorescent intensity within each region was calculated in Fiji<sup>®</sup>. The same regions of interest were used to assess mean Venus and Cerulean intensities in the same cells in all experiments. Expression of average Venus intensity was normalized to average Cerulean intensity in each region of interest (cell), and mean Venus:Cerulean ratios were compared among experimental groups via Student's *t*-test (WT vs. WT+ISO; S484A vs. S484D; WT+ISO+KN-93 vs. WT+ISO+KN-92; R481I+ISO vs. S484T+ISO). Representative summed images of cells expressing Venus and Cerulean in all experimental groups are shown in **Figure 23-25**.

As shown in the bar graph in **Figure 23**, mean Venus:Cerulean ratios were decreased with mimics of phosphorylation at S484 (S484D;  $0.38 \pm 0.01$  [mean  $\pm$  SEM]),

n=40) relative to mimics of dephosphorylation (S484A;  $0.87 \pm 0.09$ , n=37;  $p < 0.01$ ).

Similarly, mean Venus: Cerulean ratios were reduced during treatment with 100 nM ISO for 12-24 hours ( $0.38 \pm 0.03$ , n=50) relative to vehicle control ( $0.44 \pm 0.02$ , n=62;  $p < 0.05$ ).

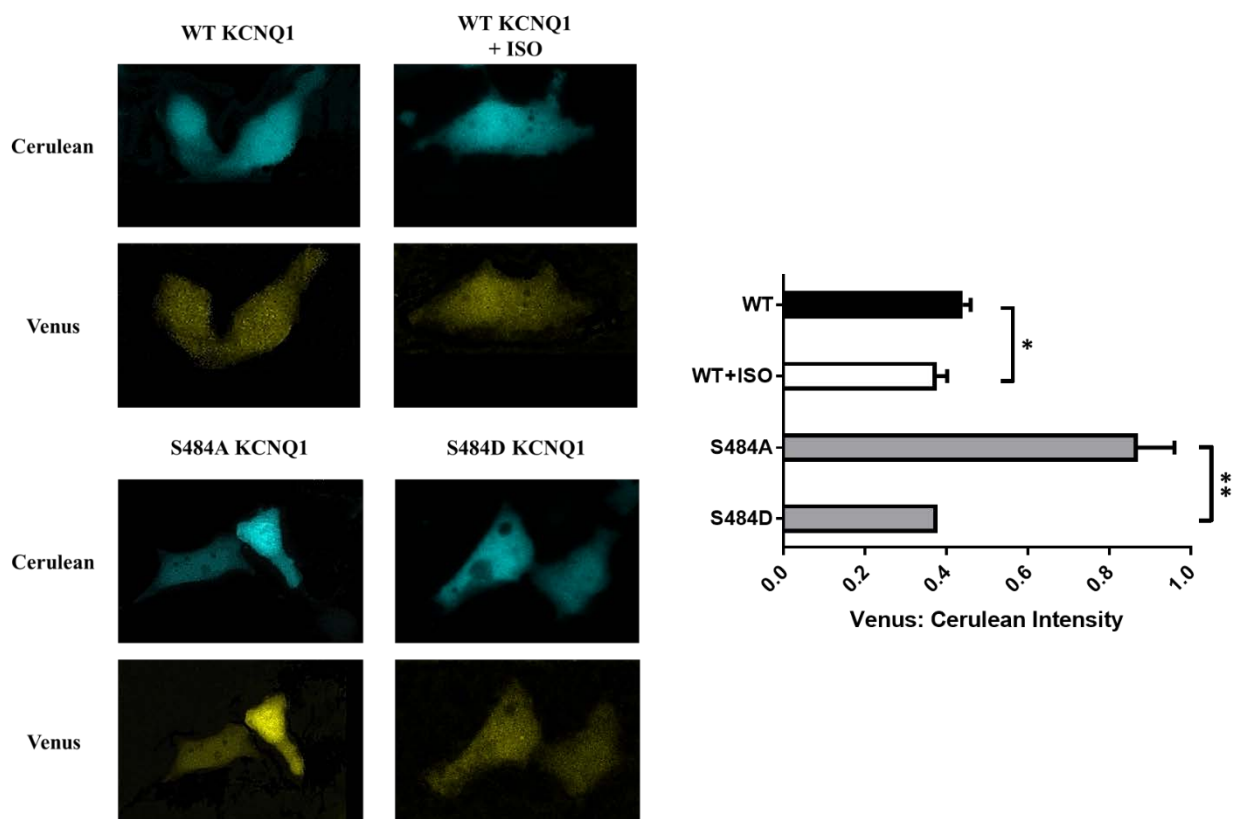


**Figure 23.** (Left) Representative summed images of HEK 293 cells transiently co-expressing cytosolic Cerulean fluorescent proteins (cyan) and Venus fluorescent proteins (yellow) encoded in plasmids containing WT KCNQ1 in control conditions, WT KCNQ1 during treatment with 100 nM ISO for 12-24 hours, S484A KCNQ1 in control conditions, and S484D KCNQ1 in control conditions along with WT KCNE1. (Right) Mean ratios of Venus: Cerulean fluorescent intensities for WT KCNQ1/KCNE1 in control conditions and during 12-24 hour treatment with 100 nM ISO, S484A KCNQ1/KCNE1, and S484D KCNQ1/KCNE1. \* $p < 0.05$ , \*\* $p < 0.01$  for comparison indicated

***CaMKII signaling disrupts the interaction between KCNQ1 and KCNE1 subunits during sustained  $\beta$ -AR stimulation via regulation at S484***

To assess the potential for CaMKII regulation at S484 to mediate the reduced cellular interaction observed between KCNQ1 and KCNE1 subunits, we utilized CaMKII

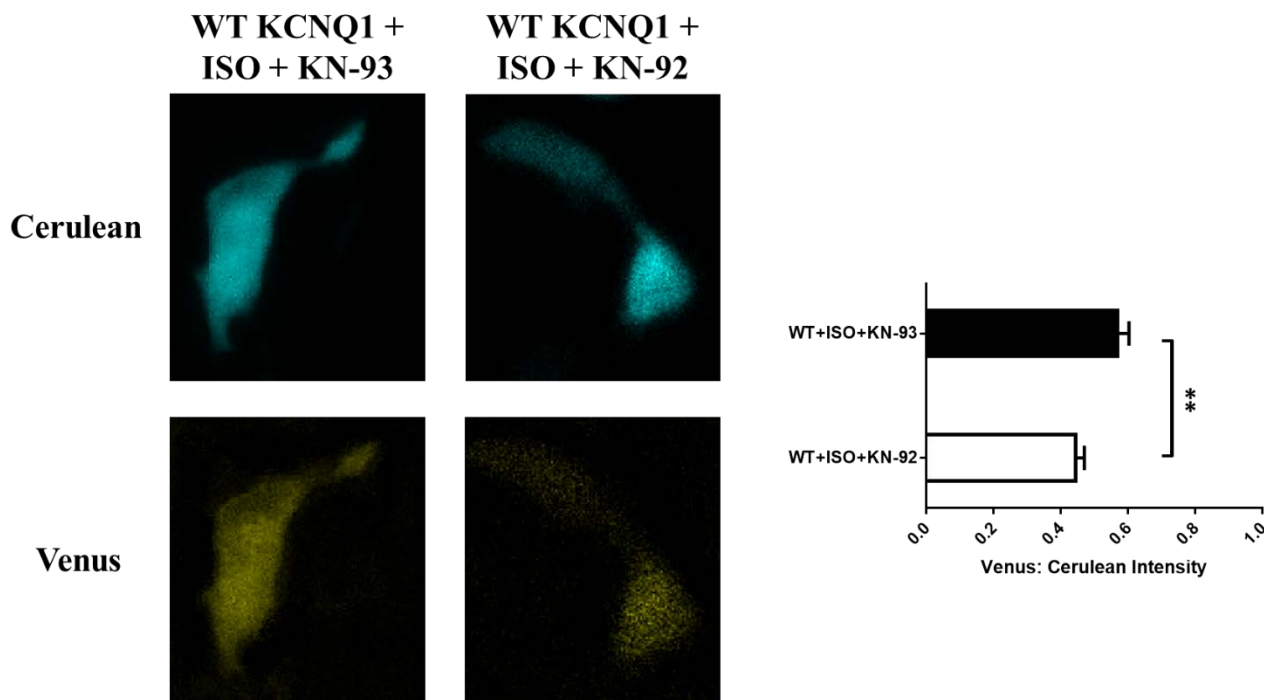


**Figure 24.** (Left) Representative summed images of HEK 293 cells transiently co-expressing cytosolic Cerulean fluorescent proteins (cyan) and Venus fluorescent proteins (yellow) encoded in plasmids containing WT KCNQ1 and KCNE1 during 12-24 hour co-treatment with 100 nM ISO and the specific CaMKII chemical inhibitor, KN-93, or its inactive analogue, KN-92 (500 nM for both). (Right) Mean ratios of Venus: Cerulean fluorescent intensities for WT KCNQ1/KCNE1 during co-treatment with ISO and KN-93 or KN-92. \*\*P<0.01 for comparison indicated

inhibition and R481I and S484T mutants during ISO treatment. HEK 293 cells expressing Venus and Cerulean plasmids were co-treated with 100 nM ISO and 500 nM of the chemical CaMKII inhibitor KN-93 or KN-92, its inactive control. As shown in the representative images and bar graph **Figure 24**, treatment with KN-93 ( $0.57 \pm 0.03$ , n=33) attenuated ISO treatment-induced reductions in Venus: Cerulean ratios relative to KN-92 control ( $0.45 \pm 0.02$ , n=37); p<0.01).

The role of CaMKII in mediating reduced KCNQ1-KCNE1 interaction via regulation at S484 was supported by our analyses with the LQT1 mutations R481I and S484T. Since the R481I mutation was shown to disrupt CaMKII phosphorylation at S484 in our peptide array experiments (**Figure 22**), we hypothesized that R481I KCNQ1 would prevent CaMKII-mediated disruption of the KCNQ1-KCNE1 interaction during sustained ISO treatment. Conversely, we hypothesized S484T KCNQ1 would not prevent CaMKII-mediated changes during sustained ISO treatment based S484T still being a site of CaMKII phosphorylation in peptide array experiments. In accordance with our hypotheses, we found that R481I KCNQ1 ( $0.53 \pm 0.04$ , n=63) attenuated ISO

treatment-induced reductions in Venus: Cerulean ratios relative to S484T KCNQ1 ( $0.41 \pm 0.01$ ,  $n=55$ ;  $p<0.01$ ; **Figure 25**).

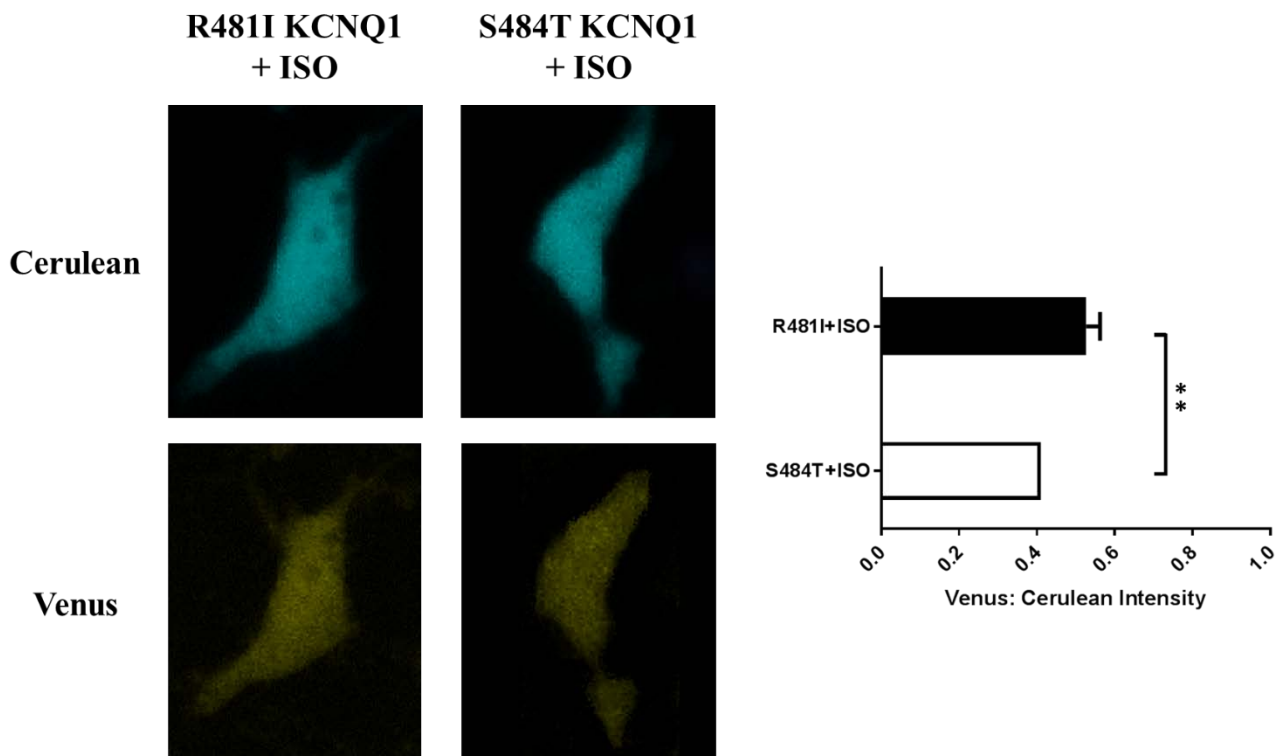


**Figure 25.** (Left) Representative summed images of HEK 293 cells transiently co-expressing cytosolic Cerulean fluorescent proteins (cyan) and Venus fluorescent proteins (yellow) encoded in plasmids containing R481I or S484T KCNQ1 during 12-24 hour treatment with 100 nM ISO. (Right) Mean ratios of Venus: Cerulean fluorescent intensities for R481I or S484T KCNQ1/WT KCNE1 during treatment with ISO. \*\* $P<0.01$  for comparison indicated

Together, these results illustrate the importance of CaMKII regulation at S484 to mediate disruption of the functional interaction between KCNQ1 and KCNE1 during sustained  $\beta$ -AR stimulation. When CaMKII is functionally inhibited or when S484 is unable to be regulated by CaMKII (such as when the arginine at 481 is replaced by an isoleucine) the effect of sustained ISO treatment in reducing the interaction of KCNQ1 and KCNE1 is blunted, as evidenced by attenuation of Venus: Cerulean ratios in these experimental conditions.

***Phosphorylation at S484 reduces plasma membrane expression of KCNQ1 and KCNE1 subunits***

To assess the potential for S484 phosphorylation to alter plasma membrane expression of KCNQ1 and/or KCNE1 subunits, we utilized a commercially available technique that utilizes N-hydroxy-succinimide reversibly conjugated to avidin to label and isolate membrane-bound proteins (Pierce Cell Surface Protein Isolation Kit, Cat. #: 89881; ThermoScientific®). S484A and S484D KCNQ1 were transiently co-expressed along with WT KCNE1 in HEK 293 cells, and labeling and isolation of membrane-bound proteins was performed at ~48 hours following transfection. Changes in subunit expression were investigated via protein immunoblot using antibodies against KCNQ1, KCNE1, and the Na<sup>+</sup>/K<sup>+</sup>-ATPase (used as a membrane-bound loading control). As shown in **Figure 26**, KCNQ1 expression (analyzed as the ratio of KCNQ1 signal [band at 75 kDa] to Na<sup>+</sup>/K<sup>+</sup>-ATPase signal [band at 113 kDa]) was reduced by ~15% with S484D (phosphorylation mimics) relative to S484A (p<0.05, n=6 per condition; **Figure 26B**). KCNE1 expression (analyzed as the ratio of KCNE1 signal [band at 17 kDa] to Na<sup>+</sup>/K<sup>+</sup>-ATPase signal [band at 113 kDa]) demonstrated an even greater reduction in expression (~33%) with S484D mutants relative to S484A (p<0.05, n=6 per condition; **Figure 26C**).

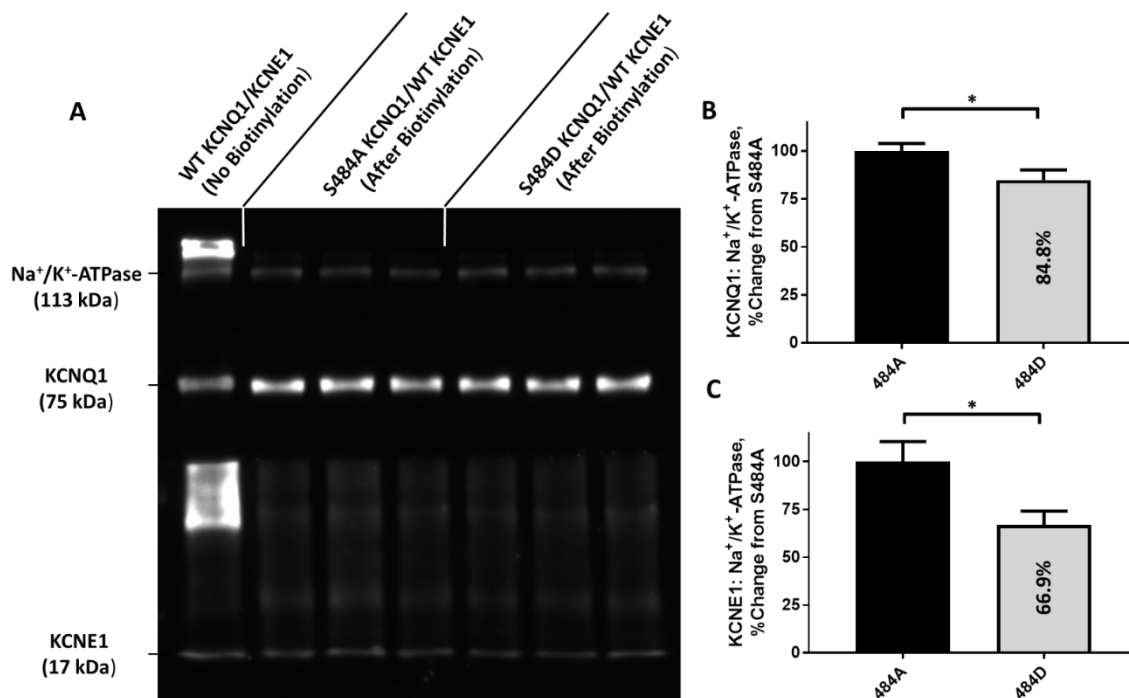


**Figure 26.** (A) Representative protein immunoblot from HEK 293 cells transiently co-expressing WT KCNQ1/KCNE1 (no biotinylation), S484A KCNQ1/WT KCNE1 (after isolation of plasma membrane-bound proteins via biotinylation), and S484D KCNQ1/WT KCNE1 (after biotinylation) following treatment with KCNQ1, KCNE1, and Na<sup>+</sup>/K<sup>+</sup>-ATPase (membrane-bound loading control) antibodies. (B) Percent change in KCNQ1:Na<sup>+</sup>/K<sup>+</sup>-ATPase ratios relative to S484A. (C) Percent change in KCNE1:Na<sup>+</sup>/K<sup>+</sup>-ATPase ratios relative to S484A. \*p<0.05

## DISCUSSION

### **Regulation of the KCNQ1 carboxyl terminus by CaMKII during sustained $\beta$ -AR stimulation**

The first specific aim examines the regulation of the KCNQ1 carboxyl terminus during sustained  $\beta$ -AR stimulation and the associated functional implications on  $I_{Ks}$ . Using a phosphoproteomics approach, we identify five KCNQ1 carboxyl terminal sites (S407, S457, T482, S484, T624) that demonstrate basal phosphorylation when expressed in HEK 293 cells. By investigating changes in KCNQ1 phosphorylation during ISO treatment, we find that two of these residues (T482 and S484) demonstrate increased phosphorylation during sustained  $\beta$ -AR stimulation. Additionally, we utilized a bioinformatics approach that predicted two of these residues (S457 and S484) as CaMKII substrates.

Based on these findings, we next investigated the functional implications of phosphorylation at S457, T482, and S484. Utilizing patch clamp electrophysiology with mimics of phosphorylation (aspartic acid) and dephosphorylation (alanine), we demonstrate that combination mimics of phosphorylation at S457, T482, and S484 recapitulate observed functional inhibition of  $I_{Ks}$  seen during sustained ISO treatment. When investigating these residues individually, we find that differential phosphorylation at S457 and S484 affect  $I_{Ks}$  function by reducing current density and causing a depolarizing shift in the voltage dependence of activation.

Specific Aim 2 investigated the potential for CaMKII signaling to mediate functional inhibition of  $I_{Ks}$  during sustained  $\beta$ -AR stimulation, including the specific phosphorylation site on KCNQ1. Utilizing protein immunoblot to assess phosphorylation

at T287 on CaMKII, an autophosphorylation site that confers constitutive kinase activity, we demonstrate the CaMKII is functionally enhanced during ISO treatment. Patch clamp experiments following co-treatment with ISO and peptide (CN21) or chemical (KN-93) CaMKII inhibitors demonstrate that CaMKII signaling mediates functional inhibition of  $I_{Ks}$  during ISO treatment. To probe for CaMKII phosphorylation sites on the KCNQ1 carboxyl terminus, we utilized peptide array experiments which assessed the potential for CaMKII to phosphorylate the five KCNQ1 residues that demonstrated basal phosphorylation via LCMS/MS analysis. These peptide array data demonstrate that S484 is a substrate for CaMKII phosphorylation, and this finding was corroborated by functional experiments in which we saw that expression of S484A KCNQ1 attenuated functional inhibition of  $I_{Ks}$  within a cell line overexpressing CaMKII.

Taken together, these results demonstrate that, in response to sustained  $\beta$ -AR stimulation, CaMKII phosphorylates KCNQ1 at S484 to inhibit  $I_{Ks}$  function. The inhibition of  $I_{Ks}$  current density is consistent with the depolarizing (inhibitory) shift in the voltage dependence of activation observed during ISO treatment and CaMKII overexpression; these inhibitory changes are also consistent with decreases in the rate constants of activation and deactivation during ISO treatment, CaMKII overexpression, and with aspartic acid mutations conferring mimics of phosphorylation. Findings from our functional analyses are consistent with our proteomic and biochemical analyses, which demonstrate that phosphorylation at S484 is enhanced during sustained  $\beta$ -AR stimulation and that S484 is a substrate for CaMKII phosphorylation. The electrophysiological changes seen independently during both CaMKII overexpression and S484 phosphorylation recapitulate the functional reductions seen during sustained

ISO treatment. These findings suggest that, at least in our cellular expression system, CaMKII-mediated phosphorylation of S484 is sufficient to account for the entirety of the functional changes in  $I_{Ks}$  during sustained  $\beta$ -AR stimulation.

An additional finding in our investigation is that phosphorylation at KCNQ1 S457, a site that demonstrated basal phosphorylation in our LCMS/MS analysis, also has inhibitory functional consequences on  $I_{Ks}$ , including inhibition of activation and tail current density and a depolarizing shift in the voltage dependence of activation. Further analyses revealed that S457 is not a site of CaMKII phosphorylation. Therefore, it remains unclear which signaling pathway regulates phosphorylation at S457 and whether the site has any pathophysiological relevance in the setting of HF.

The present work investigates the potential for  $I_{Ks}$  regulation during sustained  $\beta$ -AR stimulation by CaMKII, a serine/threonine kinase known to pathologically regulate ion channel function and excitation-contraction coupling in cardiomyocytes during HF.<sup>53</sup> Furthermore, CaMKII has been demonstrated to mediate arrhythmia development in a vast range of cardiac diseases, including HF, through aberrant calcium handling.<sup>116-118</sup> Interestingly, sustained  $\beta$ -AR stimulation has been shown to increase the function and expression of CaMKII.<sup>119-122</sup> Through regulation of cardiac ion channels, including the repolarizing potassium channels  $I_{to}$  and  $I_{K1}$ , CaMKII mediates increases in both action potential duration and arrhythmogenic propensity in HF models.<sup>97,116,118,123</sup> While CaMKII regulation of  $I_{Ks}$  has not been previously established, investigations of LQT1 mutants in the KCNQ1 carboxyl terminus demonstrate a necessary role for CaM in both  $I_{Ks}$  trafficking and channel gating.<sup>10,28-30</sup>

Several experiments from the current study suggest that the functional regulation of  $I_{Ks}$  by CaMKII occurs via phosphorylation at S484, a residue in the carboxyl terminus that lies between two CaM-binding domains in helices A and B of KCNQ1. We demonstrated the site-specific nature of regulation at S484 by means of functional investigation of  $I_{Ks}$  in a CaMKII overexpression system with KCNQ1 mutations preventing phosphorylation at S484 and the demonstration of direct CaMKII phosphorylation with peptide fragments simulating KCNQ1 S484. Interestingly, an LQT1 mutation has previously been identified at S484 (S484T), but the functional importance of the site has not been experimentally investigated outside of the present study.<sup>124</sup> LQT1 mutations have not been identified at the other two identified phosphorylation sites, S457 or T482, though our functional investigations indicate that phosphorylation at S457 has the potential to regulate  $I_{Ks}$  function.

Aflaki, et al. assessed the regulation of  $I_{Ks}$  during sustained  $\beta$ -AR stimulation in a guinea pig model using long-term ISO treatment.<sup>21</sup> In accordance with our results, they found significant  $I_{Ks}$  inhibition in response to ISO treatment for 30 hours. Additionally, their work demonstrated a role for the exchange protein directly activated by cyclic-AMP (Epac) pathway in mediating  $I_{Ks}$  inhibition during sustained  $\beta$ -AR stimulation by systematically inhibiting various elements of the Epac signaling cascade, including CaMKII. Given the established role of CaMKII as a downstream effector during Epac activation, it is not surprising that Epac-mediated functional reductions in  $I_{Ks}$  during sustained  $\beta$ -AR stimulation were reversed with CaMKII inhibition.<sup>65,75-77,125</sup> Therefore, the findings from Aflaki et al. support those of our own analyses which demonstrate that CaMKII regulates  $I_{Ks}$  during sustained  $\beta$ -AR stimulation. Utilizing a combination of

proteomic, biochemical, and electrophysiological approaches, we demonstrate novel site-specific regulation of KCNQ1 at S484 by CaMKII.

This study expands on previous findings to propose a molecular understanding of how CaMKII regulates  $I_{Ks}$  function during sustained  $\beta$ -AR stimulation, including experiments that demonstrate site-specific KCNQ1 regulation at S484. Based on its established role as a pro-arrhythmogenic mediator in HF and its demonstrated ability to inhibit  $I_{Ks}$  during sustained  $\beta$ -AR stimulation in the present study, increased CaMKII activation may contribute to the increased prevalence of arrhythmogenesis in HF patients.

A 2018 investigation by Gou, et al. demonstrates functional inhibition of  $I_{Ks}$  during treatment with angiotensin II that is mediated by PKC- $\epsilon$  and involves phosphorylation of the KCNQ1 amino terminus (S95 and T96) as well as a distal site on the accessory subunit, KCNE1 (S102).<sup>47</sup> Though the authors conclude that “PKC- $\epsilon$  mediates the inhibitory action of angiotensin II on  $I_{Ks}$  by phosphorylating distinct sites on KCNQ1/KCNE1,” their analyses only (1) investigate the functional implications of mimics of phosphorylation at nine residues predicted to be PKC- $\epsilon$  substrates by KinasePhos 2.0 and (2) demonstrate that PKC- $\epsilon$  signaling mediates inhibition of  $I_{Ks}$  by angiotensin II. As the authors do not demonstrate actual PKC- $\epsilon$ -mediated phosphorylation of KCNQ1, it is possible, particularly in the context of the surrounding literature, that PKC- $\epsilon$  is actually a mediator of signaling in this pathway rather than the effector that directly regulates KCNQ1 and thereby  $I_{Ks}$ . Multiple investigations have characterized a cellular signaling pathway in the context of sustained  $\beta$ -AR stimulation and HF that involves activation of Epac, PKC- $\epsilon$ , and finally CaMKII as the effector during sustained activation of the cardiac  $\beta_1$ -AR, as shown in **Figure 27** below<sup>76,79</sup>;

therefore, there exists the potential for this  $\text{Epac} \rightarrow \text{PKC-}\epsilon \rightarrow \text{CaMKII}$  pathway to mediate the functional results in the Gou, et al. investigation, thus tying angiotensin II and catecholaminergic signaling (the two predominant neurohormonal changes involved in HF pathophysiology) together into a single cellular signaling pathway. The potential for crosstalk between the cellular signaling cascades that mediate regulation of KCNQ1 following activation of the  $\beta$ -AR and the angiotensin II receptor type 1 (AT<sub>1</sub>) warrants further investigation.

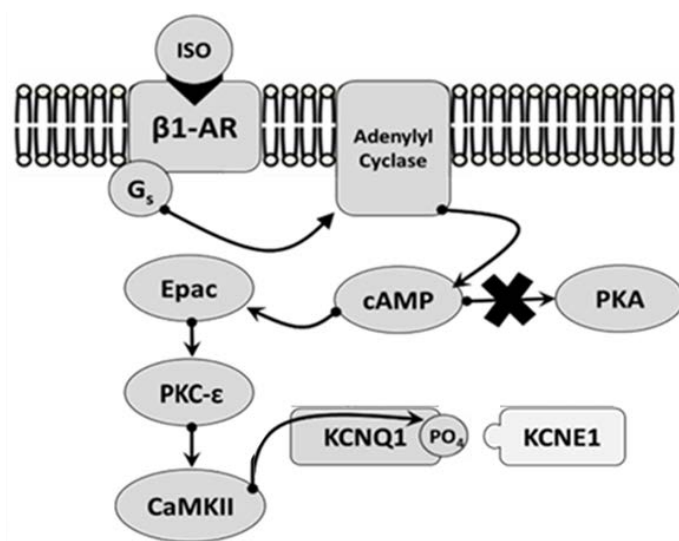


**Figure 27.** Proposed pathway of CaMKII regulation of  $I_{Ks}$  during sustained  $\beta$ -AR stimulation.

While the present study convincingly demonstrates CaMKII-mediated regulation of KCNQ1 S484 during sustained  $\beta$ -AR stimulation in an HEK 293 cellular expression system, further work is warranted to establish the relevance of these findings to human pathophysiology during HF. Specifically, CaMKII-mediated changes in KCNQ1 phosphorylation and  $I_{Ks}$  function need to be corroborated in more models more translatable to human disease, such as cardiomyocytes differentiated from human inducible pluripotent stem cells (hiPSC-CMs) or in animal models of sustained  $\beta$ -AR stimulation (rabbit or guinea pig). While hiPSC-CMs have become a popular model for

cardiac ion channel investigations due to their potential to be genetically manipulated and their relevance to human disease,  $I_{Ks}$  expression within hiPSC-CMs is known to be very low, making cellular electrophysiology experiments difficult and making LCMS/MS phosphoproteomics approaches virtually impossible. Genetic manipulation of hiPSC-CMs is both expensive and difficult, requiring synthesis and optimization of mutation-specific guide RNAs for use with CRISPR/Cas9 approaches on undifferentiated hiPSCs. Following gene editing, hiPSCs must then be differentiated using specific growth factors and culture conditions into hiPSC-CMs with appropriate expression of  $I_{Ks}$  and other ion channels (if current clamp is to be performed). Animal models of sustained  $\beta$ -AR stimulation offer a viable alternative to hiPSC-CMs, particularly the use of guinea pigs which robustly express  $I_{Ks}$ . While recording of  $I_{Ks}$  from isolated guinea pig ventricular cardiomyocytes can be reliably performed, LCMS/MS phosphoproteomic analyses have been performed far less frequently. In addition, genetic manipulation of guinea pigs requires development and maintenance of mutant animal colonies, which is not feasible. Additional details of our HEK 293 model is that our experiments were performed at room temperature ( $\sim 23^{\circ}\text{C}$ ) and in a calcium-free (use of calcium chelation reagents) environment, which must be considered when interpreting our results in the context of physiological  $I_{Ks}$  regulation during HF.

Based on these considerations regarding the experimental model, future planned experiments towards Aims 1 and 2 will be pursued in HEK 293 cells (for experiments involving genetic manipulation) and within animal models of sustained  $\beta$ -AR stimulation (for experiments involving probing of the hypothesized CaMKII signaling pathway during sustained  $\beta$ -AR stimulation). The main experimental objectives will be to: (1)

corroborate our molecular findings (increased phosphorylation at S484) and functional findings (reduced  $I_{Ks}$  current density and a depolarizing shift in the voltage dependence of activation) in an animal model of sustained  $\beta$ -AR stimulation; (2) assess the impact of CaMKII-mediated  $I_{Ks}$  inhibition on changes in APD (via assessment of  $APD_{90}$ ) via current clamp experiments in isolated guinea pig cardiomyocytes from control and ISO-treated animals; (3) utilize phosphoproteomics and cellular electrophysiology approaches to assess the proposed cellular signaling pathway (as shown in **Figure 27**) on S484 phosphorylation and functional inhibition of  $I_{Ks}$ , respectively, using inhibition of the proposed mediators (Epac and PKC- $\epsilon$ ); (4) assess constitutive activation of CaMKII in our guinea pig model of sustained  $\beta$ -AR stimulation using protein immunoblot with CaMKII T286/T287 phospho-specific antibodies (as used in **Figure 14**) on cardiomyocyte lysates from ISO-treated animals vs. those treated with vehicle.

While the potential for therapeutic inhibition of CaMKII is promising based on its pathophysiological role in modulating  $I_{Ks}$  and other key regulators of excitation-contraction coupling during HF, clinical development of CaMKII inhibitors has been complicated by a number of factors, including: the ubiquitous expression of CaMKII and its important role in mediating a number of physiologic important processes (e.g. learning and memory); and the high degree of conservation between CaMKII isoforms.<sup>126</sup> These complicating factors contribute to a high potential for off-target, deleterious effects with therapeutic inhibition of CaMKII. Accordingly, a key future objective of this line of research is to better characterize the signaling pathway involved in CaMKII activation during sustained  $\beta$ -AR stimulation to elucidate a more specific therapeutic target to prevent pathologic regulation of  $I_{Ks}$  and the expected pro-arrhythmogenic complications.

### **Assessing the mechanistic basis through which KCNQ1 S484 phosphorylation mediates functional inhibition of $I_{Ks}$ during sustained $\beta$ -AR stimulation**

In contrast to its enhancement during acute  $\beta$ -AR stimulation, sustained  $\beta$ -AR stimulation has been demonstrated to reduce  $I_{Ks}$  function by an unclear mechanism.<sup>19,21</sup> Functional deficits in  $I_{Ks}$  stemming from cardiac electrical remodeling contribute to the increased risk of ventricular arrhythmias in heart failure, and therefore it is critical to understand the molecular mechanisms that contribute to  $I_{Ks}$  regulation during chronic  $\beta$ -AR stimulation.<sup>127</sup> In Aim 1, we identified three sites located in the region connecting the two alpha-helical CaM-binding domains [helices A (residues 370-389) and B (residues 506-532)] on the KCNQ1 carboxyl terminus that are differentially phosphorylated during sustained  $\beta$ -AR stimulation. Most notably, we discovered a CaMKII-dependent pathway that reduced  $I_{Ks}$  current density during sustained  $\beta$ -AR stimulation through phosphorylation at S484 on KCNQ1. Given the well-documented arrhythmogenic role of CaMKII, its ability to regulate KCNQ1 S484 to inhibit  $I_{Ks}$  during sustained  $\beta$ -AR stimulation may contribute to arrhythmia development in HF.<sup>119-121</sup>

Functional inhibition of  $I_{Ks}$  during sustained  $\beta$ -AR stimulation has been observed in HF patients and in animal HF models. Isolated right ventricular cardiomyocytes from patients with HF demonstrate reduced  $I_{Ks}$  function relative to normal hearts.<sup>45</sup> Findings of reduced  $I_{Ks}$  function have been corroborated in animal HF models induced pharmacologically or surgically via AV nodal blockade or tachycardiac pacing.<sup>22,98-102,106</sup> The previously mentioned work by Aflaki, et al. demonstrated that Epac signaling mediated reductions in KCNE1 protein expression during sustained  $\beta$ -AR stimulation.<sup>21</sup> However, changes in the protein expression of KCNQ1 or KCNE1 in HF patients and in other animal models of sustained  $\beta$ -AR stimulation and HF have not been consistently

reproduced, suggesting that another (or an additional) mechanism may mediate reduced  $I_{Ks}$  function in HF.<sup>100,102-105</sup> Apart from changes in expression of KCNQ1 and/or KCNE1, observed reductions in  $I_{Ks}$  function during sustained  $\beta$ -AR stimulation and HF may involve other potential mechanisms, including: biophysical changes in channel gating; alterations in the interaction of KCNQ1 and KCNE1 subunits; disruption of KCNQ1 and/or KCNE1 trafficking regulated by post translational modifications; etc. Given that the arrhythmogenic potential of functional reductions in  $I_{Ks}$  have been confirmed in animal experiments that have shown the development of ventricular arrhythmias during pharmacological inhibition of  $I_{Ks}$ , elucidation of the molecular mechanism through which phosphorylation at S484 inhibits  $I_{Ks}$  function may have important clinical implications for the prevention of arrhythmias in HF patients.<sup>23,25,128</sup>

Accordingly, our final aim investigated the mechanistic basis for how S484 phosphorylation inhibits  $I_{Ks}$  function. Utilizing the LCMS/MS approach, we demonstrate reduced KCNQ1 phosphorylation at S484 during co-expression with KCNE1 versus expression of KCNQ1 alone. In addition, cellular electrophysiology experiments with mimics of phosphorylation and dephosphorylation at S484 in the presence and absence of KCNE1 demonstrate inhibition of current density with S484D mutants (relative to S484A) only during co-expression with KCNE1. Taken together, these results suggest the possibility of competition at the KCNQ1 carboxyl terminus between CaMKII-mediated S484 phosphorylation and interaction with KCNE1; increased phosphorylation at S484, as occurs during sustained  $\beta$ -AR stimulation, may reduce protein-protein interactions between KCNQ1 and KCNE1 and thereby inhibit  $I_{Ks}$  function. Since KCNQ1 interaction with KCNE1 is known to affect both channel gating (movement of

the voltage sensors) and channel conductance, alteration of the KCNQ1-KCNE1 interaction may account for both functional changes observed during sustained  $\beta$ -AR stimulation: the inhibitory shift in the voltage dependence of activation and reduced current density.

This hypothesis was investigated directly in living cells using the live-cell imaging technique BiFC, which allowed visualization of the interaction between KCNQ1 and KCNE1 subunits. The basis of this approach is that reconstitution of the fluorescent protein Venus along with co-expression of the fluorescent protein Cerulean to control for transfection/expression efficiency. Utilizing mimics of phosphorylation (S484D) and dephosphorylation (S484A), we found decreases in the Venus:Cerulean ratio, indicating reduced interaction of KCNQ1 and KCNE1, with S484D (relative to S484A) that recapitulated reductions in Venus:Cerulean ratios with WT KCNQ1 when treated with 100 nM ISO for 12-24 hours. Furthermore, reduced interaction of KCNQ1 and KCNE1 was mediated by CaMKII signaling, as evidenced by treatment with the chemical CaMKII inhibitor KN-93 attenuating reductions in Venus:Cerulean ratios relative to KN-92 control.

Finally, we sought to investigate whether CaMKII-mediated regulation of KCNQ1 during sustained ISO treatment would impact the trafficking and/or expression of KCNQ1 and/or KCNE1 at the plasma membrane. For this investigation, we utilized biotinylation to selectively tag and isolate membrane-bound proteins with extracellular lysine residues, including KCNQ1, KCNE1, and the Na<sup>+</sup>/K<sup>+</sup>-ATPase (used for loading control). After plasma membrane protein isolation, we used protein immunoblot to assess whether the phosphorylation status at KCNQ1 S484 affected plasma membrane of

expression of KCNQ1 and/or KCNE1. Using mimics of constitutive phosphorylation and dephosphorylation at S484, we demonstrated that, relative to S484A mutants, S484D mutants reduced plasma membrane expression of KCNQ1 by ~15% and KCNE1 by ~33%. Reduced plasma membrane expression of KCNQ1 and KCNE1 subunits is predicted to inhibit  $I_{Ks}$  function. Interestingly, the 33% reduction we saw in KCNE1 membrane expression is similar to the 37% reduction we observed in  $I_{Ks}$  activation currents during treatment with sustained ISO. Planned biotinylation experiments will assess: (1) the potential for sustained ISO treatment to reduce KCNQ1 and/or KCNE1 plasma membrane expression relative to control conditions; and (2) the potential for CaMKII to mediate changes in KCNQ1 and/or KCNE1 expression during ISO treatment via co-treatment with KN-93 and KN-93.

We also utilized KCNQ1 peptide arrays to assess the potential for LQT1 mutations in the vicinity of the residues at which we identified basal phosphorylation to potentially impact CaMKII phosphorylation at S407, S457, T482, S484, and T624. This investigation identified two LQT1 sites around S484 that, although they had been identified in patients with a long QT phenotype, had not been functionally characterized to assess their potential to impact  $I_{Ks}$  regulation and function. Since the LQT1 mutations R481I and S484T were seen to differentially affect CaMKII phosphorylation at S484 (R481I disrupted phosphorylation while S484T did not affect phosphorylation), we utilized these LQT1 mutations during ISO treatment as a translational approach to assess the impact of S484 phosphorylation on the KCNQ1-KCNE1 interaction and the plasma membrane trafficking of KCNQ1 and/or KCNE1. In accordance with our hypothesis, R481I KCNQ1 attenuated reductions in Venus:Cerulean ratios during sustained ISO

treatment relative to S484T. We will also assess the ability of R481I and S484T KCNQ1 to affect KCNQ1 and/or KCNE1 plasma membrane expression during sustained ISO treatment via the biotinylation approach performed above.

In summary, our work identifies (1) reduced protein-protein interaction between KCNQ1 and KCNE1 subunits and (2) reduced plasma membrane expression of KCNQ1 and KCNE1 as mechanisms that mediate  $I_{Ks}$  functional inhibition via CaMKII-dependent regulation of KCNQ1 S484 during sustained  $\beta$ -AR stimulation. Protein-protein interaction between the carboxyl termini of KCNQ1 with KCNE1 is required for formation of  $I_{Ks}$ , and disruption of the KCNQ1-KCNE1 interaction is known to result in disturbances in channel assembly, destabilization of the open-channel state, and altered kinetics of channel deactivation.<sup>129</sup> Accordingly, a limited amount of investigations have assessed disruption of the KCNQ1-KCNE1 interaction as a potential mechanism to mediate conditions in which  $I_{Ks}$  is functionally inhibited, such as with LQT1 or Long QT Syndrome Phenotype 5 (LQT5; mutations in *KCNE1*) mutations. One such investigation by Zheng, et al. demonstrated that identified LQT1 mutations in the KCNQ1 carboxyl terminus (R366W, T391I, and W392R) reduced interaction of the KCNQ1 and KCNE1 carboxyl termini via protein-protein co-immunoprecipitation and surface plasmon resonance experiments in heterologous cellular expression systems and thereby inhibited  $I_{Ks}$  function.<sup>130</sup> Of note, the T391I and W392R LQT1 mutations reside in the region connecting the CaM-binding domains in KCNQ1 carboxyl helices A and B along with S484. A study by Dvir, et al. investigated the functional implications of five LQT1 mutations within helix C of the KCNQ1 carboxyl terminus (S546L, R555C, R555H, K557E, and R562M), demonstrating that all five LQT1 mutations demonstrated reduced

$I_{Ks}$  current densities, produced depolarizing shifts in the voltage dependence of activation, demonstrated slower activation kinetics, and produced faster deactivation kinetics when expressed in Chinese hamster ovary (CHO) cells.<sup>9</sup> Mechanistically, they demonstrated that these helix C mutations reduced the KCNQ1-KCNE1 interaction (via GST pulldown assays) but did not affect plasma membrane trafficking of KCNQ1 and KCNE1 subunits (using total internal reflection fluorescence [TIRF] microscopy in CHO cells).<sup>9</sup> In addition, studies investigating LQT5 variants have also demonstrated the potential to inhibit  $I_{Ks}$  function via disruption of the KCNQ1-KCNE1 interaction. In particular, the T58P/L59P double mutation and P127T mutation have been demonstrated to reduce the KCNQ1-KCNE1 interaction via protein-protein co-immunoprecipitation and GST pulldown assays, respectively.<sup>9,131</sup> As reflected in these LQT1 and LQT5 investigations, reductions in protein-protein interactions between KCNQ1 and KCNE1 subunits, as observed in our BiFC analyses, can profoundly impair  $I_{Ks}$  function; therefore, disruption of the KCNQ1-KCNE1 interaction by CaMKII-mediated phosphorylation of S484 may account for the functional inhibition of  $I_{Ks}$  seen during sustained  $\beta$ -AR stimulation.

Defects in KCNQ1 plasma membrane trafficking and/or expression constitute one of the most common mechanisms for how LQT1 mutations disrupt  $I_{Ks}$  function.<sup>132</sup> LQT1 mutations identified to affect membrane trafficking/expression of KCNQ1 have been identified in the amino terminus and in various regions throughout the carboxyl terminus as assessed by fluorescent microscopy and immunocytochemical (detection of epitopes [e.g. c-Myc] introduced in KCNQ1 extracellular regions) approaches.<sup>6,133-135</sup> Plasma membrane trafficking/expression defects in KCNE1 have also been described, with the LQT5 mutation L51H demonstrating virtually no plasma membrane trafficking via

immunocytochemical analysis.<sup>136</sup> While it has been previously demonstrated that KCNQ1 trafficking is enhanced during co-expression of KCNE1 by a potential co-trafficking mechanism<sup>137,138</sup>, live-cell imaging approaches have since identified separate trafficking pathways for KCNQ1 and KCNE1 subunits in cellular expression systems and in cultured canine ventricular cardiomyocytes.<sup>33,139</sup> Therefore, the reduced plasma membrane expression of KCNQ1 and KCNE1 subunits observed with mimics of phosphorylation at S484 via our biotinylation approach is likely mechanistically distinct from the impaired KCNQ1-KCNE1 interaction demonstrated by our BiFC data, and is an additional mechanism that may account for functional  $I_{Ks}$  inhibition by CaMKII-mediated S484 phosphorylation during sustained  $\beta$ -AR stimulation.

Future directions towards this aim will include assessing our previously identified mechanisms for how CaMKII-mediated S484 phosphorylation inhibits  $I_{Ks}$  function within animal models of sustained  $\beta$ -AR stimulation. To assess the potential for S484 phosphorylation to disrupt the KCNQ1-KCNE1 interaction within a physiologic system, we will perform protein-protein co-immunoprecipitation experiments on lysates from isolated guinea pig cardiomyocytes to directly assess association of KCNQ1 and KCNE1 subunits. Experiments will be performed in animals treated with ISO or vehicle via osmotic mini pumps, and we will attempt to reverse expected reductions in KCNQ1-KCNE1 protein interactions in ISO-treated animals with *ex vivo* CaMKII inhibition (using tat-CN21). In order to assess whether S484 phosphorylation disrupts KCNQ1 and/or KCNE1 plasma membrane trafficking within a physiologic system, we will perform cell surface biotinylation experiments (as performed previously) to assess

membrane-bound KCNQ1 and KCNE1 on cardiomyocytes isolated from guinea pigs treated with ISO or vehicle.

Multiple investigations have demonstrated that CaM is a required auxiliary subunit that, through interaction with the CaM-binding domains in helices A and B within the carboxyl terminus, serves as a chaperone for KCNQ1 folding and channel assembly and gating.<sup>10,30,107</sup> In addition, there is a growing amount of evidence that polymorphisms in CaM can independently result in long QT phenotypes via alteration of the protein-protein interactions between CaM and various ion channel subunits.<sup>140,141</sup> In fact, an investigation by Tobelaim, et al. demonstrates a protective effect of the Ca<sup>2+</sup>-bound CaM amino lobe in limiting PIP<sub>2</sub>-mediated inhibition of I<sub>Ks</sub> function.<sup>142</sup> Finally, a crystal structure has been developed to characterize the structural interaction between CaM and KCNQ1; this investigation reveals that, during the interaction between CaM and the CaM-binding domains in KCNQ1 carboxyl terminal helices A and B, the fourth (carboxyl) lobe of CaM interacts via protein-protein interactions with the KCNQ1 carboxyl terminal region connecting helices A and B and containing S484.<sup>143</sup> Given the essential role of CaM in regulating KCNQ1 function and the close proximity (and, perhaps, involvement) of S484 in the interaction between KCNQ1 and CaM, the potential for CaMKII-mediated S484 phosphorylation to disrupt the interaction between KCNQ1 and CaM warrants investigation. Accordingly, we plan to utilize our previously described BiFC approach to assess changes in the CaM-KCNQ1 interaction during ISO treatment, with mimics of differential phosphorylation at S484, and with LQT1 mutations demonstrated to differentially affect CaMKII-regulation at S484 (R481I and S484T). Based on the role of CaM as a KCNQ1 chaperone, our assessment of the potential for

reduced CaM-KCNQ1 interaction may provide mechanistic insights to describe the reduced KCNQ1 trafficking we observed with mimics of phosphorylation at S484.

## SUMMARY & CONCLUSIONS

To investigate the potential for regulation of  $I_{Ks}$  in response to sustained  $\beta$ -AR stimulation, we first utilized an LCMS/MS approach to identify five sites of basal phosphorylation (S407, S457, T482, S484, and T624) within the carboxyl terminus of KCNQ1. Following treatment with ISO for 24 hours, phosphorylation was enhanced at two of these sites (T482 and S484). Utilizing patch clamp electrophysiology with WT or mutant KCNQ1 and KCNE1, we show that mimics of phosphorylation (aspartic acid) at S457, T482, and S484 in combination demonstrate inhibition of  $I_{Ks}$  activation current density and an inhibitory shift in the voltage dependence of activation, relative to combination mimics of dephosphorylation (alanine), that recapitulates the functional inhibition seen when WT KCNQ1 is treated with ISO for 12-24 hours. By investigating these sites individually, we find that phosphorylation mimics at S457 and S484, but not at T482, produce functional inhibition of  $I_{Ks}$  relative to their respective dephosphorylation mimics.

Next, we investigated the cellular signaling pathway responsible for functional inhibition of  $I_{Ks}$  during sustained  $\beta$ -AR stimulation, specifically assessing the potential for CaMKII and/or PKA signaling to regulate  $I_{Ks}$ . Utilizing a phospho-specific antibody directed against the CaMKII T287 (site that confers constitutive kinase activity), we demonstrate enhanced T287 phosphorylation during 24 hour ISO treatment relative to vehicle. We also show that CaMKII inhibition (using both chemical [KN-93] and peptide [CN21] inhibitors), but not PKA inhibition (using peptide [PKI] inhibition), reverses functional inhibition of  $I_{Ks}$  during sustained ISO treatment via patch clamp electrophysiology. By using individual mimics of dephosphorylation at S457 and S484

during stable expression of active (T287D)  $\delta$ CaMKII, we demonstrate that CaMKII overexpression inhibits  $I_{Ks}$  function except in S484A mutants, wherein S484 is not available for regulation. This finding is corroborated by our KCNQ1 peptide array experiments that indicate that CaMKII, but not PKA, specifically phosphorylates peptide fragments corresponding to KCNQ1 S484.

Finally, we investigate the mechanistic basis for how CaMKII-mediated phosphorylation at S484 inhibits  $I_{Ks}$  function. By performing patch clamp experiments with mimics of phosphorylation and dephosphorylation at S484 in the presence and absence of KCNE1 co-expression with KCNQ1, we find that mimics of phosphorylation only produce inhibitory functional effects during co-expression with KCNE1. In addition, LCMS/MS experiments indicate that S484 demonstrates reduced phosphorylation during co-expression with KCNE1. Based on these experiments, we hypothesized that CaMKII-mediated phosphorylation at S484, as occurs during sustained  $\beta$ -AR stimulation, may functionally inhibit  $I_{Ks}$  by disrupting the functional interaction of KCNQ1 with KCNE1. To assess KCNQ1-KCNE1 interaction, we performed BiFC imaging experiments during ISO treatment (with and without chemical CaMKII inhibition), with differential mimics of phosphorylation at S484, and with LQT1 mutants identified to differentially affect CaMKII regulation of S484. Our BiFC results demonstrate that ISO treatment reduces Venus fluorescent intensity (corresponding to interaction of expressed KCNQ1 and KCNE1 subunits) relative to vehicle; mimics of phosphorylation at S484 also reduced Venus intensity relative to dephosphorylation mimics. Reduced Venus intensity during ISO treatment is reversed, however, during CaMKII inhibition with KN-93 vs. KN-92 inactive control. In addition, LQT1 mutants

shown to disrupt CaMKII phosphorylation at S484 (R481I) show enhanced Venus intensity relative to LQT1 mutation predicted not to affect CaMKII phosphorylation (S484T) during ISO treatment. Finally, biotinylation experiments show that, relative to mimics of dephosphorylation mimics, phosphorylation mimics at S484 demonstrate reduced plasma membrane expression of both KCNQ1 and KCNE1 subunits.

In conclusion, these results demonstrate that, in response to sustained  $\beta$ -AR stimulation, CaMKII phosphorylates KCNQ1 at S484 to inhibit  $I_{Ks}$  function. Mechanistically, S484 phosphorylation inhibits  $I_{Ks}$  function by disrupting the functional interaction between KCNQ1 and KCNE1 subunits and by reducing plasma membrane expression of both KCNQ1 and KCNE1. Accordingly, CaMKII-mediated regulation of  $I_{Ks}$  may contribute to APD prolongation and increased arrhythmogenesis during pathologic states of chronic  $\beta$ -AR stimulation, such as HF.

## SUPPLEMENTARY TABLES

**Supplemental Table 1.** Best-fit values of voltages of half-maximal activation ( $V_{1/2}$ ) and slope factors from Boltzmann distribution fits of mean normalized activation curves.

<b>Mutant/Treatment</b>	<b><math>V_{1/2}</math> (mV)</b>	<b>Slope Factor</b>
WT	20.61 (0.82)	16.77 (0.75)
WT + ISO	26.10 (0.79)	14.80 (0.73)
Triple-A	19.53 (0.90)	16.43 (0.82)
Triple-A + ISO	22.34 (0.64)	14.38 (0.58)
Triple-D	20.18 (1.12)	18.44 (1.05)
Triple-D + ISO	19.19 (0.58)	16.19 (0.53)
S457A	21.55 (1.74)	18.89 (1.46)
S457D	28.55 (2.52)	20.83 (1.75)
T482A	24.72 (2.16)	16.92 (1.69)
T482D	24.77 (4.17)	20.56 (3.22)
S484A	19.62 (1.80)	17.41 (1.57)
S484D	28.34 (3.05)	18.41 (2.15)
WT + ISO + KN-92	26.41 (0.76)	14.97 (0.70)
WT + ISO + KN-93	21.40 (0.65)	14.65 (0.59)
WT in Control Lentivirus	18.51 (1.37)	16.67 (1.26)
WT in CaMKII Lentivirus	22.21 (0.76)	14.83 (0.70)
WT + ISO + CN21	13.81 (1.33)	18.60 (1.31)
WT + ISO + CN21-Alanine	20.21 (2.12)	19.67 (1.84)
WT + ISO + PKI	18.32 (1.96)	18.38 (1.78)

All data are displayed as: mean (SEM).

**Supplemental Table 2.** Peptide sequences for global KCNQ1 peptide arrays assessing  $\delta$ CaMKII phosphorylation of the intracellular regions of KCNQ1, as presented in **Figure 10**.

<b>Row/Column</b>	<b>Peptide Sequence</b>
A1	M-A-A-A-S-S-P-P-R-A-E-R-K-R-W
A2	S-S-P-P-R-A-E-R-K-R-W-G-W-G-R
A3	R-A-E-R-K-R-W-G-W-G-R-L-P-G-A
A4	K-R-W-G-W-G-R-L-P-G-A-R-R-G-S
A5	W-G-R-L-P-G-A-R-R-G-S-A-G-L-A
A6	P-G-A-R-R-G-S-A-G-L-A-K-K-C-P
A7	R-G-S-A-G-L-A-K-K-C-P-F-S-L-E
A8	G-L-A-K-K-C-P-F-S-L-E-L-A-E-G
A9	K-C-P-F-S-L-E-L-A-E-G-G-P-A-G
A10	S-L-E-L-A-E-G-G-P-A-G-G-A-L-Y

<b>A11</b>	A-E-G-G-P-A-G-G-A-L-Y-A-P-I-A
<b>A12</b>	P-A-G-G-A-L-Y-A-P-I-A-P-G-A-P
<b>A13</b>	A-L-Y-A-P-I-A-P-G-A-P-G-P-A-P
<b>A14</b>	P-I-A-P-G-A-P-G-P-A-P-P-A-S-P
<b>A15</b>	G-A-P-G-P-A-P-P-A-S-P-A-A-P-A
<b>A16</b>	P-A-P-P-A-S-P-A-A-P-A-A-P-P-V
<b>A17</b>	A-S-P-A-A-P-A-A-P-P-V-A-S-D-L
<b>A18</b>	A-P-A-A-P-P-V-A-S-D-L-G-P-R-P
<b>A19</b>	P-P-V-A-S-D-L-G-P-R-P-P-V-S-L
<b>A20</b>	S-D-L-G-P-R-P-P-V-S-L-D-P-R-V
<b>B1</b>	P-R-P-P-V-S-L-D-P-R-V-S-I-Y-S
<b>B2</b>	V-S-L-D-P-R-V-S-I-Y-S-T-R-R-P
<b>B3</b>	P-R-V-S-I-Y-S-T-R-R-P-V-L-A-R
<b>B4</b>	I-Y-S-T-R-R-P-V-L-A-R-T-H-V-Q
<b>B5</b>	R-R-P-V-L-A-R-T-H-V-Q-G-R-V-Y
<b>B6</b>	L-A-R-T-H-V-Q-G-R-V-Y-N-F-L-E
<b>B7</b>	H-V-Q-G-R-V-Y-N-F-L-E-R-P-T-G
<b>B8</b>	V-Q-G-R-V-Y-N-F-L-E-R-P-T-G-W
<b>B9</b>	Y-V-V-R-L-W-S-A-G-C-R-S-K-Y-V
<b>B10</b>	L-W-S-A-G-C-R-S-K-Y-V-G-L-W-G
<b>B11</b>	G-C-R-S-K-Y-V-G-L-W-G-R-L-R-F
<b>B12</b>	K-Y-V-G-L-W-G-R-L-R-F-A-R-K-P
<b>B13</b>	H-V-D-R-Q-G-G-T-W-R-L-L-G-S-V
<b>B14</b>	Q-G-G-T-W-R-L-L-G-S-V-V-F-I-H
<b>B15</b>	W-R-L-L-G-S-V-V-F-I-H-R-Q-E-L
<b>B16</b>	V-Q-Q-K-Q-R-Q-K-H-F-N-R-Q-I-P
<b>B17</b>	Q-R-Q-K-H-F-N-R-Q-I-P-A-A-A-S
<b>B18</b>	H-F-N-R-Q-I-P-A-A-A-S-L-I-Q-T
<b>B19</b>	Q-I-P-A-A-A-S-L-I-Q-T-A-W-R-C
<b>B20</b>	A-A-S-L-I-Q-T-A-W-R-C-Y-A-A-E
<b>C1</b>	I-Q-T-A-W-R-C-Y-A-A-E-N-P-D-S
<b>C2</b>	W-R-C-Y-A-A-E-N-P-D-S-S-T-W-K
<b>C3</b>	A-A-E-N-P-D-S-S-T-W-K-I-Y-I-R
<b>C4</b>	P-D-S-S-T-W-K-I-Y-I-R-K-A-P-R
<b>C5</b>	T-W-K-I-Y-I-R-K-A-P-R-S-H-T-L
<b>C6</b>	Y-I-R-K-A-P-R-S-H-T-L-L-S-P-S
<b>C7</b>	A-P-R-S-H-T-L-L-S-P-S-P-K-P-K
<b>C8</b>	H-T-L-L-S-P-S-P-K-P-K-K-S-V-V
<b>C9</b>	S-P-S-P-K-P-K-K-S-V-V-V-K-K-K
<b>C10</b>	K-P-K-K-S-V-V-V-K-K-K-K-F-K-L
<b>C11</b>	S-V-V-V-K-K-K-K-F-K-L-D-K-D-N

<b>C12</b>	K-K-K-K-F-K-L-D-K-D-N-G-V-T-P
<b>C13</b>	F-K-L-D-K-D-N-G-V-T-P-G-E-K-M
<b>C14</b>	K-D-N-G-V-T-P-G-E-K-M-L-T-V-P
<b>C15</b>	V-T-P-G-E-K-M-L-T-V-P-H-I-T-C
<b>C16</b>	E-K-M-L-T-V-P-H-I-T-C-D-P-P-E
<b>C17</b>	T-V-P-H-I-T-C-D-P-P-E-E-R-R-L
<b>C18</b>	I-T-C-D-P-P-E-E-R-R-L-D-H-F-S
<b>C19</b>	P-P-E-E-R-R-L-D-H-F-S-V-D-G-Y
<b>C20</b>	R-R-L-D-H-F-S-V-D-G-Y-D-S-S-V
<b>D1</b>	H-F-S-V-D-G-Y-D-S-S-V-R-K-S-P
<b>D2</b>	D-G-Y-D-S-S-V-R-K-S-P-T-L-L-E
<b>D3</b>	S-S-V-R-K-S-P-T-L-L-E-V-S-M-P
<b>D4</b>	K-S-P-T-L-L-E-V-S-M-P-H-F-M-R
<b>D5</b>	L-L-E-V-S-M-P-H-F-M-R-T-N-S-F
<b>D6</b>	S-M-P-H-F-M-R-T-N-S-F-A-E-D-L
<b>D7</b>	F-M-R-T-N-S-F-A-E-D-L-D-L-E-G
<b>D8</b>	N-S-F-A-E-D-L-D-L-E-G-E-T-L-L
<b>D9</b>	E-D-L-D-L-E-G-E-T-L-L-T-P-I-T
<b>D10</b>	L-E-G-E-T-L-L-T-P-I-T-H-I-S-Q
<b>D11</b>	T-L-L-T-P-I-T-H-I-S-Q-L-R-E-H
<b>D12</b>	P-I-T-H-I-S-Q-L-R-E-H-H-R-A-T
<b>D13</b>	I-S-Q-L-R-E-H-H-R-A-T-I-K-V-I
<b>D14</b>	R-E-H-H-R-A-T-I-K-V-I-R-R-M-Q
<b>D15</b>	R-A-T-I-K-V-I-R-R-M-Q-Y-F-V-A
<b>D16</b>	K-V-I-R-R-M-Q-Y-F-V-A-K-K-K-F
<b>D17</b>	R-M-Q-Y-F-V-A-K-K-K-F-Q-Q-A-R
<b>D18</b>	F-V-A-K-K-K-F-Q-Q-A-R-K-P-Y-D
<b>D19</b>	K-K-F-Q-Q-A-R-K-P-Y-D-V-R-D-V
<b>D20</b>	Q-A-R-K-P-Y-D-V-R-D-V-I-E-Q-Y
<b>E1</b>	P-Y-D-V-R-D-V-I-E-Q-Y-S-Q-G-H
<b>E2</b>	R-D-V-I-E-Q-Y-S-Q-G-H-L-N-L-M
<b>E3</b>	E-Q-Y-S-Q-G-H-L-N-L-M-V-R-I-K
<b>E4</b>	Q-G-H-L-N-L-M-V-R-I-K-E-L-Q-R
<b>E5</b>	N-L-M-V-R-I-K-E-L-Q-R-R-L-D-Q
<b>E6</b>	R-I-K-E-L-Q-R-R-L-D-Q-S-I-G-K
<b>E7</b>	L-Q-R-R-L-D-Q-S-I-G-K-P-S-L-F
<b>E8</b>	L-D-Q-S-I-G-K-P-S-L-F-I-S-V-S
<b>E9</b>	I-G-K-P-S-L-F-I-S-V-S-E-K-S-K
<b>E10</b>	S-L-F-I-S-V-S-E-K-S-K-D-R-G-S
<b>E11</b>	S-V-S-E-K-S-K-D-R-G-S-N-T-I-G
<b>E12</b>	K-S-K-D-R-G-S-N-T-I-G-A-R-L-N

<b>E13</b>	R-G-S-N-T-I-G-A-R-L-N-R-V-E-D
<b>E14</b>	T-I-G-A-R-L-N-R-V-E-D-K-V-T-Q
<b>E15</b>	R-L-N-R-V-E-D-K-V-T-Q-L-D-Q-R
<b>E16</b>	V-E-D-K-V-T-Q-L-D-Q-R-L-A-L-I
<b>E17</b>	V-T-Q-L-D-Q-R-L-A-L-I-T-D-M-L
<b>E18</b>	D-Q-R-L-A-L-I-T-D-M-L-H-Q-L-L
<b>E19</b>	A-L-I-T-D-M-L-H-Q-L-L-S-L-H-G
<b>E20</b>	D-M-L-H-Q-L-L-S-L-H-G-G-S-T-P
<b>F1</b>	Q-L-L-S-L-H-G-G-S-T-P-G-S-G-G
<b>F2</b>	L-H-G-G-S-T-P-G-S-G-G-P-P-R-E
<b>F3</b>	S-T-P-G-S-G-G-P-P-R-E-G-G-A-H
<b>F4</b>	S-G-G-P-P-R-E-G-G-A-H-I-T-Q-P
<b>F5</b>	P-R-E-G-G-A-H-I-T-Q-P-C-G-S-G
<b>F6</b>	G-A-H-I-T-Q-P-C-G-S-G-G-S-V-D
<b>F7</b>	T-Q-P-C-G-S-G-G-S-V-D-P-E-L-F
<b>F8</b>	G-S-G-G-S-V-D-P-E-L-F-L-P-S-N
<b>F9</b>	S-V-D-P-E-L-F-L-P-S-N-T-L-P-T
<b>F10</b>	E-L-F-L-P-S-N-T-L-P-T-Y-E-Q-L
<b>F11</b>	P-S-N-T-L-P-T-Y-E-Q-L-T-V-P-R
<b>F12</b>	L-P-T-Y-E-Q-L-T-V-P-R-R-G-P-D
<b>F13</b>	Y-E-Q-L-T-V-P-R-R-G-P-D-E-G-S
<b>F14</b>	Blank
<b>F15 (top blot in Figure 10)</b>	K-K-A-L-R-R-Q-E-A-V-D-A-L (AC-2 Negative Control)
<b>F16 (top)</b>	Blank
<b>F17 (top)</b>	K-K-A-L-R-R-Q-E-T-V-D-A-L (AC-2 Positive Control)
<b>F18 (top)</b>	Blank
<b>F19 (top)</b>	L-R-R-A-S-L-G (Kemptide Control[Weak Substrate])
<b>F20 (top)</b>	Blank
<b>F15 (bottom blot in Figure 10)</b>	Blank
<b>F16 (bottom)</b>	K-K-A-L-R-R-Q-E-A-V-D-A-L (AC-2 Negative Control)
<b>F17 (bottom)</b>	Blank
<b>F18 (bottom)</b>	Blank
<b>F19 (bottom)</b>	Blank
<b>F20 (bottom)</b>	Blank

**Supplemental Table 3.** Peptide sequences for KCNQ1 peptide array assessing  $\delta$ CaMKII phosphorylation of specific identified LCMS sites, as presented in **Figure 15**.

<b>Residue</b>	<b>Alteration</b>	<b>Peptide Sequence</b>
<b>S407</b>	<b>WT</b>	P-R-S-H-T-L-L-S-P-S-P-K-P-K-K
<b>S407</b>	<b>A</b>	P-R-S-H-T-L-L-A-P-S-P-K-P-K-K
<b>S407</b>	<b>KO</b>	P-R-A-H-A-L-L-A-P-A-P-K-P-K-K
<b>S457</b>	<b>WT</b>	E-R-R-L-D-H-F-S-V-D-G-Y-D-S-S
<b>S457</b>	<b>A</b>	E-R-R-L-D-H-F-A-V-D-G-Y-D-S-S
<b>S457</b>	<b>KO</b>	E-R-R-L-D-H-F-A-V-D-G-Y-D-A-A
<b>T482</b>	<b>WT</b>	S-M-P-H-F-M-R-T-N-S-F-A-E-D-L
<b>T482</b>	<b>A</b>	S-M-P-H-F-M-R-A-N-S-F-A-E-D-L
<b>T482</b>	<b>KO</b>	A-M-P-H-F-M-R-A-N-S-F-A-E-D-L
<b>S484</b>	<b>WT</b>	P-H-F-M-R-T-N-S-F-A-E-D-L-D-L
<b>S484</b>	<b>A</b>	P-H-F-M-R-T-N-A-F-A-E-D-L-D-L
<b>S484</b>	<b>KO</b>	P-H-F-M-R-A-N-A-F-A-E-D-L-D-L
<b>T624</b>	<b>WT</b>	L-S-L-H-G-G-S-T-P-G-S-G-G-P-P
<b>T624</b>	<b>A</b>	L-S-L-H-G-G-S-A-P-G-S-G-G-P-P
<b>T624</b>	<b>KO</b>	L-A-L-H-G-G-A-A-P-G-A-G-G-P-P

## BIBLIOGRAPHY

1. Wu W, Sanguinetti MC. Molecular Basis of Cardiac Delayed Rectifier Potassium Channel Function and Pharmacology. *Card Electrophysiol Clin.* 2016;8(2):275-284.
2. Chen L, Sampson KJ, Kass RS. Cardiac Delayed Rectifier Potassium Channels in Health and Disease. *Cardiac electrophysiology clinics.* 2016;8(2):307-322.
3. Napolitano C, Priori SG, Schwartz PJ, et al. Genetic testing in the long QT syndrome: development and validation of an efficient approach to genotyping in clinical practice. *Jama.* 2005;294(23):2975-2980.
4. Splawski I, Shen J, Timothy KW, et al. Spectrum of mutations in long-QT syndrome genes. KVLQT1, HERG, SCN5A, KCNE1, and KCNE2. *Circulation.* 2000;102(10):1178-1185.
5. Sanguinetti MC, Curran ME, Zou A, et al. Coassembly of K(V)LQT1 and minK (IsK) proteins to form cardiac I(Ks) potassium channel. *Nature.* 1996;384(6604):80-83.
6. Aromolaran AS, Subramanyam P, Chang DD, Kobertz WR, Colecraft HM. LQT1 mutations in KCNQ1 C-terminus assembly domain suppress IKs using different mechanisms. *Cardiovasc Res.* 2014;104(3):501-511.
7. Wiener R, Haitin Y, Shamgar L, et al. The KCNQ1 (Kv7.1) COOH terminus, a multitiered scaffold for subunit assembly and protein interaction. *The Journal of biological chemistry.* 2008;283(9):5815-5830.
8. Yu H, Lin Z, Mattmann ME, et al. Dynamic subunit stoichiometry confers a progressive continuum of pharmacological sensitivity by KCNQ potassium channels. *Proceedings of the National Academy of Sciences of the United States of America.* 2013;110(21):8732-8737.
9. Dvir M, Strulovich R, Sachyani D, et al. Long QT mutations at the interface between KCNQ1 helix C and KCNE1 disrupt I(KS) regulation by PKA and PIP(2). *Journal of cell science.* 2014;127(Pt 18):3943-3955.

10. Ghosh S, Nunziato DA, Pitt GS. KCNQ1 assembly and function is blocked by long-QT syndrome mutations that disrupt interaction with calmodulin. *Circulation research*. 2006;98(8):1048-1054.
11. Howard RJ, Clark KA, Holton JM, Minor DL, Jr. Structural insight into KCNQ (Kv7) channel assembly and channelopathy. *Neuron*. 2007;53(5):663-675.
12. Schwake M, Athanasiadu D, Beimgraben C, et al. Structural determinants of M-type KCNQ (Kv7) K<sup>+</sup> channel assembly. *The Journal of neuroscience : the official journal of the Society for Neuroscience*. 2006;26(14):3757-3766.
13. Charpentier F, Merot J, Loussouarn G, Baro I. Delayed rectifier K(+) currents and cardiac repolarization. *Journal of molecular and cellular cardiology*. 2010;48(1):37-44.
14. Nerbonne JM, Kass RS. Molecular physiology of cardiac repolarization. *Physiol Rev*. 2005;85(4):1205-1253.
15. Jost N, Virag L, Bitay M, et al. Restricting excessive cardiac action potential and QT prolongation: a vital role for IKs in human ventricular muscle. *Circulation*. 2005;112(10):1392-1399.
16. Volders PG, Stengl M, van Opstal JM, et al. Probing the contribution of IKs to canine ventricular repolarization: key role for beta-adrenergic receptor stimulation. *Circulation*. 2003;107(21):2753-2760.
17. Stengl M, Volders PG, Thomsen MB, Spatjens RL, Sipido KR, Vos MA. Accumulation of slowly activating delayed rectifier potassium current (IKs) in canine ventricular myocytes. *J Physiol*. 2003;551(Pt 3):777-786.
18. Li Y, Chen L, Kass RS, Dessauer CW. The A-kinase anchoring protein Yotiao facilitates complex formation between adenylyl cyclase type 9 and the IKs potassium channel in heart. *The Journal of biological chemistry*. 2012;287(35):29815-29824.
19. Marx SO, Kurokawa J, Reiken S, et al. Requirement of a macromolecular signaling complex for beta adrenergic receptor modulation of the KCNQ1-KCNE1 potassium channel. *Science (New York, NY)*. 2002;295(5554):496-499.

20. Terrenoire C, Houslay MD, Baillie GS, Kass RS. The cardiac IKs potassium channel macromolecular complex includes the phosphodiesterase PDE4D3. *The Journal of biological chemistry*. 2009;284(14):9140-9146.
21. Aflaki M, Qi XY, Xiao L, et al. Exchange protein directly activated by cAMP mediates slow delayed-rectifier current remodeling by sustained beta-adrenergic activation in guinea pig hearts. *Circulation research*. 2014;114(6):993-1003.
22. Li D, Melnyk P, Feng J, et al. Effects of experimental heart failure on atrial cellular and ionic electrophysiology. *Circulation*. 2000;101(22):2631-2638.
23. Cheng HC, Incardona J. Models of torsades de pointes: effects of FPL64176, DPI201106, dofetilide, and chromanol 293B in isolated rabbit and guinea pig hearts. *Journal of pharmacological and toxicological methods*. 2009;60(2):174-184.
24. Goldenberg I, Moss AJ. Long QT syndrome. *Journal of the American College of Cardiology*. 2008;51(24):2291-2300.
25. Lengyel C, Varro A, Tabori K, Papp JG, Baczko I. Combined pharmacological block of I(Kr) and I(Ks) increases short-term QT interval variability and provokes torsades de pointes. *British journal of pharmacology*. 2007;151(7):941-951.
26. Tester DJ, Will ML, Haglund CM, Ackerman MJ. Compendium of cardiac channel mutations in 541 consecutive unrelated patients referred for long QT syndrome genetic testing. *Heart rhythm : the official journal of the Heart Rhythm Society*. 2005;2(5):507-517.
27. Levine E, Rosero SZ, Budzikowski AS, Moss AJ, Zareba W, Daubert JP. Congenital long QT syndrome: considerations for primary care physicians. *Cleve Clin J Med*. 2008;75(8):591-600.
28. Diamant UB, Vahedi F, Winbo A, et al. Electrophysiological phenotype in the LQTS mutations Y111C and R518X in the KCNQ1 gene. *Journal of applied physiology (Bethesda, Md : 1985)*. 2013;115(10):1423-1432.
29. Winbo A, Stattin EL, Nordin C, et al. Phenotype, origin and estimated prevalence of a common long QT syndrome mutation: a clinical, genealogical and molecular genetics study including Swedish R518X/KCNQ1 families. *BMC Cardiovasc Disord*. 2014;14:22.

30. Shamgar L, Ma L, Schmitt N, et al. Calmodulin is essential for cardiac IKs channel gating and assembly: impaired function in long-QT mutations. *Circulation research*. 2006;98(8):1055-1063.
31. Kurokawa J, Bankston JR, Kaihara A, Chen L, Furukawa T, Kass RS. KCNE variants reveal a critical role of the beta subunit carboxyl terminus in PKA-dependent regulation of the IKs potassium channel. *Channels (Austin, Tex)*. 2009;3(1):16-24.
32. Chen L, Marquardt ML, Tester DJ, Sampson KJ, Ackerman MJ, Kass RS. Mutation of an A-kinase-anchoring protein causes long-QT syndrome. *Proceedings of the National Academy of Sciences of the United States of America*. 2007;104(52):20990-20995.
33. Jiang M, Wang Y, Tseng GN. Adult Ventricular Myocytes Segregate KCNQ1 and KCNE1 to Keep the IKs Amplitude in Check Until When Larger IKs Is Needed. *Circulation Arrhythmia and electrophysiology*. 2017;10(6).
34. Piccini I, Fehrmann E, Frank S, Muller FU, Greber B, Seeböhm G. Adrenergic Stress Protection of Human iPS Cell-Derived Cardiomyocytes by Fast Kv7.1 Recycling. *Front Physiol*. 2017;8:705.
35. Francis GS, Cogswell R, Thenappan T. The heterogeneity of heart failure: will enhanced phenotyping be necessary for future clinical trial success? *Journal of the American College of Cardiology*. 2014;64(17):1775-1776.
36. Bui AL, Horwich TB, Fonarow GC. Epidemiology and risk profile of heart failure. *Nat Rev Cardiol*. 2011;8(1):30-41.
37. Mozaffarian D, Benjamin EJ, Go AS, et al. Executive Summary: Heart Disease and Stroke Statistics--2016 Update: A Report From the American Heart Association. *Circulation*. 2016;133(4):447-454.
38. Tomaselli GF, Zipes DP. What causes sudden death in heart failure? *Circulation research*. 2004;95(8):754-763.
39. Coronel R, Wilders R, Verkerk AO, Wiegeler RF, Benoist D, Bernus O. Electrophysiological changes in heart failure and their implications for arrhythmogenesis. *Biochimica et biophysica acta*. 2013;1832(12):2432-2441.

40. Cutler MJ, Rosenbaum DS, Dunlap ME. Structural and electrical remodeling as therapeutic targets in heart failure. *J Electrocardiol.* 2007;40(6 Suppl):S1-7.
41. CIBIS-Investigators. A randomized trial of beta-blockade in heart failure. The Cardiac Insufficiency Bisoprolol Study (CIBIS). CIBIS Investigators and Committees. *Circulation.* 1994;90(4):1765-1773.
42. Yusuf S, Pitt B, Davis CE, Hood WB, Cohn JN. Effect of enalapril on survival in patients with reduced left ventricular ejection fractions and congestive heart failure. *The New England journal of medicine.* 1991;325(5):293-302.
43. Kurokawa J, Abriel H. Neurohormonal regulation of cardiac ion channels in chronic heart failure. *Journal of cardiovascular pharmacology.* 2009;54(2):98-105.
44. Hartzell HC. Regulation of cardiac ion channels by catecholamines, acetylcholine and second messenger systems. *Prog Biophys Mol Biol.* 1988;52(3):165-247.
45. Li GR, Lau CP, Leung TK, Nattel S. Ionic current abnormalities associated with prolonged action potentials in cardiomyocytes from diseased human right ventricles. *Heart rhythm : the official journal of the Heart Rhythm Society.* 2004;1(4):460-468.
46. Gonzalez-Juanatey JR, Garcia-Acuna JM, Pose A, et al. Reduction of QT and QTc dispersion during long-term treatment of systemic hypertension with enalapril. *Am J Cardiol.* 1998;81(2):170-174.
47. Gou X, Wang W, Zou S, Qi Y, Xu Y. Protein kinase C epsilon mediates the inhibition of angiotensin II on the slowly activating delayed-rectifier potassium current through channel phosphorylation. *Journal of molecular and cellular cardiology.* 2018;116:165-174.
48. Rivard K, Paradis P, Nemer M, Fiset C. Cardiac-specific overexpression of the human type 1 angiotensin II receptor causes delayed repolarization. *Cardiovasc Res.* 2008;78(1):53-62.
49. Lymperopoulos A, Rengo G, Koch WJ. Adrenergic nervous system in heart failure: pathophysiology and therapy. *Circulation research.* 2013;113(6):739-753.
50. Cui J, Melman Y, Palma E, Fishman GI, McDonald TV. Cyclic AMP regulates the HERG K(+) channel by dual pathways. *Curr Biol.* 2000;10(11):671-674.

51. Ruiz-Hurtado G, Morel E, Dominguez-Rodriguez A, et al. Epac in cardiac calcium signaling. *Journal of molecular and cellular cardiology*. 2013;58:162-171.
52. Metrich M, Lucas A, Gastineau M, et al. Epac mediates beta-adrenergic receptor-induced cardiomyocyte hypertrophy. *Circulation research*. 2008;102(8):959-965.
53. Anderson ME, Brown JH, Bers DM. CaMKII in myocardial hypertrophy and heart failure. *Journal of molecular and cellular cardiology*. 2011;51(4):468-473.
54. Hund TJ, Mohler PJ. Role of CaMKII in cardiac arrhythmias. *Trends Cardiovasc Med*. 2015;25(5):392-397.
55. Backs J, Backs T, Neef S, et al. The delta isoform of CaM kinase II is required for pathological cardiac hypertrophy and remodeling after pressure overload. *Proceedings of the National Academy of Sciences of the United States of America*. 2009;106(7):2342-2347.
56. Erickson JR, Joiner ML, Guan X, et al. A dynamic pathway for calcium-independent activation of CaMKII by methionine oxidation. *Cell*. 2008;133(3):462-474.
57. Meyer T, Hanson PI, Stryer L, Schulman H. Calmodulin trapping by calcium-calmodulin-dependent protein kinase. *Science (New York, NY)*. 1992;256(5060):1199-1202.
58. Erickson JR, Nichols CB, Uchinoumi H, Stein ML, Bossuyt J, Bers DM. S-Nitrosylation Induces Both Autonomous Activation and Inhibition of Calcium/Calmodulin-dependent Protein Kinase II delta. *The Journal of biological chemistry*. 2015;290(42):25646-25656.
59. Erickson JR, Pereira L, Wang L, et al. Diabetic hyperglycaemia activates CaMKII and arrhythmias by O-linked glycosylation. *Nature*. 2013;502(7471):372-376.
60. Wu Y, Temple J, Zhang R, et al. Calmodulin kinase II and arrhythmias in a mouse model of cardiac hypertrophy. *Circulation*. 2002;106(10):1288-1293.
61. Swaminathan PD, Purohit A, Hund TJ, Anderson ME. Calmodulin-dependent protein kinase II: linking heart failure and arrhythmias. *Circulation research*. 2012;110(12):1661-1677.

62. J OU, Komukai K, Kusakari Y, et al. alpha1-adrenoceptor stimulation potentiates L-type Ca<sup>2+</sup> current through Ca<sup>2+</sup>/calmodulin-dependent PK II (CaMKII) activation in rat ventricular myocytes. *Proceedings of the National Academy of Sciences of the United States of America*. 2005;102(26):9400-9405.
63. Zhu W, Zou Y, Shiojima I, et al. Ca<sup>2+</sup>/calmodulin-dependent kinase II and calcineurin play critical roles in endothelin-1-induced cardiomyocyte hypertrophy. *The Journal of biological chemistry*. 2000;275(20):15239-15245.
64. Mangmool S, Shukla AK, Rockman HA. beta-Arrestin-dependent activation of Ca(2+)/calmodulin kinase II after beta(1)-adrenergic receptor stimulation. *J Cell Biol*. 2010;189(3):573-587.
65. Pereira L, Metrich M, Fernandez-Velasco M, et al. The cAMP binding protein Epac modulates Ca<sup>2+</sup> sparks by a Ca<sup>2+</sup>/calmodulin kinase signalling pathway in rat cardiac myocytes. *J Physiol*. 2007;583(Pt 2):685-694.
66. Zhu WZ, Wang SQ, Chakir K, et al. Linkage of beta1-adrenergic stimulation to apoptotic heart cell death through protein kinase A-independent activation of Ca<sup>2+</sup>/calmodulin kinase II. *J Clin Invest*. 2003;111(5):617-625.
67. Ling H, Zhang T, Pereira L, et al. Requirement for Ca<sup>2+</sup>/calmodulin-dependent kinase II in the transition from pressure overload-induced cardiac hypertrophy to heart failure in mice. *J Clin Invest*. 2009;119(5):1230-1240.
68. Zhang T, Maier LS, Dalton ND, et al. The deltaC isoform of CaMKII is activated in cardiac hypertrophy and induces dilated cardiomyopathy and heart failure. *Circulation research*. 2003;92(8):912-919.
69. Khoo MS, Li J, Singh MV, et al. Death, cardiac dysfunction, and arrhythmias are increased by calmodulin kinase II in calcineurin cardiomyopathy. *Circulation*. 2006;114(13):1352-1359.
70. Sag CM, Wadsack DP, Khabbazzadeh S, et al. Calcium/calmodulin-dependent protein kinase II contributes to cardiac arrhythmogenesis in heart failure. *Circulation Heart failure*. 2009;2(6):664-675.
71. Li J, Marionneau C, Zhang R, et al. Calmodulin kinase II inhibition shortens action potential duration by upregulation of K<sup>+</sup> currents. *Circulation research*. 2006;99(10):1092-1099.

72. Zhong P, Quan D, Huang Y, Huang H. CaMKII Activation Promotes Cardiac Electrical Remodeling and Increases the Susceptibility to Arrhythmia Induction in High-fat Diet-Fed Mice With Hyperlipidemia Conditions. *Journal of cardiovascular pharmacology*. 2017;70(4):245-254.
73. Zhong P, Quan D, Peng J, et al. Role of CaMKII in free fatty acid/hyperlipidemia-induced cardiac remodeling both in vitro and in vivo. *Journal of molecular and cellular cardiology*. 2017;109:1-16.
74. Schulman H, Anderson ME. Ca/Calmodulin-dependent Protein Kinase II in Heart Failure. *Drug Discov Today Dis Mech*. 2010;7(2):e117-e122.
75. Metrich M, Morel E, Berthouze M, et al. Functional characterization of the cAMP-binding proteins Epac in cardiac myocytes. *Pharmacological reports : PR*. 2009;61(1):146-153.
76. Oestreich EA, Malik S, Goonasekera SA, et al. Epac and phospholipase Cepsilon regulate Ca<sup>2+</sup> release in the heart by activation of protein kinase Cepsilon and calcium-calmodulin kinase II. *The Journal of biological chemistry*. 2009;284(3):1514-1522.
77. Oestreich EA, Wang H, Malik S, et al. Epac-mediated activation of phospholipase C(epsilon) plays a critical role in beta-adrenergic receptor-dependent enhancement of Ca<sup>2+</sup> mobilization in cardiac myocytes. *The Journal of biological chemistry*. 2007;282(8):5488-5495.
78. Pereira L, Cheng H, Lao DH, et al. Epac2 mediates cardiac beta1-adrenergic-dependent sarcoplasmic reticulum Ca<sup>2+</sup> leak and arrhythmia. *Circulation*. 2013;127(8):913-922.
79. Pereira L, Ruiz-Hurtado G, Morel E, et al. Epac enhances excitation-transcription coupling in cardiac myocytes. *Journal of molecular and cellular cardiology*. 2012;52(1):283-291.
80. Beckendorf J, van den Hoogenhof MMG, Backs J. Physiological and unappreciated roles of CaMKII in the heart. *Basic research in cardiology*. 2018;113(4):29.

81. Bers DM, Grandi E. Calcium/calmodulin-dependent kinase II regulation of cardiac ion channels. *Journal of cardiovascular pharmacology*. 2009;54(3):180-187.
82. Anderson ME, Braun AP, Schulman H, Premack BA. Multifunctional Ca<sup>2+</sup>/calmodulin-dependent protein kinase mediates Ca(2+)-induced enhancement of the L-type Ca<sup>2+</sup> current in rabbit ventricular myocytes. *Circulation research*. 1994;75(5):854-861.
83. Hudmon A, Schulman H, Kim J, Maltez JM, Tsien RW, Pitt GS. CaMKII tethers to L-type Ca<sup>2+</sup> channels, establishing a local and dedicated integrator of Ca<sup>2+</sup> signals for facilitation. *J Cell Biol*. 2005;171(3):537-547.
84. Anderson ME, Braun AP, Wu Y, et al. KN-93, an inhibitor of multifunctional Ca<sup>++</sup>/calmodulin-dependent protein kinase, decreases early afterdepolarizations in rabbit heart. *J Pharmacol Exp Ther*. 1998;287(3):996-1006.
85. Welsby PJ, Wang H, Wolfe JT, Colbran RJ, Johnson ML, Barrett PQ. A mechanism for the direct regulation of T-type calcium channels by Ca<sup>2+</sup>/calmodulin-dependent kinase II. *The Journal of neuroscience : the official journal of the Society for Neuroscience*. 2003;23(31):10116-10121.
86. Ferron L, Capuano V, Ruchon Y, Deroubaix E, Coulombe A, Renaud JF. Angiotensin II signaling pathways mediate expression of cardiac T-type calcium channels. *Circulation research*. 2003;93(12):1241-1248.
87. Izumi T, Kihara Y, Sarai N, et al. Reinduction of T-type calcium channels by endothelin-1 in failing hearts in vivo and in adult rat ventricular myocytes in vitro. *Circulation*. 2003;108(20):2530-2535.
88. Ashpole NM, Herren AW, Ginsburg KS, et al. Ca<sup>2+</sup>/calmodulin-dependent protein kinase II (CaMKII) regulates cardiac sodium channel NaV1.5 gating by multiple phosphorylation sites. *The Journal of biological chemistry*. 2012;287(24):19856-19869.
89. Veldkamp MW, Viswanathan PC, Bezzina C, Baartscheer A, Wilde AA, Balser JR. Two distinct congenital arrhythmias evoked by a multidysfunctional Na(+) channel. *Circulation research*. 2000;86(9):E91-97.

90. Wagner S, Dybkova N, Rasenack EC, et al. Ca<sup>2+</sup>/calmodulin-dependent protein kinase II regulates cardiac Na<sup>+</sup> channels. *J Clin Invest*. 2006;116(12):3127-3138.
91. Verkerk AO, Veldkamp MW, van Ginneken AC, Bouman LN. Biphasic response of action potential duration to metabolic inhibition in rabbit and human ventricular myocytes: role of transient outward current and ATP-regulated potassium current. *Journal of molecular and cellular cardiology*. 1996;28(12):2443-2456.
92. Sergeant GP, Ohya S, Reihill JA, et al. Regulation of Kv4.3 currents by Ca<sup>2+</sup>/calmodulin-dependent protein kinase II. *Am J Physiol Cell Physiol*. 2005;288(2):C304-313.
93. Xiao L, Coutu P, Villeneuve LR, et al. Mechanisms underlying rate-dependent remodeling of transient outward potassium current in canine ventricular myocytes. *Circulation research*. 2008;103(7):733-742.
94. Beuckelmann DJ, Nabauer M, Erdmann E. Alterations of K<sup>+</sup> currents in isolated human ventricular myocytes from patients with terminal heart failure. *Circulation research*. 1993;73(2):379-385.
95. Piao L, Li J, McLerie M, Lopatin AN. Cardiac IK1 underlies early action potential shortening during hypoxia in the mouse heart. *Journal of molecular and cellular cardiology*. 2007;43(1):27-38.
96. Pogwizd SM, Schlotthauer K, Li L, Yuan W, Bers DM. Arrhythmogenesis and contractile dysfunction in heart failure: Roles of sodium-calcium exchange, inward rectifier potassium current, and residual beta-adrenergic responsiveness. *Circulation research*. 2001;88(11):1159-1167.
97. Wagner S, Hacker E, Grandi E, et al. Ca/calmodulin kinase II differentially modulates potassium currents. *Circulation Arrhythmia and electrophysiology*. 2009;2(3):285-294.
98. Li GR, Lau CP, Ducharme A, Tardif JC, Nattel S. Transmural action potential and ionic current remodeling in ventricles of failing canine hearts. *American journal of physiology Heart and circulatory physiology*. 2002;283(3):H1031-1041.

99. Ramakers C, Vos MA, Doevendans PA, et al. Coordinated down-regulation of KCNQ1 and KCNE1 expression contributes to reduction of I(Ks) in canine hypertrophied hearts. *Cardiovasc Res.* 2003;57(2):486-496.
100. Rose J, Armoundas AA, Tian Y, et al. Molecular correlates of altered expression of potassium currents in failing rabbit myocardium. *American journal of physiology Heart and circulatory physiology.* 2005;288(5):H2077-2087.
101. Tsuji Y, Opthof T, Kamiya K, et al. Pacing-induced heart failure causes a reduction of delayed rectifier potassium currents along with decreases in calcium and transient outward currents in rabbit ventricle. *Cardiovasc Res.* 2000;48(2):300-309.
102. Tsuji Y, Zicha S, Qi XY, Kodama I, Nattel S. Potassium channel subunit remodeling in rabbits exposed to long-term bradycardia or tachycardia: discrete arrhythmogenic consequences related to differential delayed-rectifier changes. *Circulation.* 2006;113(3):345-355.
103. Akar FG, Wu RC, Juang GJ, et al. Molecular mechanisms underlying K<sup>+</sup> current downregulation in canine tachycardia-induced heart failure. *American journal of physiology Heart and circulatory physiology.* 2005;288(6):H2887-2896.
104. Borlak J, Thum T. Hallmarks of ion channel gene expression in end-stage heart failure. *FASEB J.* 2003;17(12):1592-1608.
105. Watanabe E, Yasui K, Kamiya K, et al. Upregulation of KCNE1 induces QT interval prolongation in patients with chronic heart failure. *Circ J.* 2007;71(4):471-478.
106. Volders PG, Sipido KR, Vos MA, Kulcsar A, Verduyn SC, Wellens HJ. Cellular basis of biventricular hypertrophy and arrhythmogenesis in dogs with chronic complete atrioventricular block and acquired torsade de pointes. *Circulation.* 1998;98(11):1136-1147.
107. Yus-Najera E, Santana-Castro I, Villarroel A. The identification and characterization of a noncontinuous calmodulin-binding site in noninactivating voltage-dependent KCNQ potassium channels. *The Journal of biological chemistry.* 2002;277(32):28545-28553.

108. Imredy JP, Penniman JR, Dech SJ, Irving WD, Salata JJ. Modeling of the adrenergic response of the human IKs current (hKCNQ1/hKCNE1) stably expressed in HEK-293 cells. *American journal of physiology Heart and circulatory physiology*. 2008;295(5):H1867-1881.
109. Lai X. Reproducible method to enrich membrane proteins with high purity and high yield for an LC-MS/MS approach in quantitative membrane proteomics. *Electrophoresis*. 2013;34(6):809-817.
110. Lai X, Bacallao RL, Blazer-Yost BL, Hong D, Mason SB, Witzmann FA. Characterization of the renal cyst fluid proteome in autosomal dominant polycystic kidney disease (ADPKD) patients. *Proteomics Clin Appl*. 2008;2(7-8):1140-1152.
111. Keller A, Nesvizhskii AI, Kolker E, Aebersold R. Empirical statistical model to estimate the accuracy of peptide identifications made by MS/MS and database search. *Anal Chem*. 2002;74(20):5383-5392.
112. Nesvizhskii AI, Keller A, Kolker E, Aebersold R. A statistical model for identifying proteins by tandem mass spectrometry. *Anal Chem*. 2003;75(17):4646-4658.
113. Lai X, Wang L, Tang H, Witzmann FA. A novel alignment method and multiple filters for exclusion of unqualified peptides to enhance label-free quantification using peptide intensity in LC-MS/MS. *J Proteome Res*. 2011;10(10):4799-4812.
114. Ashpole NM, Hudmon A. Excitotoxic neuroprotection and vulnerability with CaMKII inhibition. *Mol Cell Neurosci*. 2011;46(4):720-730.
115. Rezazadeh S, Claydon TW, Fedida D. KN-93 (2-[N-(2-hydroxyethyl)]-N-(4-methoxybenzenesulfonyl)]amino-N-(4-chlorocinnamyl)-N -methylbenzylamine), a calcium/calmodulin-dependent protein kinase II inhibitor, is a direct extracellular blocker of voltage-gated potassium channels. *The Journal of pharmacology and experimental therapeutics*. 2006;317(1):292-299.
116. Maier LS, Zhang T, Chen L, DeSantiago J, Brown JH, Bers DM. Transgenic CaMKII $\delta$ C overexpression uniquely alters cardiac myocyte Ca<sup>2+</sup> handling: reduced SR Ca<sup>2+</sup> load and activated SR Ca<sup>2+</sup> release. *Circulation research*. 2003;92(8):904-911.

117. Vincent KP, McCulloch AD, Edwards AG. Toward a hierarchy of mechanisms in CaMKII-mediated arrhythmia. *Frontiers in pharmacology*. 2014;5:110.
118. Wagner S, Ruff HM, Weber SL, et al. Reactive oxygen species-activated Ca/calmodulin kinase II $\delta$  is required for late I(Na) augmentation leading to cellular Na and Ca overload. *Circulation research*. 2011;108(5):555-565.
119. Ai X, Curran JW, Shannon TR, Bers DM, Pogwizd SM. Ca<sup>2+</sup>/calmodulin-dependent protein kinase modulates cardiac ryanodine receptor phosphorylation and sarcoplasmic reticulum Ca<sup>2+</sup> leak in heart failure. *Circulation research*. 2005;97(12):1314-1322.
120. Hoch B, Meyer R, Hetzer R, Krause EG, Karczewski P. Identification and expression of delta-isoforms of the multifunctional Ca<sup>2+</sup>/calmodulin-dependent protein kinase in failing and nonfailing human myocardium. *Circulation research*. 1999;84(6):713-721.
121. Kirchhefer U, Schmitz W, Scholz H, Neumann J. Activity of cAMP-dependent protein kinase and Ca<sup>2+</sup>/calmodulin-dependent protein kinase in failing and nonfailing human hearts. *Cardiovasc Res*. 1999;42(1):254-261.
122. Wang W, Zhu W, Wang S, et al. Sustained beta1-adrenergic stimulation modulates cardiac contractility by Ca<sup>2+</sup>/calmodulin kinase signaling pathway. *Circulation research*. 2004;95(8):798-806.
123. Nagy N, Acsai K, Kormos A, et al. [Ca<sup>2+</sup>]<sub>i</sub>-induced augmentation of the inward rectifier potassium current (IK1) in canine and human ventricular myocardium. *Pflugers Archiv : European journal of physiology*. 2013;465(11):1621-1635.
124. Aydin A, Bahring S, Dahm S, et al. Single nucleotide polymorphism map of five long-QT genes. *J Mol Med (Berl)*. 2005;83(2):159-165.
125. Ruiz-Hurtado G, Dominguez-Rodriguez A, Pereira L, et al. Sustained Epac activation induces calmodulin dependent positive inotropic effect in adult cardiomyocytes. *Journal of molecular and cellular cardiology*. 2012;53(5):617-625.
126. Pellicena P, Schulman H. CaMKII inhibitors: from research tools to therapeutic agents. *Frontiers in pharmacology*. 2014;5:21.

127. Kaab S, Nuss HB, Chiamvimonvat N, et al. Ionic mechanism of action potential prolongation in ventricular myocytes from dogs with pacing-induced heart failure. *Circulation research*. 1996;78(2):262-273.
128. Guo X, Gao X, Wang Y, Peng L, Zhu Y, Wang S. IKs protects from ventricular arrhythmia during cardiac ischemia and reperfusion in rabbits by preserving the repolarization reserve. *PloS one*. 2012;7(2):e31545.
129. Chen J, Zheng R, Melman YF, McDonald TV. Functional interactions between KCNE1 C-terminus and the KCNQ1 channel. *PLoS One*. 2009;4(4):e5143.
130. Zheng R, Thompson K, Obeng-Gyimah E, et al. Analysis of the interactions between the C-terminal cytoplasmic domains of KCNQ1 and KCNE1 channel subunits. *Biochem J*. 2010;428(1):75-84.
131. Harmer SC, Wilson AJ, Aldridge R, Tinker A. Mechanisms of disease pathogenesis in long QT syndrome type 5. *Am J Physiol Cell Physiol*. 2010;298(2):C263-273.
132. Bohnen MS, Peng G, Robey SH, et al. Molecular Pathophysiology of Congenital Long QT Syndrome. *Physiol Rev*. 2017;97(1):89-134.
133. Dahimene S, Alcolea S, Naud P, et al. The N-terminal juxtamembranous domain of KCNQ1 is critical for channel surface expression: implications in the Romano-Ward LQT1 syndrome. *Circulation research*. 2006;99(10):1076-1083.
134. Kanki H, Kupersmidt S, Yang T, Wells S, Roden DM. A structural requirement for processing the cardiac K<sup>+</sup> channel KCNQ1. *The Journal of biological chemistry*. 2004;279(32):33976-33983.
135. Seebohm G, Strutz-Seebohm N, Ureche ON, et al. Long QT syndrome-associated mutations in KCNQ1 and KCNE1 subunits disrupt normal endosomal recycling of IKs channels. *Circulation research*. 2008;103(12):1451-1457.
136. Bianchi L, Shen Z, Dennis AT, et al. Cellular dysfunction of LQT5-minK mutants: abnormalities of IKs, IKr and trafficking in long QT syndrome. *Hum Mol Genet*. 1999;8(8):1499-1507.
137. Aldridge R, Berber R, Wilson AJ, Bitner-Glindzicz M, Tinker A. Effect of KCNE1 mutations on the trafficking of KCNQ1 in CHO-K1 cells. *J Physiol*. 2005;565P:PC91.

138. Vanoye CG, Welch RC, Tian C, Sanders CR, George AL, Jr. KCNQ1/KCNE1 assembly, co-translation not required. *Channels (Austin, Tex)*. 2010;4(2):108-114.
139. Aromolaran A, Kobertz WR, Colecraft HM. Illuminating Trafficking of KCNQ1/KCNE1 Channels in Heart. *Biophys J*. 2012;102(3, Supplement 1):34a-35a.
140. Boczek NJ, Gomez-Hurtado N, Ye D, et al. Spectrum and Prevalence of CALM1-, CALM2-, and CALM3-Encoded Calmodulin Variants in Long QT Syndrome and Functional Characterization of a Novel Long QT Syndrome-Associated Calmodulin Missense Variant, E141G. *Circ Cardiovasc Genet*. 2016;9(2):136-146.
141. Jimenez-Jaimez J, Palomino Doza J, Ortega A, et al. Calmodulin 2 Mutation N98S Is Associated with Unexplained Cardiac Arrest in Infants Due to Low Clinical Penetrance Electrical Disorders. *PLoS One*. 2016;11(4):e0153851.
142. Tobelaim WS, Dvir M, Lebel G, et al. Competition of calcified calmodulin N lobe and PIP2 to an LQT mutation site in Kv7.1 channel. *Proceedings of the National Academy of Sciences of the United States of America*. 2017;114(5):E869-e878.
143. Sun J, MacKinnon R. Cryo-EM Structure of a KCNQ1/CaM Complex Reveals Insights into Congenital Long QT Syndrome. *Cell*. 2017;169(6):1042-1050.e1049.